Spin Determination at the Large Hadron Collider

A dissertation presented
by

Itay Yavin

to
The Department of Physics
in partial fulfillment of the requirements
for the degree of
Doctor of Philosophy
in the subject of

Physics

Harvard University
Cambridge, Massachusetts
June 2006

Thesis advisor
Nima Arkani-Hamed

Author
Itay Yavin

Spin Determination at the Large Hadron Collider

Abstract

The quantum field theory describing the Electroweak sector demands some new physics at the TeV scale in order to unitarize the scattering of longitudinal W bosons. If this new physics takes the form of a scalar Higgs boson then it is hard to understand the huge hierarchy of scales between the Electroweak scale $\sim$ TeV and the Planck scale $\sim 10^{19}$ GeV. This is known as the Naturalness problem. Normally, in order to solve this problem, new particles, in addition to the Higgs boson, are required to be present in the spectrum below a few TeV. If such particles are indeed discovered at the Large Hadron Collider it will become important to determine their spin. Several classes of models for physics beyond the Electroweak scale exist. Determining the spin of any such newly discovered particle could prove to be the only means of distinguishing between these different models. In the first part of this thesis, we present a thorough discussion regarding such a measurement. We survey the different potentially useful channels for spin determination and a detailed analysis of the most promising channel is performed.

The Littlest Higgs model offers a way to solve the Hierarchy problem by introducing heavy partners to Standard Model particles with the same spin and quantum numbers. However, this model is only good up to ~ 10 TeV. In the second part of

this thesis we present an extension of this model into a strongly coupled theory above ~ 10 TeV. We use the celebrated AdS/CFT correspondence to calculate properties of the low-energy physics in terms of high-energy parameters. We comment on some of the tensions inherent to such a construction involving a large-N CFT (or equivalently, an AdS space).

Contents

Citations to Previously Published Work

The first part of this work is based on a paper written with Lian-Tao Wang,

[1] *Spin Measurements in Cascade Decays at the LHC*, Lian-Tao Wang and Itay Yavin, hep-ph/0605296

The second part of this work is based on a paper written with Jesse Thaler,

[2] *The Littlest Higgs in Anti-de Sitter Space*, Jesse Thaler and Itay Yavin, JHEP 0508 (2005) 022, hep-ph/0501036

Work that I have done during my Ph.D., but will not be included in this thesis can be found in the following papers,

[3] *Effect of a magnetic field gradient and gravitational acceleration on a time-domain grating-echo interferometer*, M. Weel, I. Chan, S. Beattie, A. Kumarakrishnan, I. Yavin - accepted to PRA, to be published upon proofing.

[4] *Curvature as a remedy or discretizing gravity in warped dimensions*, Jason Gallicchio and Itay Yavin, JHEP 0306 (2006) 3, hep-th/0507105.

[5] *Evolution in time of an N-atom system: II. Calculation of the eigenstates* , Terry Rudolph, Itay Yavin and Helen Freedhoff, Phys. Rev. A 69 , 013815.

Acknowledgments

First and foremost I would like to thank my advisor, Nima Arkani-Hamed, for taking me as his student and providing me with guidance. I am certain it has not been easy for him. Yet, he was always patient at explaining things to me, never frowning or disrespecting. In this regard, I am impressed by Nima as a person even more than I am impressed by him as a physicist. His kindness and encouragement have elevated my spirit many a times during the last four years. Needless to say, I have learned more physics from Nima than anyone before. It has been truly a great privilege to be his student.

I would also like to thank the other members on my thesis committee, Melissa Franklin and Howard Georgi, for accepting the burden of serving on the committee.

The work appearing in the first part of this dissertation was done in collaboration with Lian-Tao Wang. I thank Lian-Tao for his constant encouragement and his will to listen to my frequently wrong ideas.

The second part of this dissertation is comprised of work I have done with Jesse Thaler. I would like to thank Jesse for baring with my creeping pace. It has been a delightful experience working with Jesse and learning from him.

The third successful project during my Ph.D. was done with Jason Gallicchio. It involved the deconstruction of AdS space and I did not include it in this dissertation since it is slightly off topic. Nonetheless, I would like to thank Jason for the many hours of stimulating conversations we had while working on this project.

When not doing physics I spent many memorable hours with my dear friends Adilet Imambekov and Dima Abanin. They are like family to me. Through our adventures in the mountains of New-Hampshire and Mexico, Adilet has taught me a

great deal. He taught me patience, organization and perseverance. If nothing else, these skills proved useful during difficult times while completing my Ph.D., and I must thank him for that. My thanks also go to Dima, for always reminding me not to take myself too seriously, and for being an unwavering source of happiness in my life. I was also fortunate enough to have David Mattoon Thompson to share Jefferson 465 with me. Mattoon became much more than a fantastic office mate. He was, and still is an inspiration to me as a scientist, a humanist, and a friend.

I would also like to thank Sheila Ferguson who was always there, not only to help with any administrative difficulties, but also to provide a listening ear and a sound advice. Her true care for the students and their problems, far and beyond her duty, is remarkable.

I suppose this is also a wonderful opportunity to tell my parents how grateful I am. Above all, they gave me the gift of freedom to choose my path in life. They never imposed themselves on me, never told me what to study, where to live or who to love. They were happy and proud of my decisions even when those did not meet their expectations or hopes. I could not ask for better parents.

Finally I would like to thank Mina for being on my mind.

Dedicated to my father and mother, Yossi and Zipi Yavin.

Part I:

Determining the Spin of Prospective New Particles at the Large Hadron Collider

1

Introduction

Naturalness of the weak scale implies the existence of new physics beyond the Standard Model at the scale $\sim$ TeV. Typical new physics scenarios predict the existence of a set of new particles at that scale. The Large Hadron Collider (LHC) gives us a great opportunity for discovering those particles.

In order to understand the nature of the new physics, it is necessary to measure its properties in detail. One of the obvious tasks is to reconstruct the masses and gauge quantum numbers of the new physics particles from experimental data. A recent study [12] demonstrated the challenges of such a goal and suggested possible directions in achieving it.

On the other hand, there is another, at least equally important, LHC inverse problem: how do we determine the spin of any newly discovered particle? The proposed new particles in several main candidates of new physics scenarios typically have similar gauge interactions. They could often be organized as partners of the known Standard Model particles with the same gauge quantum number, such as

quark partners, lepton partners and gauge boson partners. A typical example is the set of superpartners in supersymmetry, including squarks, sleptons, gauginos, and so on. Another interesting scenario is the theory space models inspired by [9]. The duplication of the Standard Model states in this scenario comes from introducing more copies of the Standard Model gauge group. Typical examples are little Higgs models [1]. Measuring the partners' spin becomes a crucial, sometimes single, way to distinguish those scenarios.

Motivated by electroweak precision constraints and the existence of Cold Dark Matter, many new physics scenarios incorporate some discrete symmetry which guarantees the existence of a lightest stable neutral particle, LSNP. Well-known examples of such discrete symmetries include R-parity in supersymmetry, KK-parity in universal extra-dimension models [6], or similarly, T-parity in Little Higgs Models [22, 23, 60, 24]. The existence of such a neutral particle at the end of the decay chain results in large missing energy events in which new physics particles are produced. This fact helps to separate them from the Standard Model background. On the other hand, it also makes the spin measurement more complicated because it is almost impossible to reconstruct the momentum, and therefore the rest frame, of the decaying particles.

The question of spin determination has been revisited recently. The total cross section might serve as an initial hint to the spin of the new particles discovered [35]. This is not entirely satisfactory because certain model dependence is inevitable when using the rate information. For example, a fermion can be faked by two closely de-

[1] Another well-known example is the the extra-dimensional setup with the corresponding KK particles. As we learned in the past few years, this is very related to the theory space models via deconstruction

generate scalars. Moreover, such a determination is only possible if we could measure the masses of the particle using kinematical information. As demonstrated in [24, 65], typical "transverse" kinematical observables are not sensitive to the absolute mass of particles. One can only deduce the mass difference between the decaying particle and the neutral particle escaping the detector. With some assumptions regarding the underlaying model there are more subtle kinematical observables which, in combination with the rate information, could determine the spin [65]. To what extent this could be generalized to a broader classes of new physics particles is currently under investigation.

Therefore, it is important to investigate other possible ways of directly measuring the spin of new particles. The typical way of measuring the spin of a decaying particle start with reconstructing its rest frame from the decay products. Then, the angular distribution in the rest frame contains the full spin information, independent of the boost. As discussed above, we do not have enough kinematical information to boost to the rest frame of the decaying particle if the spectrum contains a LSNP. Therefore, it is natural to consider distributions as a function of relativistic invariants constructed out of the decay products of a single decaying particle. We will focus on this possibility in this paper.

Various new physics models always have some detailed differences in their spectra. But, such differences are very model dependent. Although in principle they could carry interesting information, we will focus on spin determination based on Standard Model partners only. What we have in mind are two classes of models with almost identical gauge quantum numbers and maximal flexibility in their mass spectra. In

other words, they would look very similar except for their spin content.

One obvious scenario is low energy supersymmetry, parameterized by the MSSM with a conserved R-parity.

As a contrasting scenario we consider a framework in which all new particles have the same spin as their Standard Model counter parts. The existence of a LSNP, is guaranteed by the assumption that all the new physics particles are odd under a certain Z_2 parity. Special cases of this scenario could be the first KK level of UED or T-parity little Higgs. However, what we have in mind is a more generic setup and we will not constrain ourselves to any special mass or coupling relations imposed by these two scenarios. To emphasize its generic nature, we will call it the Same Spin scenario in this paper. We will use symbols with primes to label the new particles in the Same Spin scenario. For example, we will use q' to label the quark partner, and so on. We will assume the LSNP in this case is a vector and label it as A'.

Typical new physics scenarios have many complicated decay channels. Many kinematical distributions can be constructed from them. One of the main goals of this paper is to present a systematical survey of the observability of spin correlations in a wide variety of decay chains which are generically present in new physics scenarios. We identify interesting decay channels to focus on for spin measurements. It is important to notice, as will be clear from our discussion, that the usefulness of any particular channel is restricted to a specific range of parameters. We describe the kinematical requirements for each of the channels we analyze. There is no obvious golden channel. For different points in the parameter space, we will generically have different decay channels available. Therefore, we will have to devise different strategies depending

on mass spectra of underlying models.

One of the important tools we develop in this paper is a set of simple rules, which summarizes many well-known results concerning spin correlations. Such simple rules allows one to gain insight into the angular correlations in decay, without the necessity of going through a lengthy calculation. They can be useful in other, potentially more complicated, scenarios than the ones considered hereafter.

Barr [16] investigated a typical supersymmetry cascade involving a squark decay. He found that angular correlations exist between the decay products. Barr's method relies on the fact that more squarks are produced than anti-squarks in a proton-proton collider. There are several follow-up studies along the same lines [36, 73, 5]. References [73] and [36] went further and contrasted supersymmetry with the universal extra-dimensions scenario [6],[25]. Reference [73] found that with a mass spectrum given by the SPS point 1a, the SUSY model is distinguishable from the UED case. In their study, they assumed the lepton can be perfectly correlated with the correct jet. That might be possible if complete kinematic information is available, but in practice seems quite difficult. In general jet combinatorics must be taken into account.

One limitation of these investigations is the need for a light leptonic partner. It must be lighter than the second lightest neutral gauge boson partner, such as the second lightest neutralino (which must be a wino or bino), in supersymmetry. While true in some special benchmark models [4], there is no reason to assume this is a generic feature of supersymmetry breaking. In fact, it is more generic to assume otherwise, especially if one is driven by the problem of naturalness.

We present a detailed study of spin correlations in the decay chain $\tilde{q} \to q + \tilde{C}_1^{\pm} \to$

$q + W^{\pm} + \tilde{N}_1$ in supersymmetry and its counter part $q' \to q + W'^{\pm} \to q + W^{\pm} + A'$ in the Same Spin scenario. Such a decay chain does not require the leptonic partner to be lighter than the gauge boson partner and is certainly more generic in parameter space. We will assume that the mass splitting between the two lightest states is greater than $m_{\mathrm{W,Z}}$. Therefore, the on-shell decay to W/Z always dominates[2]. Our result shows that it is possible to observe spin correlation in this decay chain. As a demonstration of the result of our general discussion, we map out the parameter region in which this decay channel is useful.

As part of the analysis we used HERWIG 6.507 [32] which implements a spin correlation algorithm. This algorithm was first used for QCD parton showers [29, 57, 59, 58] and later extended by Richardson to supersymmetric and top processes [71]. We supplemented the code to include the decays of massive gauge bosons (such as KK partners of the gluon) and the details are spelled out in appendix B. To the best of the authors' knowledge, HERWIG is the only simulator that implements such an algorithm and is therefore suitable for spin determination studies.

This part of the thesis is organized as follows: In Section 2 we try to build some intuition by looking at the effects of spin on the angular distributions of simple decays. In Section 3, we present a survey of spin correlations in various decay channels. Our detailed study of the decay chain with $qW^{\pm}$ final states is presented in Section 4. There, we take up the task of constructing an observable signal to distinguish SUSY from the Same Spin scenario in the absence of any leptonic partners. Finally, in section 6, we comment on possible future directions and present our conclusions.

[2]If the mass splitting is less than $m_{\mathrm{W,Z}}$, sometimes, the off-shell diagram via a squark and slepton can be important. Although it is a special case of the mass spectrum, it is certainly worthwhile exploring it further.

2

Simple Spin Correlations

In this section we review some basic angular distributions from simple decays. These distributions will serve as building blocks in our understanding of the spin correlations in more complicated decay chains which we will consider later.

2.1 Scalar decay

A scalar does not pick any special direction in space and so its decay is isotropic. It does not mean that the existence of scalars spoils any hope for distinguishing them away from phase-space. The production of bosons (via a Z^0 for example) has a different angular distribution about the beam axis than that of fermions. This discrepancy can be employed in determining the spin of lepton partners (see for example, [17]). However, in our study we will concentrate on a single branch in which case it is not possible to distinguish a scalar from phase-space.

2.2 Fermion decay

First, we consider the decay of a fermion ψ_1 into another fermion ψ_2 and a scalar ϕ, via an interaction of the form

$$y_L \phi \bar{\psi}_2 P_L \psi_1 + y_R \phi \bar{\psi}_2 P_R \psi_1 \tag{2.1}$$

Depending on the model, this coupling could be either chiral, $y_L \neq y_R$, or non-chiral, $y_L = y_R$. We will see examples of both cases in our study.

If the coupling in Eq. 2.1 is chiral, ψ_2 is produced in a chirality eigenstate. If ψ_2 is boosted then it is in a helicity eigenstate, i.e., polarized. However, ψ_1 is, in general, not polarized and therefore the decay is isotropic, even if the coupling (2.1) is chiral and ψ_2 is boosted. It is easy to see how this comes about. If it is a Left handed coupling, $y_R = 0$, then ψ_2 is mostly a right-handed particle, $|\downarrow\rangle$. From the transformation of a spinor under a rotation by an angle θ we have that,

$$\begin{aligned} |\uparrow\rangle &\rightarrow \cos\left(\frac{\theta}{2}\right) |\uparrow\rangle + \sin\left(\frac{\theta}{2}\right) |\downarrow\rangle \\ |\downarrow\rangle &\rightarrow -\sin\left(\frac{\theta}{2}\right) |\uparrow\rangle + \cos\left(\frac{\theta}{2}\right) |\downarrow\rangle \end{aligned}$$

The angle θ is defined with respect to ψ_1 polarization axis. Notice that if ψ_1 is left-handed polarized, $|\uparrow\rangle$, its decay probability is $\propto \sin^2\left(\frac{\theta}{2}\right)$. On the other hand, if it is right-handed polarized, $|\downarrow\rangle$, its decay probability $\propto \cos^2\left(\frac{\theta}{2}\right)$. These decay distributions are shown in Fig.(2.1) as a function of $\cos(\theta)$. Unfortunately, ψ_1 itself is normally not polarized and averaging over the two process the decay is indeed isotropic.

However, if ψ_1 came from the decay of another particle and that vertex was chiral then the situation is different. In that case ψ_1 is polarized and its subsequent decay

is governed by a non-trivial angular distribution as shown in Fig. (2.1). Whether the decay involves a helicity flip or not determines the sign of the slope.

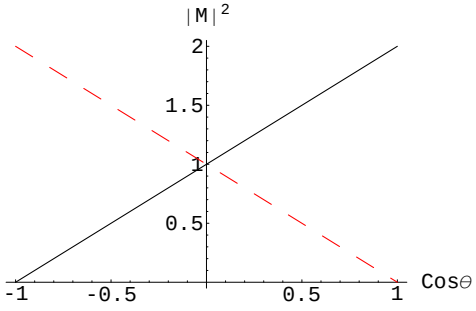

Figure 2.1: The decay probability for a fermion into a scalar and another fermion of the same helicity (solid-black) or opposite helicity (dashed-red) as a function of $\cos\theta$. θ is defined with respect to the axis of polarization of the decaying fermion.

Next, we consider the decay of a fermion into another fermion and a gauge-boson via an interaction of the form

$$g_L \bar{\psi}_2 \gamma^\mu P_L \psi_1 A_\mu + g_R \bar{\psi}_2 \gamma^\mu P_R \psi_1 A_\mu \tag{2.2}$$

As before, we consider the case where ψ_2 is boosted. If the interaction is chiral ψ_2 is in a definite helicity state. The fermionic current that couples to A^μ is of the form $\bar{\psi}_{\dot{\alpha}} \sigma_\mu^{\dot{\alpha}\beta} \psi_\beta$. If the emitted gauge-boson is longitudinally polarized the distributions are the same as the decay into a fermion and a scalar. If it transversely polarized it is precisely opposite (i.e. same helicity corresponds to $\sin^2\theta/2$ and opposite helicity to $\cos^2\theta/2$).

The most important feature of the fermion's decay is the linear dependence of the decay probability on $\cos\theta$. It is also clear that chiral vertices must be involved in order to observe spin correlations (unless the fermion is a Majorana particle, a possibility we discuss below).

2.3 Gauge-boson decay

When a gauge-boson decay (2-body), relativity forces the products to be two bosons or two fermions. As is well known, when the products are two fermions the angular distribution is given by,

$$P_{\rm trans}(\cos\theta) = \frac{1}{4}\left(1+\cos^2\theta\right) \qquad P_{\rm long}(\cos\theta) = \frac{1}{2}\left(1-\cos^2\theta\right) \tag{2.3}$$

If a gauge boson decays into two scalars via the interaction

$$g\phi_2^* \overleftrightarrow{\partial}_\mu \phi_1 A^\mu, \tag{2.4}$$

the angular distribution has the opposite structure,

$$P_{\rm trans}(\cos\theta) = \frac{1}{2}(1-\cos^2\theta) \qquad P_{\rm long}(\cos\theta) = \cos^2\theta \tag{2.5}$$

where the subscript on P denotes the initial gauge-boson's polarization. As usual θ is defined about the polarization axis. The decay of a gauge-boson into two other gauge-bosons has the same angular distribution as Eq. (2.5). These are shown in Fig.(2.2). As usual there are finite mass effects that come into play when the products are not

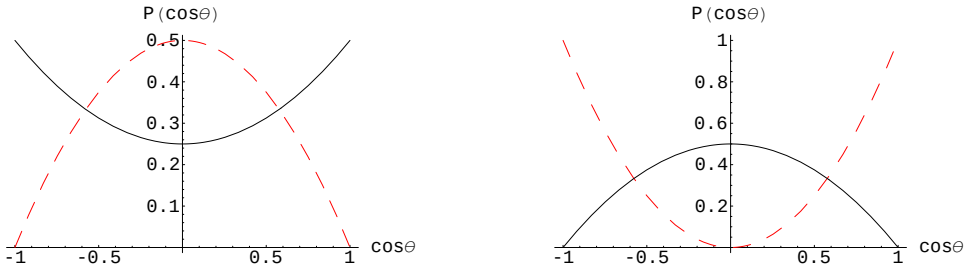

Figure 2.2: The decay probability for a gauge-boson into two fermions (left) and two bosons (right) for transverse (solid-black) and longitudinal polarization (dashed-red) as a function of $\cos\theta$.

highly boosted. Those tend to wash out any angular dependence of the amplitude. Generically these contributions scale as m^2/E^2. Therefore, as noted before there has to be an appreciable difference between the mass of the decaying particle and its products so that $m^2/E^2 \lesssim 1/2$.

The contrast with the previous case is clear as the dependence of the amplitude on $\cos\theta$ is quadratic. It is also important to note that the vertex need not be chiral.

2.4 Higher spin

By noting that a rotation by θ of a state of spin j is given by $e^{i\theta j\sigma_y}$ it is easy to see that the amplitude for the decay of a particle with spin j is some polynomial of degree $2j$,

$$P_\lambda(\cos\theta) = a_{2j}(\cos\theta)^{2j} + a_{2j-1}(\cos\theta)^{2j-1} + \ldots + a_0 \tag{2.6}$$

The coefficients a_i are such that when we sum over all polarizations λ we get,

$$\sum_\lambda P_\lambda(\cos\theta) = 1 \tag{2.7}$$

since an unpolarized particle has no preferred direction. In this paper we concentrate on spin 0,1/2, and 1 and will not consider higher spin. Nonetheless, this is an important issue to address. For example, if the partners of the graviton are indeed detected it would be good to know whether it is a supersymmetric spin-3/2 object or a Same-Spin spin-2 resonance.

3

Angular Correlations in Cascade Decays

In this section, we present a systematic study of spin correlations in a wide variety of cascade decay channels. Aside from the matrix element, the kinematics also play a crucial role in the observability of spin effects. We lay out the conditions for observing spin correlations in each of the decay channels we discuss. Whether any of the channels is open or not depends on the particular mass spectrum. However, it is not unreasonable to expect several such channels to be open in a generic model. This is important because the signal from any one channel might not be sufficiently strong. In this case we would have to combine the signal from a few channels to obtain a high confidence spin determination.

We focus on a class of specific kinematical observable. It is constructed from the momenta of two of the observed final state particles. More complicated decay patterns and observables consisting of more than two observable particles could also

be interesting.

A generic feature of this type of observables is that spin information of the *intermediate* particle, which has observable decay products on both sides, in the decay chain always manifest itself as some polynomial structure in the distribution. Indeed, a particle of spin j, if polarized, will result in a polynomial of degree $2j$. On the other hand, such a method is not useful for determining the spin of any particle at the top or bottom of the decay chain. For the same reason, very short decay chains such as $\tilde{q} \to q + \text{LSP}$ won't contain much information.

As discussed in Section 2, a key requirement for the existence of any spin correlations is for the intermediate state particle to be polarized[1]. A boost invariant way to know whether a particle is polarized or not is to study this question in its rest frame using a direction defined by its mother particle and the other decay products. We will see examples of such analysis in the decay channels we consider below. From the discussion in the previous section, it is clear that there are only a few ways for a particle to be polarized in its rest frame,

1. For Majorana fermions a spin flip results in a different process with different end products. We must be able to tell those apart (measuring a leptons vs. anti-lepton). We will see this in detail in the discussion to follow.

2. Dirac fermions must be produced from a (partially) chiral coupling and decay through a (partially) chiral interaction.

3. In general the spectrum of new particles needs not be left-right symmetric. In

[1]Strictly speaking, this requirement only applies for on-shell particles. For off-shell particles, the spin correlation could have new interesting properties. We will examine the off-shell decay in Section 3.9

this case, the interaction of these particles is effectively chiral even if the gauge-coupling is vector like. A typical example is the asymmetric QCD production of left and right squarks when their masses are very different[2].

4. For a gauge boson, it must come from the decay of a boosted particle (in the gauge-boson rest frame).

We will see detailed realizations of all of these requirements in various decay channels we study in this section.

We will organize our discussion in terms of different final states.

3.1 Weak Decay with $q\ell^{\pm}$ final state

We will go through the logic of establishing spin correlation this channel in more detail because many other channels can be understood following very similar arguments.

We first consider the supersymmetric case. Here, the decay to $q\ell^{\pm}$ final states will proceed through either Dirac or Majorana fermion intermediate states. We consider the case of a Dirac fermion first (i.e., chargino intermediate state) and compare it with the corresponding process in the Same Spin scenario where the intermediate state is a massive gauge boson W'. We will comment on the case of Majorana fermion briefly. For more details, see [16].

In the case of a Dirac fermion there are two possible ways for the particle to be polarized. If it is off-shell then one of the helicities dominates over the other simply

[2]We would like to thank M. Peskin for bringing this fact to our attention.

because $m^2/q^2 \neq 1$, where q is the fermion 4-momenta (this possibility is also open to a Majorana fermion). This might become important if a decay must proceed through an off-shell particle simply because no other channel is available. We will not pursue this possibility further, but we comment on it in section (3.9).

The other possibility for a Dirac fermion to be polarized is when both its mother vertex and its daughter vertex are at least partially chiral. As an example, consider the decay of a squark into a quark, slepton and anti-lepton through a Chargino, as shown in Fig.(3.1). Using the rules we developed in the previous section it is straightforward to understand what angular correlations are expected.

In the rest frame of the Chargino, the decaying squark and outgoing quark define a polarization axis. Since the interaction is chiral the Chargino is polarized. Since the second vertex is also polarized, we have a polarized fermion decaying into another fermion (lepton) and a scalar (slepton). As we saw before, this decay is governed by a first order polynomial of $\cos\theta$. However, notice that $\cos\theta$ is related to the relativistically invariant quantity, t_{ql},

$$t_{ql} = (p_q + p_l)^2 = 2\frac{\left(m_{\tilde{q}}^2 - m_{\tilde{C}}^2\right)\left(m_{\tilde{C}}^2 - m_{\tilde{l}}^2\right)}{4m_{\tilde{C}}^2}(1 - \cos\theta) \tag{3.1}$$

where the last equality only holds in the Chargino's rest frame. We can immediately conclude that the relativistically invariant amplitude is at most a linear function of t_{ql} with the sign given by the explicit details of the couplings. Of course, this can be easily confirmed by an explicit computation of the amplitude, as shown in Fig.3.1).

In contrast with the supersymmetric case let us consider the decay chain $q' \to q + W'^{\pm} \to q + W^{\pm} + \nu'$, where we have assumed that W' couples like a Standard Model W. The relevant diagram is shown in Fig.(3.2). If the spectrum is not too

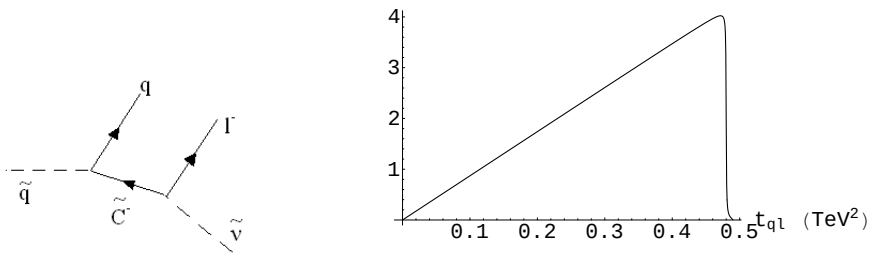

Figure 3.1: The decay of a squark through a chargino involves two chiral vertices. As a result the lepton's direction is correlated with that of the outgoing quark. On the right we plot the amplitude as a function of t_{ql} for $m_{\tilde{q}} = 1000$ GeV, $m_{\tilde{C}} = 500$ GeV and $m_{\tilde{\nu}} = 300$ GeV. The graph is normalized to unit area.

degenerate then in the rest frame of the W', both the incoming q' and the outgoing q are boosted and mostly left-handed. Therefore, the W' longitudinal polarization dominates over the transverse one. Another way of seeing the same thing is to note that in the rest frame of W' the fermionic current can be written in terms of the gauge-boson polarizations,

$$g_A \bar{u}_2 \gamma^\mu P_A u_1 \propto \left(\epsilon_{\text{long}} + \frac{m_{q'}}{E_{q'}} \left(c_L \epsilon_L + c_R \epsilon_R \right) \right) \tag{3.2}$$

where we have neglected m_q. c_L and c_R are $\mathcal{O}(1)$ coefficients depending on the precise nature of the interaction. Notice the suppression of the transverse polarization with respect to the longitudinal one by a factor of $m_{q'}/E_{q'}$ in the amplitude. It is clear that when the fermions' mass difference is comparable to the W' mass, $m_{q'} - m_q \sim m_{W'}$, the resulting polarization is negligible, since $m_{q'}/E_{q'} \sim 1$ in the rest frame of the W'.

Since the W' is longitudinally polarized, its subsequent decay into $l^+ \nu'$ is governed by a $1 - \cos^2\theta$. Here, θ is the angle of the outgoing leptons with respect to the axis of polarization defined by the quarks. Therefore, the relativistically invariant amplitude squared must be a *quadratic* function of t_{ql} with a negative coefficient in front of

the leading power. Notice that a gauge-boson does not require the vertices to be

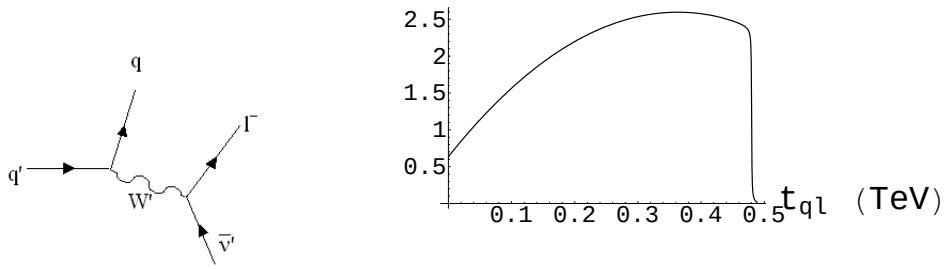

Figure 3.2: When q' decays the intermediate W' is longitudinally polarized if the incoming q' and outgoing q are both boosted in its rest frame. This in turn will result in angular correlations between the directions of the quark and the lepton. On the right we plot the amplitude as a function of t_{ql} for $m_{q'} = 1000$ GeV, $m_{W'} = 500$ GeV and $m_{\nu'} = 300$ GeV. The graph is normalized to unit area.

chiral. This is important and potentially useful in determining the gluon partner's spin. However, it is also more susceptible to mass difference effects (see equation (3.2)). In contrast, the fermionic counterpart remains polarized even when $m_{\tilde{q}}$ is not very different from $m_{\tilde{C}}$, as long as the coupling is chiral and the outgoing quark is boosted.

Finally, we briefly consider the decay of the squark into $q\ell^{\pm}$ final states via a Majorana fermion intermediate state. The relevant diagrams are shown in Fig.(3.3). For the propagator to flip its spin we must place a mass insertion. However, due to the Majorana nature of the Neutralino, this corresponds to a different process with different final states than the one without a mass insertion. Therefore, the propagator has a definite helicity for each of the processes and there are angular correlations between the quark and the lepton. This fact was exploited by A. Barr [16] to determine the spin of the Neutralino and further details can be found in the

reference. One can study $q\ell^+$ and $q\ell^-$ distributions to uncover the spin information. However, there is a further complication due the Majorana nature of the Neutralino. There is always another diagram starting from anti-squark with opposite sign of its charge which contributes to the same process but with the opposite helicity structure as shown in Fig.(3.4). As Barr noted, in a proton-proton collider more squarks are produced than anti-squarks and therefore the angular correlations are not washed out completely.

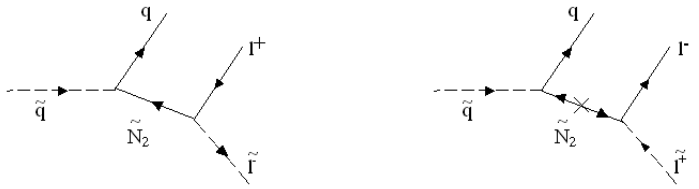

Figure 3.3: The two possible modes for a decay through a Neutralino. A spin flip requires a mass insertion (right), which results in a different process.

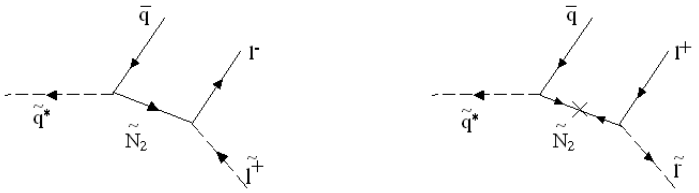

Figure 3.4: The two conjugate modes starting from an anti-squark for the decay through a Neutralino.

3.2 Weak Decay with $q\bar{q}$ final states

In principle, the decay into $q\bar{q}$ final states could contain similar spin correlations, since it just replace the leptons in the second stage of the decay chains discussed in the previous section with quarks. However, in general we can not determine the charge of the initial jet. Once we are forced to average over the two final states shown in Fig.(3.3), all angular correlations are washed out.

On the other hand, if the decay products of the second decay are a third generation quark and quark partner we could, in principle, recover some charge information. It will then be possible to extract some spin correlation from such decay chains. The effectiveness of such decay channels require further careful studies taking into account the efficiency of identifying charge of the third generation quarks.

3.3 Weak Decay with $qW^{\pm}$ final state

If the charged gauge boson partner is lighter than the leptonic partner then its decay into a $W^{\pm}$ and LSNP through a non-Abelian vertex is usually the dominant decay mode. This channel is shown in Fig.(3.5) In the supersymmetric case this coupling is at least partially chiral if $\tan\beta \neq 1$ and the higgsino is not considerably heavier than the gauginos. If $m_{\tilde{q}} - m_{\tilde{C}} >> m_q$, than the chargino is at least partially polarized (with respect to the axis defined by the incoming squark and outgoing quark in its rest frame). In this case, since the chargino-neutralino-W coupling is also in general chiral, correlations between the quark and the outgoing $W^{\pm}$ are present. The situation is a little more subtle than that since the contributions from a cascade

initiated by an up-type partner cancel those initiated by a anti-down-type partner. However, due to the initial asymmetry between up quarks and anti-down quarks in the incoming PDFs the signal is not washed out. This decay exhibits a linear dependence on the variable $t_{qW} = (p_q + p_W)^2$.

The corresponding distribution for the Same Spin scenario is very different. In the rest frame of the W' both the incoming q' and the outgoing q are boosted and are mostly left-handed or mostly right handed. Hence the W' is longitudinally polarized. As a result, this decay exhibits a quadratic dependence on t_{qW} with a positive coefficient.

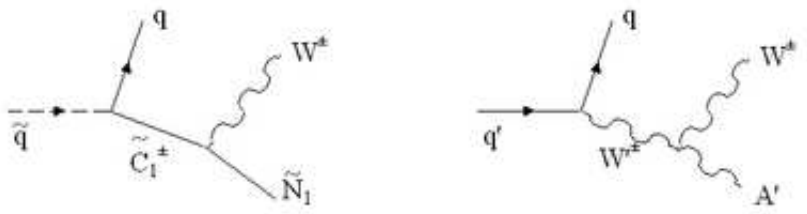

Figure 3.5: The weak cascade decay of a quark partner through the non-Abelian vertex in supersymmetry (left) and Same-Spin theories (right).

We will present a detailed study of this channel in Section 4. At this point, we just remark that this is a more generic channel comparing with the channel requiring on-shell lepton partner in the decay chain. In fact, the existence this decay channel is based on a very minimal set of assumptions about the spectrum, in which only a heavy quark partner, a charged gauge boson partner and a LSNP are present. If the spectrum does not even allow for this decay chain, we will not be able to extract any information from weak decays. This appears to be the most promising channel.

3.4 Weak Decay with qZ final state

There is a similar channel with a neutralino as the intermediate particle and a Z^0 in the final state (due to the higgsino-higgsino-Z^0 coupling). This could be a potentially golden channel considering the leptonic decay of the Z^0. Unfortunately, there are no angular correlations since the $\bar{\tilde{N}}_i \gamma_\mu P_\lambda \tilde{N}_j Z^\mu$ vertex is not even partially chiral. The Same-Spin counterpart is slightly ambiguous. If the intermediate particle is a heavy scalar partner of the higgs, there are no correlations. However, if the intermediate particle is some heavy Z' this might be the easiest channel to discover. As this is not a very generic case we will not pursue it any further.

There is an additional complication concerning this process. When the Z^0 decays into quarks, this process is experimentally indistinguishable from the previous one we consider involving a $W^\pm$. However, in most models it is suppressed by a factor of $10 - 50$ with respect to the chargino channel owing to the higgsino origin of the coupling. Therefore it does not present a serious background to it.

3.5 Weak Decay with qh final state

The neutralino could also decay into a Higgs and LSP. This is shown in Fig.(3.6). In the supersymmetric case this process is possible because of mixing with the higgsino. Unfortunately, the $h\bar{\tilde{N}}_1\tilde{N}_2$ vertex is not chiral and no correlation exists between the quark and higgs directions.

In the Same-Spin scenario this process is realized through the higgs coupling to the heavy gauge-bosons $g'vZ'_\mu A'^\mu h$. In this case, a correlation between the higgs and

outgoing quark exists and follow the same as those for a massive gauge-boson decay into two bosons (the amplitude has a quadratic dependence on the variable t_{qh} with a positive coefficient).

This channel is quite generic and it is important to investigate it further. In certain cases, it might be possible to replace the outgoing quark with an outgoing lepton (for example heavy slepton production as discussed below in subsection 3.8). In a sense this is an orthogonal channel to that considered by Barr [16] as it relies on the existence of heavy leptonic partners rather than light ones.

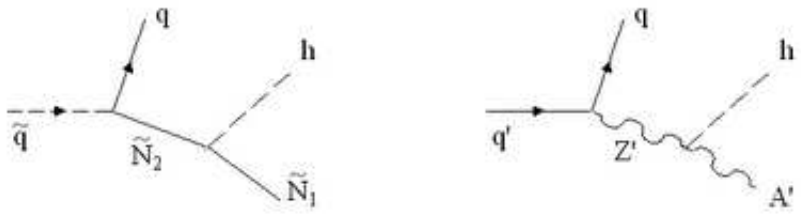

Figure 3.6: The weak cascade decay of a quark partner through a heavy neutralino into a higgs and LSP, in supersymmetry (left) and Same-Spin theories (right).

3.6 Decay of Gluon partner

In this section, we discuss the decay of the gluon partner into a quark and the quark partner. The quark partner subsequently decays into another quark and missing energy. This is shown in Fig.(3.7). This would certainly be the dominant channel of producing new physics particles if gluon partners are present in the spectrum. This diagram might prove to be the dominant decay mode into missing energy. Unfortunately, neither SUSY nor its Same-Spin counterpart have any spin effects

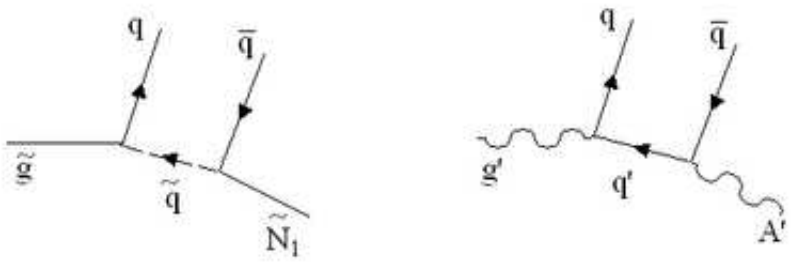

Figure 3.7: The cascade decay of the gluon partner in supersymmetry (left) and Same-Spin theories (right).

present. The supersymmetric diagram certainly does not involve any correlations between the two outgoing jets owing to the scalar nature of the intermediate squark. In contrast the Same-Spin quark is indeed a fermion, however, its coupling to the gluon partner is vector like. Therefore, it is unpolarized and its subsequent decay is isotropic. In the present work we will not consider this channel any further, leaving a detailed study to a future publication.

If the spectrum is such that the gluon partner must decay into the LNSP via an off-shell quark the situation is quite different. We discuss this issue further in subsection 3.9.

3.7 Strong Decay of Quark Partner

Next we consider the strong decay of a quark partner. This scenario is slightly specialized as it relies on the existence of a squark heavier than the gluino, but it is still generic enough to warrant consideration. The relevant diagram is shown in Fig.(3.8). If such a quark partner indeed exist this will be its dominant decay mode.

The supersymmetric case still has no angular correlations between the outgoing jets

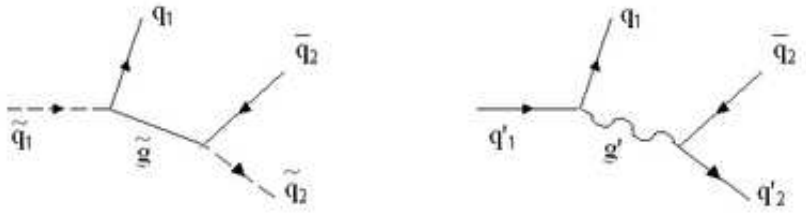

Figure 3.8: The strong cascade decay of a heavy quark partner in supersymmetry (left) and Same-Spin theories (right).

owing to our experimental limitations. As discussed above, the Majorana nature of the gluino makes it possible to observe correlations without having chiral vertices. There are two diagrams, one with a mass insertion and the other without. The former involves two outgoing quarks and the latter a quark and an antiquark. Unfortunately, all that we observe in the lab are two jets and must average over the two contributions. Therefore the decay should have no dependence on the variable $t_{q_1 q_2} = (p_{q_1} + p_{q_2})^2$.

The Same-Spin case, however, does posses angular correlations between the outgoing jets and is distinguishable from the supersymmetric one. As discussed above, the Same-Spin gluon is longitudinally polarized and we expect the decay to be a quadratic function of the variable $t_{q_1 q_2}$. The biggest challenge such a measurement faces is the signficant background due to Standard Model processes. This may not be an insurmountable impasse. The subsequent decay of q' together with hard cuts on missing energy might reduce the background dramatically. This is an important enough channel with a clear enough signature (if isolated) to warrant further study which we hope to address in a future publication.

Notice that the second stage of the decay chain could involve third generation

quarks and squarks. In this case, since we might recover some charge information, this decay can be useful to determine the spin of the gluino. It is not uncommon that the third generation squarks are lighter than the first two generation squarks. In particular, RGE running and a large third generation Yukawa coupling usually results in a lighter third generation squarks. Therefore, if $m_{\tilde{q}_3} \geq M_{\tilde{g}}$ or just slightly lighter, and $m_{\tilde{q}_{1,2}} > m_{\tilde{q}_3}$ there could be a significant enhancement of branching ratio into third generation quark and quark partners. Even in the Same Spin scenario, decaying into third generation quark and quark partner could help reduce the combinatorial background.

As mentioned above, in the case of left-right asymmetric spectrum, the two vertexes are effectively chiral and that will effect the angular correlations.

3.8 Decay from leptonic initial states

Many of the channels discussed above, involved the weak decay of a quark partner. If lepton partners are heavy enough, all such channels can be initiated by a lepton partner decay instead. The angular correlations are the same, only we replace an outgoing jet with an outgoing lepton. Such a scenario can be realized through the Drell-Yan production of heavy lepton partners.

Such a cascade has several advantages. First, jet combinatorics is not a problem. Second, we gain a lot more information because charge and flavor is now available to us. This is extremely helpful. For example, in the weak decay with $l, W^{\pm}$ final state, there is only one channel to consider and no averaging is needed.

On the other hand, a lepton partner at the beginning of a cascade is harder to

come by. It could come from the decay of heavy electroweak gauge boson partner, or a Z' coupled to leptons. But, that is more model dependent. We also require there to be several states below the lepton partner. This could sometimes require special arrangements. For example, in the MSSM, we would require a mass hierarchy such as $M_2 > m_{\tilde{\ell}} > M_1 > \mu$. This avenue looks promising in certain regions of parameter space.

3.9 Off-shell decays

So far, we have only considered on-shell decay processes. We saw that if the intermediate particle is a Dirac fermion the interactions involved must be at least partially chiral. This conclusion is modified if that particle is off-shell. Although on-shell decays usually dominate, there are special kinematical regions where we are forced to have off-shell decays. For example:

1. If the quark partner is heavier than the gluon partner, gluon partner will be forced to decay through an off-shell quark partner.

2. The decay of a gauge boson partner to LNSP will be forced to go through an off-shell W/Z and lepton/quark partners if the mass splitting is small. The virtual lepton-partner and virtual quark channels could be particularly interesting since it brings in new spin information about the lepton partner. It could be important over a large mass range of the lepton partner since the decay to off-shell W/Z is usually suppressed by mixing.

To illustrate this point we consider the first example where the gluon partner decays through an off-shell quark partner. The relevant diagrams are shown in Fig.(3.7). The SUSY channel obviously has no correlations since the squark is a scalar. However, in the Same-Spin scenario correlations are present. The amplitude for this process is

$$\sum_{\text{pol}} |\mathcal{M}|^2 \propto 2\frac{(m_{q'}^2 - q^2)(q^2 - 2m_{g'}^2)(q^2 - 2m_{A'}^2)}{m_{g'}^2 m_{A'}^2}\, t_{q\bar{q}} + f_0(q^2), \tag{3.3}$$

where we neglected the trivial denominator. $f_0(q^2)$ is some complicated function of q^2, the momentum of the internal quark partner, and the masses. It is irrelevant for this discussion. Notice that when the quark partner is off-shell $q^2 \neq m_{q'}^2$ and the coefficient of $t_{q\bar{q}} = (p_q + p_{\bar{q}})^2$ is non-zero. This linear dependence of the cross-section on $t_{q\bar{q}}$ can in principle be distinguished from the SUSY case where there is no dependence on $t_{q\bar{q}}$. Further study is needed to explore the observability of this effect in different models.

Similar considerations apply for the other case of a gauge-boson partner decay to LNSP via an off-shell slepton.

4

Determining Spin without Leptonic Partners

In this section we will explore the decay of a quark partner into a charged weak partner which consequently decays into a $W^{\pm}$ and missing energy. Let's begin with the supersymmetric case. The squark-quark-chargino vertex is given by [26] (we are ignoring the CKM and super-CKM matrices as they are quite irrelevant to the following discussion),

$$\mathcal{L}_{q\tilde{q}\tilde{C}^{+}} = -g_2 \left(\bar{u} P_R (U_{11}\tilde{C}_1 + U_{21}\tilde{C}_2)\tilde{d} + \bar{d} P_R (V_{11}\tilde{C}_1^c + V_{21}\tilde{C}_2^c)\tilde{u} \right) \tag{4.1}$$

where U_{ij}, V_{ij} are the matrices diagonalizing the Chargino's' mass matrix. We are assuming that the chargino is dominantly a gaugino and ignore the direct quark-squark-higgsino couplings. The more important vertex is the chargino-W^{+}-neutralino coupling,

$$\mathcal{L}_{W^{-}\tilde{C}\tilde{N}} = g_2 W_{\mu}^{-} \bar{\tilde{N}}_i \gamma^{\mu} \left(O_{ij}^{L} P_L + O_{ij}^{R} P_R \right) \tilde{C}_j \tag{4.2}$$

where,

$$\begin{aligned} O^L_{ij} &= -\frac{1}{\sqrt{2}} N_{i4} V^*_{j2} + N_{i2} V^*_{j1} \\ O^R_{ij} &= \frac{1}{\sqrt{2}} N^*_{i3} U_{j2} + N^*_{i2} U_{j1} \end{aligned} \tag{4.3}$$

and N_{ij} are the mixing matrices for the Neutralino. This interaction is usually at least partially chiral (when $tan\beta \neq 1$. Therefore we expect the amplitude to have some $t_{qW} = (p_q + p_W)^2$ dependence, with a coefficient given by the difference of the couplings in equation (4.3). Indeed, in the narrow width approximation $q^2 \to m^2_{\tilde{C}}$ we get,

$$|\mathcal{M}|^2 \propto \frac{1}{2} \left(\frac{m^2_{\tilde{C}}(m^2_{\tilde{C}} - m^2_{\tilde{N}} - 2m^2_W)}{m^2_W} \right) \; (a^2_L - a^2_R) \; t_{qW} + f_0(q^2, m_i) \tag{4.4}$$

where $f_0(S, m_i)$ is a polynomial given in appendix A. The 3-body phase-space differential volume can be written in terms of q^2 and t_{qW} (see for example [15]),

$$dPS_3 = \frac{1}{128\pi^3 m^2_1} dq^2 dt_{qW} \tag{4.5}$$

with appropriate kinematic boundaries. In the narrow-width approximation the integration over q^2 is trivial and simply removes the denominator in equation (4.4) and replaces $q^2 \to m^2_{\tilde{C}}$. Therefore, the angular correlations in this decay depend on the difference $(a^2_L - a^2_R)$.

In Fig.(4.1) we plot the ratio a^2_R/a^2_L as a function of $\tan\beta$ for a few values of μ-parameter with $M_1 = 100$ GeV and $M_2 = 500$ GeV. This ratio is quite different than unity for most choices of the parameters.

There is one additional complication in the SUSY case. As seen from equation (4.1) there are two contributions to any process involving the chargino. One comes from the coupling to the up squark, while the other comes from the coupling to the

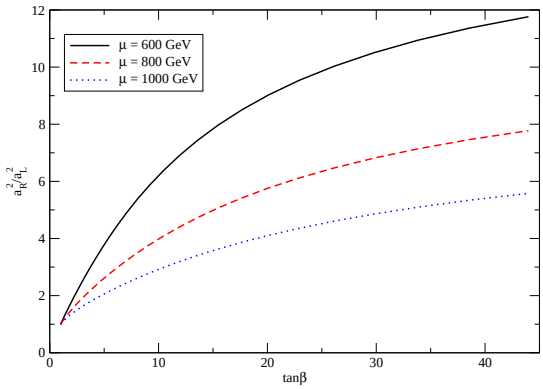

Figure 4.1: The ratio of the right to left couplings a_R^2/a_L^2 as a function of $\tan\beta$ for three different values of the μ-parameter. $M_1 = 100$ GeV and $M_2 = 500$ GeV are fixed.

anti-down squark. Therefore, as shown in details in appendix A these two contributions differ by the sign of the coefficient of t_{qW}. Since we cannot distinguish between a jet coming from a down quark and that coming from an anti-up quark, we must average over the two contributions. Fortunately, due to the composition of the proton there are more up-like squarks produced than down-like squarks. Their ratio in production is shown in Fig.(4.2) as a function of their mass and gluino mass.

Let us contrast this with the corresponding process in Same-Spin theories. The intermediate particle is a spin-1 Same-Spin $W^{\pm}$. As we argued before in equation (3.2) it is dominated by the longitudinal mode. Therefore its subsequent decay is dominated by the angular distribution of the second equation in (2.5). Therefore the W^+ boson is preferentially collinear or anti-collinear with the jet. We expect $a_2(t_{qW})^2 + a_1 t_{qW} + a_0$ dependence with $a_2 > 0$ and $a_1 \leq 0$. The computation is quite

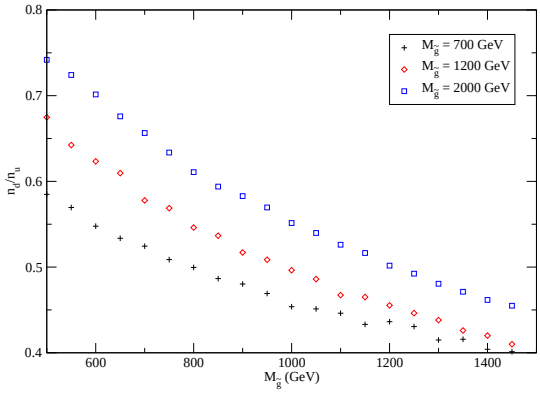

Figure 4.2: The ratio of down squarks to up squarks in production as a function of their mass for different gluino masses, $m_{\tilde{g}} = 700,\ 1200,\ 2000$ GeV (black-solid, red-dashed, green-points).

involved, but the final expression is indeed,

$$|\mathcal{M}|^2 = \frac{1}{(q^2 - M^2)^2}\left(F_0(q^2, m_i) + F_1(q^2, m_i)t_{qW} + F_2(q^2, m_i)(t_{qW})^2\right) \tag{4.6}$$

where the F_i's are given in appendix A. It is not hard to show that $F_2(M^2, m_i) > 0$ and $F_1(M^2, m_i) < 0$. The shape of the resulting cross-section is plotted in Fig.(4.3) against the corresponding SUSY cross-section. The behavior for small t_{qW} is distinctly different than the supersymmetric case. The reason is clear. Small values of t_{qW} corresponds to W^+ being collinear with the jet, which is forbidden in the supersymmetric process, but preferred in the Same-Spin case. We have also included in Fig.(4.3) the results of the Monte-Carlo simulation.

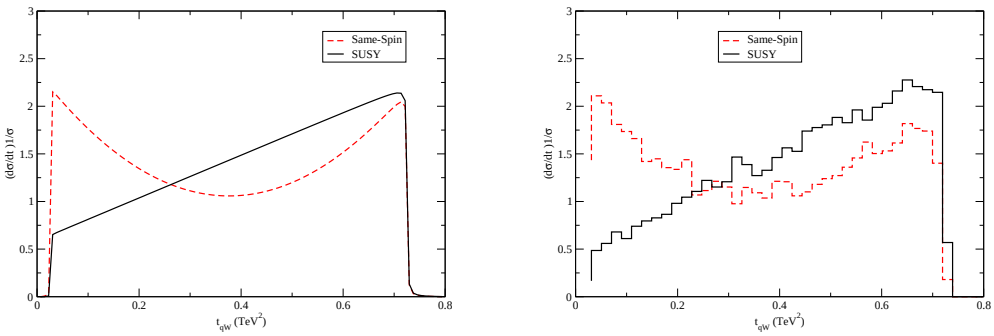

Figure 4.3: Theoretical curves (Left graph) for the q-W correlations in the two models (solid,black - SUSY, dashed,red - Same-Spin). Cross-section is plotted against the t_{ql} variable. The right plot shows the Monte-Carlo simulation. Both graphs are normalized to unit area.

5

Experimental Observables

We must take into account the fact that W^+ cannot be observed directly and only its decay products can be measured. If it decays into quarks and it is possible to distinguish these two jets from the rest by reconstructing the W^+ (as it is on-shell) the signal might still be very strong. We include standard cuts to reduce Standard Model background. We also consider the contribution from other new physics processes with identical final states. We argue that this signal is still a strong candidate for spin determination[1]. There is also the possibility of a semi-leptonic decay with the W decaying into a lepton and the corresponding neutrino.

5.1 Lepton-jet correlation

In this subsection, we concentrate on the semi-leptonic decay of the $W^{\pm}$. The main challenge we face is that we cannot reconstruct the W^+ as the neutrino is unob-

[1]A detailed study of Standard Model background with sophisticated jet analysis is beyond the scope of this paper. We will begin to address this issue in future publications.

servable. To investigate the resulting signal we used the Monte-Carlo event generator HERWIG [32]. We implemented spin-correlations for massive spin-1 particles and the details can be found in appendix B. For the Same-Spin production matrix elements we used the ones quoted in [73] [2]

We expect much of the difference to be washed out once the W^+ is allowed to decay into leptons. The only observables we are left with are the momenta of the outgoing jet and that of the lepton. Therefore, we will plot the cross-section as a function of the invariant mass $t_{ql} = (p_q + p_l)^2$. Fig.(5.1) shows the Monte-Carlo simulation results when the lepton is correlated with the jet from it own branch. In practice we have no why to tell which jet came from which branch and we amend this below.

While the behavior is indistinguishable at high t_{ql}, it is certainly very different at low t_{ql}. We can attribute this to the fact that in the SUSY model, the W^+ is very unlikely to be collinear with the jet, whereas the opposite is true for the Same-Spin model.

This plot suggests that the two models are still distinguishable from one another even if the W cannot be fully reconstructed. When taking into account the jet combinatorics by pairing the lepton with both jets in the event the results do alter. In Fig.(5.2) we plot the cross-section against t_{ql} for events with two jets and one or two leptons (the two-leptons case corresponds to both branches decaying into a lepton).

[2] Except for the matrix element $\mathcal{M}(qq \to q_1^* q_1^*)$ which was taken from [62] since the one quoted in [73] seemed to give production rates which are too large. Strictly speaking, those are inappropriate for the model we consider (as they assume degenerate spectrum and only one mass scale, namely $1/R$, the compactification radius). However, nothing in our discussion seems to relay heavily on the precise production cross-section and we do not expect any major modification to the conclusions below. To simplify the analysis we switched off cluster formation, heavy hadron decays and the underlying soft event.

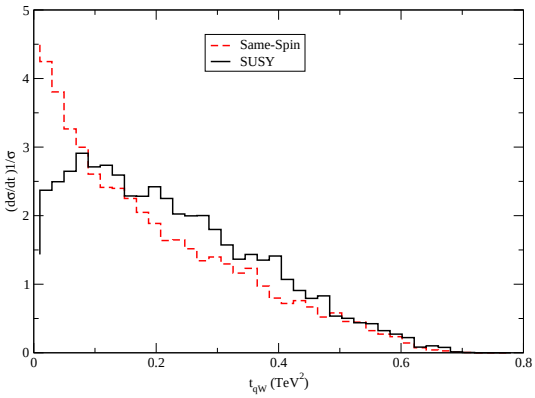

Figure 5.1: Monte-Carlo simulation for the quark-lepton correlations in the two models (solid,black - SUSY, dashed,red - Same-Spin). Normalized cross-section is plotted against the t_{ql} variable. The data sets contain $\sim 13,000$ events each.

The single lepton diagram still exhibits the flattening of the cross-section in the SUSY case for low t_{ql}. This is in contrast with the rising cross-section for the Same-Spin model. It is possible that close analysis of low t_{ql} can pick up this difference once real data is available. There is no obviously observable spin dependence in the second case with two leptons in the final state.

5.2 Jet-W correlation

In this subsection we take up the second possibility, namely that the $W^{\pm}$ decays into two jets. The advantage is the ability of fully reconstructing the four momenta of the $W^{\pm}$'s. There are disadvantages as well. First and foremost, very naively the Standard Model background is significant. Second, since jets are involved, momentum determination involves some amount of smearing. This would affect the reconstruc-

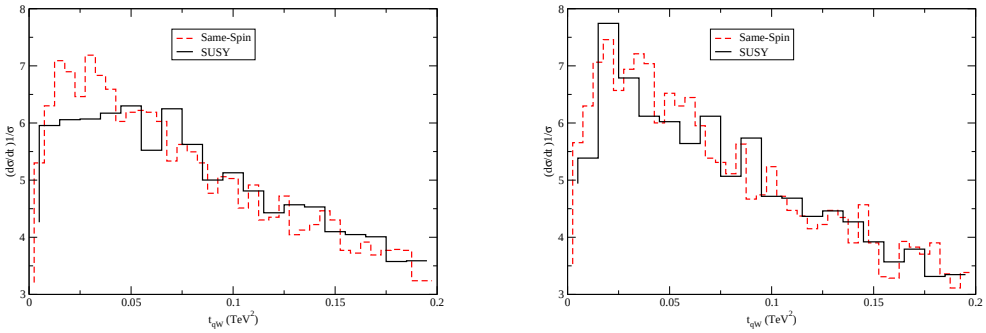

Figure 5.2: Monte-Carlo simulation for the jet-lepton correlations in the two models (solid,black - SUSY, dashed,red - Same-Spin) with no knowledge of the correct pairing. Normalized cross-section is plotted against the t_{ql} variable. The graph on the left is for 2 jets and 1 lepton events. The graph on the right corresponds to 2 jets 2 opposite sign leptons events. The data sets contain $\sim$ 17,000 events with 1 lepton and $\sim$ 9,000 events with 2 leptons for each of the models.

tion of $W^{\pm}$ as well as the angular correlations. Third, it is very hard to distinguish between a $W^{\pm}$ and a Z^0 and so when investigating background we must consider both. We do not attempt a full Standard Model background analysis, however, there are several reasons why it might be possible to reduce such a background. First, hard cuts on missing energy can yield a fairly clean sample of beyond the standard model physics. Second, we can easily have additional leptons in the process we consider. Simply let the quark partner in the other branch (shown in Fig. (5.4)) to decay into a Z' or W'. It is not hard to imagine other possible channels for producing leptons in the final state. The problem of background reduction is beyond the scope of this paper and we will assume that some non-negligible set of events, containing new physics, can be isolated and analyzed.

We consider 4-jet events with a typical event topology shown in Fig.(5.4) together

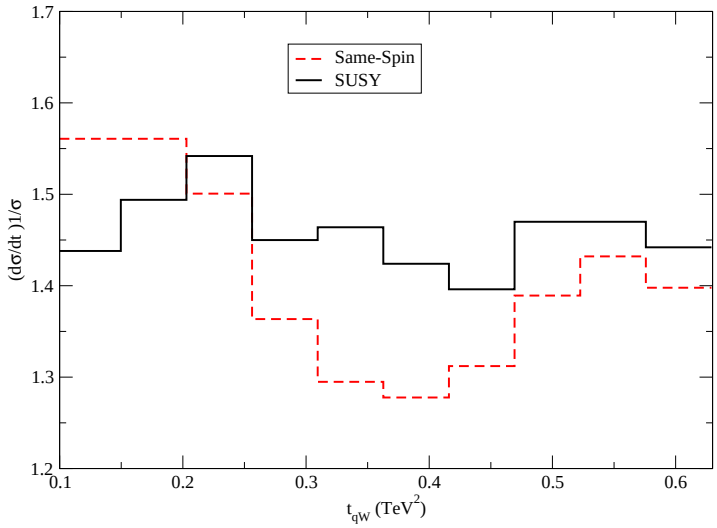

Figure 5.3: Considering only 4-jet events this is a histogram of the invariant mass $t_{W,jl}$ for each of the models: SUSY (solid-black), Same-Spin (dashed-red). The histogram is normalized to unit area. The two data sets contained $\sim 9,000$ and $2,000$ events, respectively. The normalized error is approximately $\sqrt{N} \sim 0.04$.

with a possible background from another new physics process. In every event we try to reconstruct the $W^{\pm}$ from two of the 4 jets and then form the invariant mass t_{qW} with the two remaining jets. If more than one pairing reconstructs W it is regarded as failure and the event is discarded. Our cuts involve $\not{P}_T > 200$ GeV and $\eta < 4.0$. We make no attempt in trying to order the jets by the magnitude of their transverse momentum or some more sophisticated ordering (This very naive approach yields a significant difference between the two models as shown in Fig.(5.3)). There can certainly be potential improvements on this measurement by using more kinematical information of the jets. The linear behavior vs. the the quadratic behavior is still visible on top of the background coming from the wrong pairing.

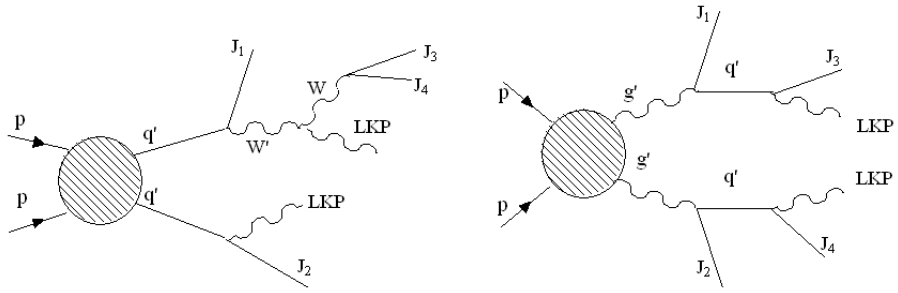

Figure 5.4: 4-jet event topology for the Same-Spin theory. The diagram we are interested in (left) together with a possible Same-Spin irreducible background (right)

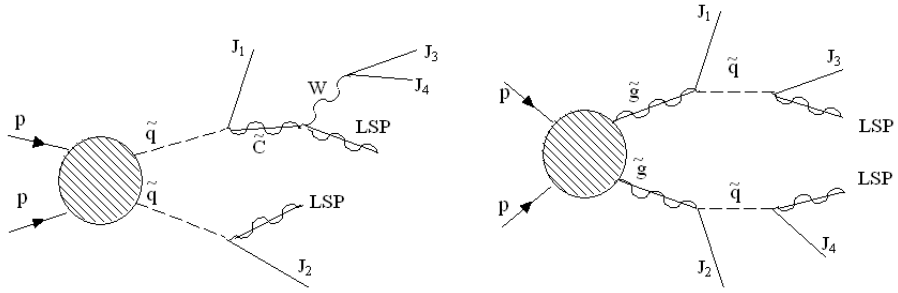

Figure 5.5: 4-jet event topology for SUSY. The diagram we are interested in (left) together with a possible SUSY irreducible background (right)

There could also be background from different processes in the same model of new physics with identical final states. One such channel is shown on the right in Fig. (5.4) for Same-Spin theory and Fig. (5.5) for the SUSY case. We consider all events with 4-jets. Then we construct the invariant mass $m^2_{j_k,j_l} = (p_k + p_l)^2$ for every possible pair. We use HERWIG internal algorithm for jet formation. We include jet smearing effects [47] using the ATLAS specs [1]. The results are shown in Fig.(5.6). It is clear the background from the model itself is not an issue and the reconstruction of the W should be fairly easy. This should come as no surprise. With a random pairing of

such energetic jets, the chance of reconstructing a quantity with < 100 GeV is fairly low. This can probably be made even sharper with some simple cuts on jet energy. For example, the initial jets from the squark decay tend to be more energetic than those coming from the W.

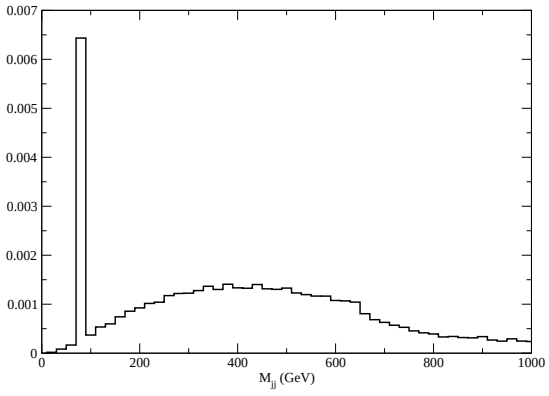

Figure 5.6: Considering only 4-jet events we plot a histogram of the invariant mass $m^2_{j_k,j_l} = (p_k + p_l)^2$ of all possible pairs of jets. The graph is normalized to unit area.

5.3 Scanning M_1 and M_2

It is important to map out the regions of parameter space in which the different channels are useful. In this section we present the results of a scan covering the subspace spanned by (M_1, M_2). We also set $m_{W'} = M_2$ and $m_{A'} = M_1$. While there are other parameters which effect the results (such as $\tan\beta$, $m_{\tilde{q}}$, μ, etc.) we focus on those two parameters, (M_1, M_2), which are the most determinantal to the observability of angular correlations for the channel we consider.

When performing such a scan, we wish to assign a number to quantify the dif-

ference between, say, the distribution describing the SUSY scenario and that of the Same-Spin scenario. There is no unique choice for such a number. Moreover, such an assignment can be problematic as it can overlook differences that a more careful analysis would pick up. Therefore, the results of this section should be understood with the following proviso in mind: the numbers assigned for the different points in parameter space carry only relative importance among themselves and have very little absolute meaning. They indicate that in certain regions spin determination is easier as compared with other regions.

There is one more point to keep in mind. We will compare the distributions produced for the two models by matching their spectrum. This is incorrect. One should match the cross-section first as that is the actual experimental observable. Unfortunately, we had poor control over the production rates for the Same-Spin scenario[3] However, this is not entirely misleading. As part of our results we will consider the observability of each of the models against phase-space. Therefore, if nothing else, we are able to tell when spin effects are present at all.

To quantify the difference between the distributions we use the Kolmogorov-Smirnov test for goodness-of-fit. In this test, the cumulative distribution functions (CDF) of both data sets are compared. The D-statistics is simply the maximum vertical difference between the CDF's. In other words,

$$D = sup\,|F_1(x) - F_2(x)| \tag{5.1}$$

where $F_1(x)$ and $F_2(x)$ are the CDF's for the two data sets. The p-value assigned to the D-statistics is low when the two data sets come from different underlying distri-

[3]The production cross-sections given in [73] for the Same-Spin theory have only one adjustable parameter, namely the inverse compactification radius.

butions. There are several advantages to the Kolmogorov-Smirnov test. First, it is a non-parametric test so it applies to general distributions. Second, it is independent of the way we choose to histogram the data.

In Fig. (5.7) we plot the p-value as a function of M_2 for three different values of M_1. The quark partner mass is $m_{\tilde{q},q'} = 1000$ GeV, the gluon partner mass is $m_{\tilde{g},g'} = 1200$ GeV. We set $\tan\beta = 10$ in the supersymmetric case. For every value of the parameters we produced $100,000$ events out of which only about 10% passed the different cuts.

The scan matches our expectations. When $M_2 \to M_1$ the LSP and the W are produced at rest and there the correlations with the polarization axis defined by the quark partner are diminished. Also, when $M_2 \to m_{\tilde{q},q'}$ it becomes harder to distinguish the two data sets. This is also expected because in the Same-Spin case the quark partner, q', is not at all boosted in the rest frame of the W'. Therefore, W' is not polarized.

The results are encouraging. While a more sophisticated analysis (better cuts, better fitting, more realistic collider simulation, etc.) is certainly warranted, these initial results seem to indicate that spin determination is possible. As pointed out before, one should not confine the analysis to special benchmark points, but rather attempt a scan over the parameter space. In this way, an inclusive strategy, combining several channels, can be devised to cover different exclusive regions of the parameter space.

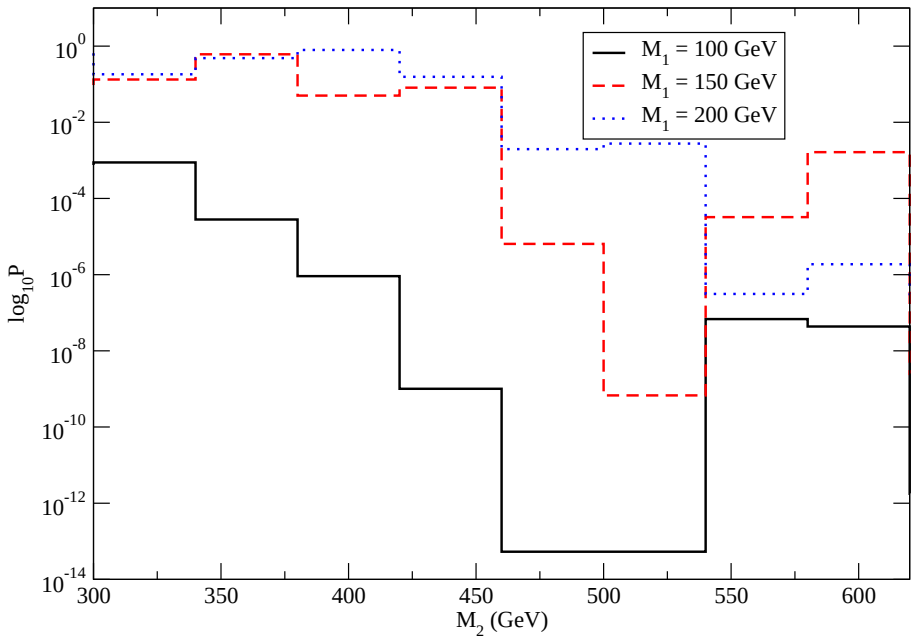

Figure 5.7: A plot of the p-value vs M_2 for different values of M_1. We set $m_{W'} = M_2$ and $m_{A'} = M_1$. The p-value is lower when the two data sets are more distinguishable. The other parameters were fixed at $m_{\tilde{q},q'} = 1000$ GeV,$m_{\tilde{g},g'} = 1200$ GeV. We set $\tan\beta = 10$ in the supersymmetric case. Both data sets contained $\sim 10,000$ events. Notice that when the mass splitting between M_1 and M_2 is small, i.e. the left-hand side of the plot, it is harder to distinguish these two scenarios. Supersymmetry and Same-Spin scenario become more distinguishable as the mass splitting increases. However, as M_2 approaches $m_{\tilde{q},q'}$ the difference is again diminished.

6

Conclusions and Future Directions

We have systematically studied the possibility of measuring the spin of new particles in a variety of cascade decays. Generally, the existence of a LNSP renders the reconstruction of the momenta of new physics particles impossible. Therefore, we focused on distributions of relativistically invariant variables. We identified a set of decay channels which are useful for spin determination.

A general lesson of this study is that even though spin correlations are present in a variety of decay channels, the viability of any particular channel is always confined to certain kinematical regions. As a result, different models of new physics with different spectra tend to give very different useful channels for spin determination. Different strategies will have to be employed at the LHC. Therefore, we emphasize that it is important not to confine ourselves to any particular benchmark model or any particular decay mode. We should instead explore the effective range of all possible decay channels and devise techniques for using them efficiently. In this sense, our survey of potentially useful decay channels is the initial step of an important task for

which many detailed studies still need to be done.

As part of this program we studied the decay channel $\tilde{q} \to q + \tilde{C}^{\pm} \to q + W^{\pm} + LSP$. A scan over the chargino and neutralino masses was performed. We found that as long as the spectrum is not too degenerate the prospects for spin determination are rather good.

One of the most important challenges is to measure the spin of gluon partners. The difficulty in such a study is that the decay products carrying the spin information of the gluon partner are usually jets, missing the charge information. In addition, such channels usually have larger combinatorial background and Standard Model background. A similarly challenging task is a direct measurement of the spin of the quark partner.

We have considered only kinematical variables constructed out of two objects of the decay products. It is in principle interesting to study the possibility of using more complicated kinematical variables.

Notice that decay channels involving leptons are generally more promising than those involving only jets. This result stems from the fact that we have charge and flavor information from the lepton, which could help us in separating the channels. We have assumed no such information from jets. Therefore, we have limited information from channels decaying into quarks, except for the third generation. Moreover, losing charge and flavor information from the jet significantly increases the combinatorial background, since typical new physics signals for the scenarios considered in this paper almost always contain several hard jets. Therefore, any potential information about the charge and flavor of the initial parton of the jet will be very helpful in spin

determination.

We would like to remark that reducing combinatorial background is very important in extracting more information about the underlaying new physics. This lead the authors of [12] to conclude that to what extent jet charge could be measured is an important study for LHC experiments.

We have not studied the possibility of measuring spin in the production. This is certainly a very important area to be investigated carefully. Barr [17] has studied the measurement of the spin of muon partners using angular distribution from pair production. In principle, angular distributions of production of other partners should carry similar information. This is a subject currently under investigation. One of the main complications is the existence of t-channel productions. Such production channels bring in more partial-waves and tend to wash out characteristic angular distributions.

We would also like to emphasize that although we have only compared SUSY with the Same-spin scenario, the general rules we have developed in the paper are easily applicable to any generic scenario with different spin content of new physics particles.

Part II:

An Example of a Model for Beyond the Standard Model physics

7

Introduction

The little Higgs mechanism [10, 11, 7, 8, 44, 61, 53, 72] offers a fascinating way to stabilize the electroweak scale. Like the Georgi-Kaplan composite Higgs [51, 52, 38, 39, 37], the little Higgs is naturally light because it is a pseudo-Goldstone boson of a spontaneously broken approximate global symmetry. What is novel about the little Higgs mechanism is that it implements collective breaking. That is, the interactions of the theory are arranged such that turning on any one interaction preserves enough of the global symmetry to protect the Higgs mass. Therefore, quadratic divergences to the Higgs mass can only appear at mutliloop order, and generically the Higgs boson is two loop-factors lighter than the scale of spontaneous symmetry breaking. In principle, this allows us to push the cutoff of the standard model as high as 10 TeV without fine-tuning the Higgs mass. In addition, specific little Higgs models, such as models with a custodial $SU(2)$ symmetry [20, 19] and models which implement T-parity [22, 23, 60], automatically satisfy precision electroweak constraints [48, 33, 34, 43, 55, 21, 78]. Therefore, it is reasonable to say that the little Higgs mechanism is a

fully realistic theory for perturbative physics up to 10 TeV.

Despite the phenomenological successes of little Higgs mechanism, there are questions that one might be interested in answering that cannot be unambiguously calculated in a theory with a 10 TeV cutoff. In particular, four-fermion operators that generate flavor-changing neutral currents (FCNCs) generically require a cutoff of $\Lambda \sim 1000$ TeV, so in a theory with a 10 TeV cutoff, we have no natural way of explaining why FCNCs are so suppressed. Also, in the original little Higgs papers, the Higgs potential is governed by operators with quadratically sensitive couplings, and estimates of these couplings were generated using the Coleman-Weinberg potential [27] and naïve dimensional analysis [64, 40]. While we have no *a priori* reason for not trusting these estimates, there are always $\mathcal{O}(1)$ effects (including sign ambiguities) accompanying UV sensitive physics. For these reasons, we wish to present a possible UV completion of the little Higgs mechanism in which the UV sensitive physics is finite and calculable.

Here, we will focus on the simplest little Higgs model, the littlest Higgs [7]. The littlest Higgs is based on an $SU(5)/SO(5)$ non-linear sigma model, and there are two obvious UV completions one might explore. The most naïve UV completion is a linear sigma model with a Mexican-hat potential, but such a theory cannot address the hierarchy problem because the mass of the linear sigma field is quadratically sensitive to the Planck scale. Alternatively, the $SU(5) \to SO(5)$ symmetry breaking pattern could be generated by technicolor-like strong dynamics. This is the path taken in [54] based on an $SO(7)$ confining gauge group, and the $SU(5)/SO(5)$ non-linear sigma model arises analogously to the pions of QCD.

Another type of strong dynamics is suggested by the AdS/CFT correspondence [63, 46, 77] and its phenomenological interpretation [13, 70]. As noted in [30], the Higgs can emerge as a composite state of a strongly coupled 4D quasi-conformal field theory, and while the details of the strong dynamics are difficult to calculate, UV sensitive parameters such as the Higgs potential can be determined in the weakly coupled AdS dual of the quasi-CFT. In all composite Higgs models, some separation between the confinement scale and the electroweak scale is necessary in order to satisfy precision electroweak constraints. Recently, the Higgs as a holographic pseudo-Goldstone boson has been incorporated into a realistic model [2] where this separation is achieved by a mild fine-tuning between radiative contributions in the fermion sector. In the littlest Higgs, the Higgs quartic coupling is naturally large and parametrically of order the standard model gauge coupling, so it is particularly interesting to study the composite littlest Higgs in the context of AdS/CFT. We can imagine a quasi-CFT with an $SU(5)$ global symmetry spontaneously broken to $SO(5)$ at the scale of conformal symmetry breaking, and the $SU(5)/SO(5)$ non-linear sigma model will naturally emerge as composites of the strong dynamics.

In this part of the thesis, we construct a simple AdS_5 model [69, 68] that includes all the major features of the littlest Higgs. We consider a slice of AdS_5 space bounded by a UV brane and an IR brane. In AdS language, it is easy to see why the Higgs potential will be finite and calculable. The non-linear sigma field that contains the Higgs doublet lives on the IR brane, and all interactions on the IR brane respect the global symmetries that leave the Higgs massless. These global symmetries are only broken on the UV brane, so a quantum effective potential for the Higgs is generated

through loops that stretch from the IR brane to the UV brane. Because these loops are non-local in the bulk of AdS, they are manifestly finite.

Even more interesting is what collective breaking looks like in AdS language. In the original littlest Higgs model, the global $SU(5)$ symmetry that protects the Higgs mass is broken by gauging two subgroups of the $SU(5)$ in such a way that the Higgs is exactly massless unless both gauge couplings are non-zero. In our AdS model, two subgroups of the bulk $SU(5)$ gauge bosons are given different boundary conditions on the Planck brane, and collective breaking in AdS language is now a statement about collectively choosing these boundary conditions. Whereas the low-energy Coleman-Weinberg potential involved combinations of coupling constants, the full 5D Coleman-Weinberg potential involves differences of Greens functions in a way that makes collective breaking manifest.

Though the radiatively generated Higgs potential is parametrically of the right form to successfully trigger electroweak symmetry breaking, when we look at the model in numerical detail, we find an interesting tension that is already evident in the low energy phenomenology and which is exacerbated by the AdS construction. The littlest Higgs contains a top partner t' and electroweak gauge partners W' that cancel quadratic divergences coming from standard model fermion and gauge loops. The ratio of the t' mass to the W' mass is generically of order $4\lambda_{\rm top}/\sqrt{g_1^2+g_2^2}$, where $\lambda_{\rm top}$ is the top Yukawa coupling, g_i are $SU(2)_i$ gauge couplings, and the electroweak gauge coupling is determined by $g_{\rm EW} = g_1 g_2/\sqrt{g_1^2+g_2^2}$. For phenomenological reasons, we would like the t' and W' to be nearly degenerate, and therefore we would like to make $g_2 \gg g_1$. However, in a large N CFT, gauge couplings are infrared free, so we either

have to shrink the conformal window in order to enforce a large separation between g_1 and g_2, or we have to reckon with dangerously light W' gauge bosons.

In the limit where $g_1 = g_2$, we may be able to live with a light W' if the theory has T-parity, and in section (14), we work towards constructing a realistic AdS_5 model that implements T-parity. T-parity is a $\mathbf{Z}_2$ symmetry under which standard model fields are even but new fields at the TeV scale are odd. This symmetry forbids standard model dimension six operators from being generated by tree-level exchange of the new particles, so corrections to precision electroweak observables are generically suppressed by a loop factor. However, we will see a tension between implementing T-parity and trying to capitalize on the past successes of AdS_5 model building (see [3] for a summary). In particular, there is natural way to generate hierarchies among the Yukawa couplings by putting standard model fermions in the bulk of AdS space with different bulk masses [45, 41, 50, 49], and as an added bonus, this setup naturally leads to suppressed FCNCs. Unfortunately, the same mechanism that generates Yukawa hierarchies also leads to a hierarchy in the masses of T-odd fermion partners, and the lightest T-odd fermion is far lighter than the current experimental bound. This tension between precision electroweak constraints and FCNCs appears to be a problem for any AdS_5 model with T-parity. In this light, it may be interesting to look at the AdS implementation of little Higgs theories with a custodial $SU(2)$ symmetry, where the mechanism that protects precision electroweak corrections can coexist with the AdS mechanism of suppressing FCNCs.

Putting aside these detailed model building questions, the littlest Higgs in AdS space is a technically natural extension of the standard model that makes sense up to

the Planck scale (or some suitably high UV scale when $g_1 \neq g_2$). In CFT language, the hierarchy between the Planck scale and the electroweak scale is generated in two steps. First, the hierarchy between $M_{\rm Pl}$ and confinement scale is generated through dimensional transmutation. Second, the hierarchy between confinement scale and the electroweak scale is guaranteed by collective breaking. We expect it to be straightforward to generalize this AdS_5 construction to other little Higgs theories, allowing us to embed a class of phenomenologically successful models into a UV complete framework.

In the next section, we review the holographic description of spontaneous symmetry breaking and apply it to generic little Higgs theories. We present the littlest Higgs in AdS space in Section 9, and match this theory to the well-known low energy description in Section 10. We comment on the tensions between the low energy theory and a large N CFT description in Section 11. In Sections 12 and 13 we calculate the radiatively generated potential for the Higgs doublet and show that there is a wide range of parameters with realistic values for the Higgs mass. Finally, in Section 14 we sketch how to implement T-parity in AdS space, and conclude with a preview of future directions in little Higgs model building.

8

The Little Higgs Mechanism through AdS/CFT

The little Higgs mechanism is ideally suited for a holographic interpretation because the underlying physics involves symmetry breaking patterns and not the specific mechanism for symmetry breaking. The generalization of the AdS/CFT conjecture to AdS_5 with boundaries [13, 67] can only give us limited information about the structure of the CFTs dual to AdS models. Given an RS1-type model with a warped dimension [69], there is a corresponding 4D quasi-conformal field theory coupled to gravity and an elementary sector, and this quasi-CFT confines at the scale of the IR brane. But in any RS1-type model, we are ignorant about physics on the IR brane at energies near the IR scale because the KK gravitons are strongly coupled there. The dual description of 5D ignorance is 4D ignorance, so while the AdS/CFT correspondence can tell us a lot about the low-energy bound states of the dual CFT, we do not have an unambiguous understanding of physics near the confinement scale.

Our goal is to understand the UV sensitive parameters of the littlest Higgs model, and we can arrange the interactions of the theory such that the Higgs potential is insensitive to the details of physics near the confinement scale. In 5D language, this feature will be obvious, as the Higgs boson is physically separated in the warped dimension from the fields that radiatively generate the Higgs potential. In 4D language, the Higgs potential is generated through interactions between the quasi-CFT and the elementary sector and is therefore independent of the details of CFT dynamics.

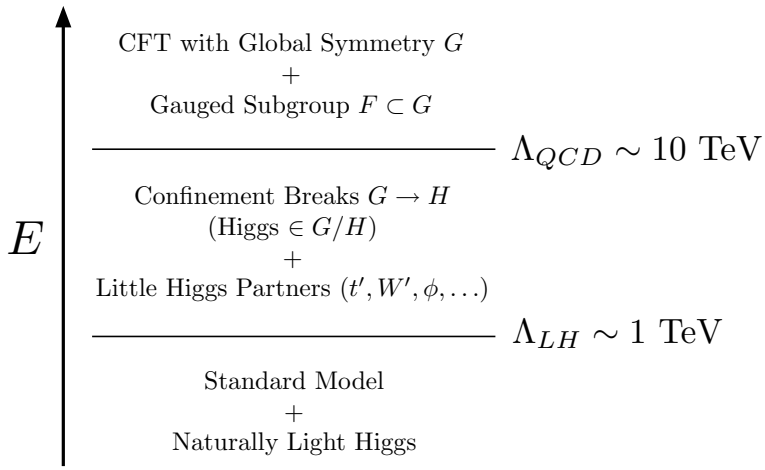

Figure 8.1: Schematic of a generic 4D little Higgs theory. The scale Λ_{LH} is the mass of the particles responsible for collective breaking and is roughly of order f_π, the pion decay constant of the CFT. The scale Λ_{QCD} is where we see any particles not directly involved in collective breaking, namely the ρ mesons of the CFT.

Ignoring the fermion sector, all little Higgs models involve a global symmetry G that is spontaneously broken to H at an energy $\Lambda \sim 10$ TeV. We will assume that the breaking $G \to H$ is triggered by QCD-like confinement, and the Goldstone bosons of G/H emerge as bound states of the strong dynamics, analogously to the pions of QCD. (See Figure 8.1.) A subgroup $F \subset G$ is gauged and contains two copies of

the electroweak gauge group $W_i = SU(2)_i \times U(1)_i$ for $i = 1, 2$, but H only contains the diagonal electroweak gauge group $W_1 + W_2$. (In the model we construct in the next section, we only introduce one copy of $U(1)_Y$, so $W_i = SU(2)_i$.) The Higgs sector is embedded in the pseudo-Goldstone bosons of G/H such that the Higgs field transforms as a (diagonal) electroweak doublet. To implement collective breaking, the structure of the symmetry groups is chosen such that the Higgs is an exact Goldstone boson if only one of the electroweak gauge groups is turned on.

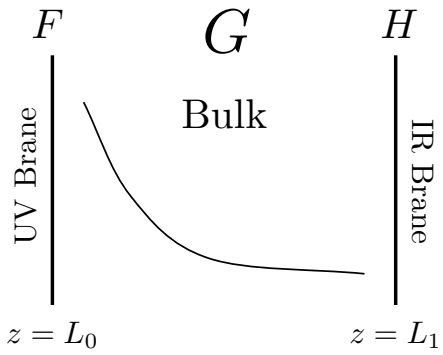

Figure 8.2: The gauge symmetries in AdS_5 for a generic little Higgs theory where there is a G/H non-linear sigma model at low energies with $F \subset G$ gauged. The reduced gauge symmetries F and H on the UV/IR branes can be accomplished through boundary conditions or linear sigma models. We will work as closely as possible to boundary condition breaking.

If the strong sector of this theory is a strongly coupled conformal field theory, then there is a simple AdS metaphor for this symmetry breaking pattern. Consider a slice of AdS_5 bounded by a UV brane and a IR brane as in Figure 8.2. The metric for AdS_5 is

$$ds^2 = \frac{1}{(kz)^2}(\eta_{\mu\nu}dx^\mu dx^\nu - dz^2), \tag{8.1}$$

where $k \sim M_{\rm Pl}$ is the AdS curvature, and z parametrizes distance in the the warped

dimension. The UV brane sits at $z = L_0 \sim 1/M_{\rm Pl}$ and the IR brane sits at $z = L_1 \sim 1/(\text{a few TeV})$. It is also convenient to introduce the parameter $\epsilon = L_0/L_1$. In general, fields that "live" on the UV brane correspond to 4D elementary fields that are outside of the CFT, and fields that live on the IR brane correspond to composites of the strong dynamics. Fields living in the bulk of AdS_5 encode information about the operator content of the CFT. In particular, the global symmetry G of the CFT corresponds to bulk G gauge bosons in AdS_5. Gauging a subgroup F of G in 4D language corresponds to reducing the bulk G gauge symmetry to F on the UV brane. Spontaneously breaking $G \to H$ at $\Lambda \sim 10$ TeV corresponds to reducing the bulk G gauge symmetry to H on the IR brane.

As shown in [30], we could work entirely in the language of boundary conditions in AdS space, imposing Dirichlet boundary conditions on the appropriate modes of the gauge bosons A_μ^a to reduce the gauge symmetries on the boundaries. In this case, the uneaten Goldstone modes (including our Higgs boson) correspond to A_5^a zero modes. For our purposes, we work instead in $A_5 = 0$ gauge and reduce the gauge symmetry on the IR brane via a linear sigma field Φ that takes a non-zero vacuum expectation value. For low energy physics $E <$ a few TeV, the boundary condition language and the linear sigma field language give identical results, and we will go to a limit which is maximally similar to boundary condition breaking. We prefer the Φ language because the fluctuations Σ about $\langle\Phi\rangle$ *are* the pseudo-Goldstone bosons associated with G/H, so the fact that the Φ field lives on the IR brane makes it intuitively obvious that the pseudo-Goldstone bosons Σ are composite states of the strong dynamics.

We still have enough gauge freedom to use boundary conditions to reduce the

gauge symmetry on the UV brane to F. As we will see explicitly, collective breaking now looks like a choice between Neumann and Dirichlet boundary conditions for the electroweak groups W_1 and W_2. If W_1 has Neumann boundary conditions but W_2 has Dirichlet boundary conditions (*i.e.* only W_1 is gauged), then the Higgs contained in Σ is still an exact Goldstone. Only when all of F has Neumann boundary condition does the Higgs pick up a mass. This is because Φ transforms as some representation of the bulk gauged G, and G-violating corrections to the Φ potential can only come through loops involving gauge bosons that stretch from the IR brane (where G is a good symmetry before Φ takes its vev) to the UV brane (where G is explicitly broken by boundary conditions). Because these loops are non-local in the warped dimension, their contribution to the Goldstone potentials are finite and calculable.

To complete the little Higgs mechanism we need to introduce fermions. Because the Higgs lives on the IR brane, standard model fermions must have some overlap with the IR brane. Standard model fermions do not come in complete G multiplets, however, and if we simply included G-violating Yukawa couplings with the Φ field on the IR brane, then the quantum effective potential for the Σ field would be sensitive to the cutoff on the IR brane, namely a few TeV. While this is not a problem from a model-building perspective, our aim was to have control over UV sensitive parameters in little Higgs models. Therefore, as for the gauge sector, we only want to explicitly break G on the UV brane, so we introduce bulk fermions in complete G multiplets. These bulk fermions couple to the Φ field on the IR brane and have explicit G-violating (but F-preserving) boundary conditions on the UV brane. Like the gauge sector, these boundary conditions are chosen collectively such that a mass for the

Higgs is only generated when there are pairs of Dirichlet boundary conditions.

While it appears that collective breaking involves a binary choice between Neumann and Dirichlet boundary conditions, we could of course break G by introducing G-violating UV brane kinetic terms for the gauge bosons and fermions. In our model, we in fact need to do this because simple boundary conditions are not enough to generate different gauge couplings for W_1 and W_2. Clearly, if we introduced a boundary mass term proportional to m, then Neumann and Direchlet boundary conditions are just the $m \to 0$ and $m \to \infty$ limits, respectively. As we will see when we write down the expression for the Higgs potential, the boundary condition language makes it easy to see how the little Higgs mechanism works in anti-de Sitter space, but the central idea is applicable for general boundary kinetic terms. We use the shorthand $(\pm, \pm)$ to indicate boundary conditions on the UV/IR branes, where $+$ indicates Neumann (or modified Neumann) boundary conditions, and $-$ indicates Dirichlet boundary conditions.

9

An AdS Implementation of the Littlest Higgs

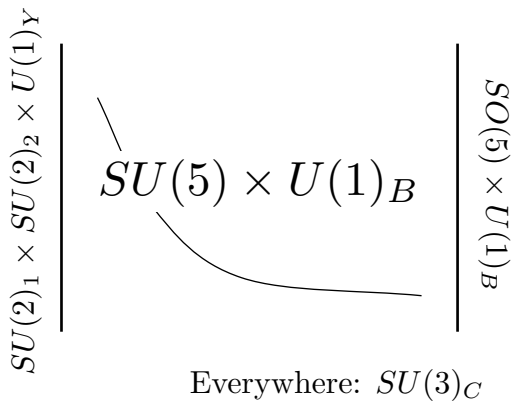

Figure 9.1: Gauge structure of the littlest Higgs in AdS_5.

The littlest Higgs [7] is based on an $SU(5)/SO(5)$ non-linear sigma model. In this section, we construct an AdS_5 model that captures the essential features of the littlest Higgs involving only the top and gauge sectors. This model roughly shares the

4D fermion content of [54]. Unlike the original littlest Higgs, we do not implement collective breaking for $U(1)_Y$ in order to avoid issues arising from mixing between heavy and light $U(1)$ gauge bosons, but because the hypercharge gauge coupling is small, this will not change the Higgs mass appreciably. In the calculations in the following sections, we simply ignore the $U(1)_Y$ contribution to the Higgs mass and quartic coupling.

In the language of the previous section, we will take

$$\begin{aligned} G &= SU(3)_C \times SU(5) \times U(1)_B \\ F &= SU(3)_C \times SU(2)_1 \times SU(2)_2 \times U(1)_Y \\ H &= SU(3)_C \times SO(5) \times U(1)_B \end{aligned} \tag{9.1}$$

where $SU(3)_C$ is color $SU(3)$, and $U(1)_B$ has nothing to do with baryon number. (See Figure 9.1.) The $SU(2)$ generators of F are imbedded in the $SU(5)$ generators as

$$Q_1^a = \begin{pmatrix} \sigma^a/2 & & \\ & & \\ & & \end{pmatrix}, \qquad Q_2^a = \begin{pmatrix} & & \\ & & \\ & & -\sigma^{*a}/2 \end{pmatrix}. \tag{9.2}$$

There is a $U(1)_A$ in $SU(5)$ generated by $A = \mathrm{diag}(1,1,0,-1,-1)/2$, and $U(1)_Y$ is defined by $Y = A+B$, where B is the $U(1)_B$ generator. For the purposes of calculating the radiative Higgs potential, we need only introduce the bulk gauge coupling g_5 for $SU(5)$. We also introduce a Planck brane boundary gauge kinetic terms for the $SU(2)_i$ subgroups proportional to z_i. Propagators for gauge fields with boundary conditions and Planck brane kinetic terms are given in Appendix C. The low energy gauge couplings g_i for the $SU(2)_i$ can be extracted by integrating out the bulk of AdS:

$$\frac{1}{g_i^2} = \frac{1}{g_5^2 L_0}\left(\log\frac{L_1}{L_0} + z_i\right) = \frac{1}{g_\rho^2}(-\log\epsilon + z_i), \tag{9.3}$$

where we have introduced $g_\rho = g_5\sqrt{L_0}$. g_ρ is the AdS perturbative expansion parameter that has the holographic interpretation $g_\rho \sim 4\pi/\sqrt{N}$ in a large N CFT [13].

The field Φ on the IR brane is a symmetric tensor that transforms as

$$\Phi \to V\Phi V^T \tag{9.4}$$

under $SU(5)$, and Φ is a singlet under $SU(3)_C \times U(1)_B$. Φ takes a vacuum expectation value

$$\langle\Phi\rangle = \Sigma_0 \equiv \begin{pmatrix} & & \mathbb{1} \\ & 1 & \\ \mathbb{1} & & \end{pmatrix}, \tag{9.5}$$

breaking $SU(5) \to SO(5)$ on the IR brane. The unbroken $SO(5)$ generators T_a and the broken $SU(5)/SO(5)$ generators X_a satisfy

$$T_a\Sigma_0 + \Sigma_0 T_a^T = 0, \qquad X_a\Sigma_0 - \Sigma_0 X_a^T = 0. \tag{9.6}$$

Performing a broken $SU(5)$ transformation on the vacuum, we can parametrize fluctuations about the Φ background as

$$\Sigma = e^{i\Pi/f_5}\Sigma_0 e^{i\Pi^T/f_5} = e^{2i\Pi/f_5}\Sigma_0, \tag{9.7}$$

where $\Pi = \pi^a X_a$ is the Goldstone matrix and f_5 is related the 4D Goldstone decay constant f_4 by $f_4 = \epsilon f_5$. As we will see, f_4 has nothing to do with what a low energy observer would call the pion decay constant, and we will actually go to the limit $f_4 \to \infty$. Three of the Goldstone bosons are eaten by the Higgsing of $SU(2)_1 \times SU(2)_2$ down to $SU(2)_{EW}$, giving rise to the gauge boson partner W'. The remainder of the

Π matrix can be written as

$$\Pi = \begin{pmatrix} (\eta/\sqrt{20})\mathbb{1} & h^\dagger/\sqrt{2} & \phi^\dagger \\ h/\sqrt{2} & -4\eta/\sqrt{20} & h^*/\sqrt{2} \\ \phi & h^T/\sqrt{2} & (\eta/\sqrt{20})\mathbb{1} \end{pmatrix}, \tag{9.8}$$

where η is a real neutral field, $h = (h^+, h^0)$ is the Higgs doublet, and ϕ is a complex symmetric two by two matrix that transforms as a charge 1 electroweak triplet.

On the IR brane, the leading lagrangian for Σ is the gauged non-linear sigma model

$$\mathcal{L}_\Sigma = \sqrt{-g_{\rm ind}}\delta(z-L_1) g_{\rm ind}^{\mu\nu}\frac{f_5^2}{8}\,\mathrm{tr}(D_\mu\Sigma)^\dagger(D_\nu\Sigma), \qquad D_\mu\Sigma = \partial_\mu\Sigma - iA_\mu\Sigma - i\Sigma A_\mu^T, \tag{9.9}$$

where $A_\mu = A_\mu^a T_a + A_\mu^b X_b$ are the 5D $SU(5)$ gauge bosons. In order to give the η field a mass and remove it from the spectrum, we introduce an explicit $SO(5)$ violating plaquette operator on the IR brane which does not substantially affect the Higgs potential. Expanding Σ in the Goldstone fields, there is a linear coupling between h and the KK gauge bosons which induces wavefunction renormalization on h. Integrating out the heavy KK states, the kinetic lagrangian for h is

$$\mathcal{L}_h = Z_h |D_\mu h|^2, \qquad Z_h = \left(1 + \frac{f_5^2 g_5^2 G_{br}}{2}\right)^{-1}, \tag{9.10}$$

where the covariant derivative now only includes electroweak gauge fields, and $G_{br} = \hat{G}(0; L_1, L_1) = L_0/2$ is the zero momentum boundary to boundary rescaled gauge boson propagator for modes with $(-,+)$ boundary conditions.

In this simplified littlest Higgs model, we only consider fermionic contributions to the Higgs mass from the top sector. We introduce two bulk 5D (Dirac) fermions $\mathbf{Q}$

and $\mathbf{Q^c}$. Under KK decomposition, $\mathbf{Q}$ and $\mathbf{Q^c}$ have upper (left-handed) and lower (right-handed) Weyl components:

$$\mathbf{Q} = \begin{pmatrix} Q \\ \overline{Q}' \end{pmatrix}, \qquad \mathbf{Q^c} = \begin{pmatrix} Q'^c \\ \overline{Q}^c \end{pmatrix}. \tag{9.11}$$

In order for the 4D masses of the KK fermion tower to have real masses, we must impose Dirichlet boundary conditions on either the upper or lower component on each of the AdS boundaries [45]. However, because we do not impose orbifold symmetry on AdS space, the choice of which mode vanishes is independent on each boundary. We choose the upper component Q of $\mathbf{Q}$ and the lower component Q^c of $\mathbf{Q^c}$ to have non-vanishing boundary conditions on the IR brane. While this choice is arbitrary, it will simplify the calculation of the fermionic contribution to the Σ effective potential.

The components Q and Q^c transform under G as:

	$SU(3)_C$	$SU(5)$	$U(1)_B$
Q	$\mathbf{3}$	$\mathbf{5}$	$+2/3$
Q^c	$\overline{\mathbf{3}}$	$\mathbf{5}$	$-2/3$

(9.12)

Expanding Q and Q^c as $SU(5)$ multiplets:

$$Q = \begin{pmatrix} \tilde{p} \\ \tilde{t} \\ \\ q \end{pmatrix}, \qquad Q^c = \begin{pmatrix} \tilde{q}^c \\ t^c \\ \\ \tilde{p}^c \end{pmatrix}. \tag{9.13}$$

Under F, these fields transform as:

	$SU(3)_C$	$SU(2)_1$	$SU(2)_2$	$U(1)_Y$	$B.C.$
q	$\mathbf{3}$	$-$	$\mathbf{2}$	$+1/6$	$(+,+)$
t^c	$\bar{\mathbf{3}}$	$-$	$-$	$-2/3$	$(+,+)$
$\tilde{t}$	$\mathbf{3}$	$-$	$-$	$+2/3$	$(-,+)$
$\tilde{q}^c$	$\bar{\mathbf{3}}$	$\mathbf{2}$	$-$	$-1/6$	$(-,+)$
$\tilde{p}$	$\mathbf{3}$	$\mathbf{2}$	$-$	$+7/6$	$(-,+)$
$\tilde{p}^c$	$\bar{\mathbf{3}}$	$-$	$\mathbf{2}$	$-7/6$	$(-,+)$

(9.14)

After $SU(2)^2$ is Higgsed to the electroweak $SU(2)$, the q and t^c fields have the right quantum numbers to be the standard model third generation quark doublet and top singlet. In order for q (t^c) to have zero modes, we take them to have Neumann boundary conditions on the UV brane, and thus the associated lower (upper) component modes have Dirichlet boundary conditions there. The tilded fields have Dirichlet boundary conditions on the UV brane, so the first KK mode is massive. The $\tilde{t}$ and $\tilde{q}^c$ fields are roughly the t' and q' fermionic partners responsible for cutting off the divergent top contribution to the Higgs mass, but the $\tilde{p}$ and $\tilde{p}^c$ are spectators that serve merely to fill out the $SU(5)$ representation.[1]

As is standard in AdS model building, we give $\mathbf{Q}$ and $\mathbf{Q^c}$ bulk masses νk and $\nu^c k$. The values of ν and ν^c affect the spectrum and wavefunctions of the KK tower. In CFT language, the values of ν and ν^c adjust the anomalous dimension of operators

[1]Though $\tilde{p}$ and $\tilde{p}^c$ have the right quantum numbers such that their zero modes could become one massive vector fermion, we will have more flexibility to choose different bulk masses for $\mathbf{Q}$ and $\mathbf{Q^c}$ if we remove the $\tilde{p}$ and $\tilde{p}^c$ zero modes.

corresponding to the zero mode of the relevant fermions [31]:

$$\gamma = |\nu - 1/2| - 1, \qquad \gamma^c = |\nu^c + 1/2| - 1. \tag{9.15}$$

(Unfortunately, we use opposite conventions from [31] for the signs of ν and ν^c.) In particular, in order to generate a large enough top Yukawa coupling, we need the top doublet and singlet to have anomalous dimension close to or less than zero. Though we will not discuss precision electroweak tests, we note that because these anomalous dimensions are indictations of couplings between the fermions with the CFT, deviations from standard model predictions for $Z \to b\bar{b}$, S, T, *etc.* are expected to be smaller the closer γ and γ^c are to zero. (See [3, 2] for details.) In Model 3 presented in Section 13, $\nu = -\nu^c \sim 1/2$ which at first glance seems to suggest large deviations from precision electroweak measurements. However, in that model, the CFT resonances appear at around 10 TeV, so while the mixing with CFT states may be large, the suppression scale for dangerous dimension six operators is much higher.

To generate the top Yukawa coupling, we introduce a Yukawa interaction on the IR brane:

$$\mathcal{L}_t = \sqrt{-g_{\rm ind}}\delta(z - L_1)\left(\lambda Q \Sigma^\dagger Q^c + h.c.\right), \tag{9.16}$$

where λ is $\mathcal{O}(1)$.[2] This interaction does not break any of the global symmetries acting on Σ. In fact, ignoring the gauge sector, there is an enhanced $SU(5)_L \times SU(5)_R$ global symmetry acting on Σ:

$$\Sigma \to L\Sigma R^T, \qquad Q \to LQ, \qquad Q^c \to RQ^c, \tag{9.17}$$

[2]This is dimensionally correct, because Q and Q^c are components of 5D fermions and have mass dimension 2.

and *both* of these $SU(5)$s must be broken in order for the Higgs to get a radiative mass from the fermion sector. Indeed, the UV brane boundary conditions on $\mathbf{Q}$ break $SU(5)_L$ and the UV brane boundary conditions on $\mathbf{Q^c}$ break $SU(5)_R$. Equivalently, at energies below the mass of the fermion KK modes, all the symmetries that protect the mass of the Higgs boson are broken, but when we see the KK modes of the tilded fields, we restore the $SU(5)_L \times SU(5)_R$ global symmetry of the fermion sector. In order for the tilded fields to naturally cancel the quadratically divergent top loop, at least one of the top partners must have mass no greater than around 2 TeV [7].

Expanding around $\Sigma = \Sigma_0$, we see that the Yukawa interaction in equation (9.16) generates kinetic mixing between the tilded and untilded fields. The overlap of the zero modes of q and t^c with the IR brane are

$$q: \ f_L(\nu) = \frac{1}{L_1^{1/2}} \sqrt{\frac{1+2\nu}{1-\epsilon^{1+2\nu}}}, \qquad t^c: \ f_R(\nu^c) = \frac{1}{L_1^{1/2}} \sqrt{\frac{1-2\nu^c}{1-\epsilon^{1-2\nu^c}}}. \tag{9.18}$$

Mixing between the zero mode of q (t^c) and the KK modes of $\tilde{q}^c$ ($\tilde{t}$) induce the following wavefunction renormalizations:

$$Z_q = 1 + \lambda^2 f_L(\nu)^2 G_{\tilde{q}^c}/\epsilon, \qquad Z_{t^c} = 1 + \lambda^2 f_R(\nu^c)^2 G_{\tilde{t}}/\epsilon, \tag{9.19}$$

where $G_{\tilde{q}^c} = \hat{G}^c(0; L_1, L_1; \nu^c)$ and $G_{\tilde{t}} = \hat{G}(0; L_1, L_1; \nu)$ are zero momentum boundary to boundary rescaled fermion propagators for modes with $(-,+)$ boundary conditions. After integrating out the heavy modes, the low energy Yukawa interaction in terms of canonically normalized fields is:

$$\mathcal{L}_t = \lambda_{\text{top}} \left(q h t^c + h.c. \right), \qquad \lambda_{\text{top}} = \frac{\lambda f_L(\nu) f_R(\nu^c) \sqrt{2}}{f_4 \sqrt{Z_h Z_q Z_{t^c}}}, \tag{9.20}$$

where using Appendix A, we have

$$Z_h = \left(1 + \frac{f_5^2 g_5^2 L_0}{4}\right)^{-1}, \qquad Z_q = 1 + \left(\lambda \frac{f_L(\nu)}{f_L(\nu^c)}\right)^2, \qquad Z_{t^c} = 1 + \left(\lambda \frac{f_R(\nu^c)}{f_R(\nu)}\right)^2. \tag{9.21}$$

In the next section, we will show how to understand this expression in terms of the t' and q' fields of the littlest Higgs.

10

Matching to the Low Energy Theory

The low energy phenomenology of the littlest Higgs is governed by the pion decay constant f_π, which sets the mass scale for the gauge boson partner W', the fermionic partners t' and q', and ultimately the electroweak scale. In our AdS construction, however, we appear to have two independent mass scales, f_4 and $1/L_1$, and it is not clear which combination we should call f_π. From the CFT point of view, we want the $SU(5)/SO(5)$ non-linear sigma field to arise directly from confinement and not from a composite linear sigma field. In other words, we would like to decouple all information about the Φ field that lived on the IR brane, and the way to do this is to send $f_4 \to \infty$. In AdS langauge, the $f_4 \to \infty$ limit is morally equivalent to describing Σ as the zero mode of A_5, though by leaving f_4 as a finite parameter, we are able to go to the computationally simpler $A_5 = 0$ gauge.

We notice immediately that all reference to f_4 vanishes in this limit. The top

Yukawa coupling in equation (9.20) involves the combination $f_4\sqrt{Z_h}$, and in this limit,

$$f_4\sqrt{Z_h} \to \frac{2\epsilon}{g_5\sqrt{L_0}} = \frac{2}{g_\rho L_1} \equiv f_\pi, \qquad \lambda_{\text{top}} \to \frac{\lambda f_L(\nu) f_R(\nu^c)\sqrt{2}}{f_\pi\sqrt{Z_q Z_{t^c}}}, \tag{10.1}$$

where we have cavalierly defined the pion decay constant f_π. To justify this choice, we need to match to the gauge sector. At large f_4, the Σ kinetic term in equation (9.9) enforces vanishing IR boundary conditions on the gauge bosons corresponding to the subgroup G/H. Gauge bosons contained in $F \cap G/H$ are the littlest Higgs W' modes. If we take $g_1 = g_2$ ($z_1 = z_2$), then using Appendix C the mass of the lightest KK mode of a $(+,-)$ gauge boson is roughly $m^2_{W'} = 2/L_1^2(-\log\epsilon + z)$. For arbitrary Planck brane gauge kinetic terms, the W' has approximate mass

$$m^2_{W'} \sim \frac{1}{L_1^2}\left(\frac{1}{-\log\epsilon + z_1} + \frac{1}{-\log\epsilon + z_2}\right) = \frac{g_1^2 + g_2^2}{g_\rho^2 L_1^2}. \tag{10.2}$$

where we have used equation (9.3) in the last step. In the littlest Higgs, the mass of the W' is [7]

$$m_{W'} = \frac{g' f_\pi}{2}, \qquad g' = \sqrt{g_1^2 + g_2^2}. \tag{10.3}$$

Therefore, to match the low energy theory, we should identify f_π with

$$f_\pi \equiv \frac{2}{g_\rho L_1}, \tag{10.4}$$

in agreement with equation (10.1). The mass of the lightest KK mode of a $(+,+)$ or $(-,+)$ gauge boson is roughly $m_\rho \sim 3\pi/4L_1$, which sets the scale for the ρ-like resonances of the CFT. In terms of f_π and $g_\rho \sim 4\pi/\sqrt{N}$:

$$f_\pi \sim \frac{m_\rho}{g_\rho} \sim \frac{m_\rho}{4\pi}\sqrt{N}, \tag{10.5}$$

which reproduces the expected $\sqrt{N}$ scaling of f_π in strongly coupled theories [74]. Because we want a large separation between the scale of new physics m_ρ and the pion decay constant f_π, we would like to take N small (g_ρ large). For reference, the electroweak gauge coupling g_{EW} in terms of g_1 and g_2 is

$$g_{EW} = \frac{g_1 g_2}{\sqrt{g_1^2 + g_2^2}}. \tag{10.6}$$

Now that we understand how to identify f_π in the gauge sector, we want to know whether this choice is consistent with the fermion sector. Using the fermion content of [54] and a notation suggestive of equation (9.14), the low energy littlest Higgs fermion sector has the lagrangian

$$\mathcal{L}_t = \lambda_1(qht^c + \alpha_q f_\pi q\tilde{q}^c + \alpha_t f_\pi \tilde{t}t^c) + \lambda_2 f_\pi \tilde{q}\tilde{q}^c + \lambda_3 f_\pi \tilde{t}\tilde{t}^c, \tag{10.7}$$

where α_i are $\mathcal{O}(1)$ parameters inserted for reasons that will become clear shortly.[1] The fields q, $\tilde{t}$, t^c, and $\tilde{q}^c$ are familar from equation (9.14), and the interaction proportional to λ_1 would arise from the leading expansion of equation (9.16). Because $\tilde{q}^c$ and $\tilde{t}$ are $(-,+)$ modes, they do not have zero modes, and $\tilde{q}$ and $\tilde{t}^c$ are the components of Q'^c and Q' that pair with $\tilde{q}^c$ and $\tilde{t}$ to form Dirac masses. We see that a linear combination of q and $\tilde{q}$ marries with $\tilde{q}^c$ to become the q', and a linear combination of t^c and $\tilde{t}^c$ marries with $\tilde{t}$ to become the t'. The partners q' and t' cut off fermionic quadratic divergences in the Higgs potential, and their masses are

$$m_{q'} = f_\pi\sqrt{\alpha_q^2\lambda_1^2 + \lambda_2^2}, \qquad m_{t'} = f_\pi\sqrt{\alpha_t^2\lambda_1^2 + \lambda_3^2}. \tag{10.8}$$

[1] From the low energy point of view, α_q and α_t account for any effects from wave function renormalization.

After integrating out t' and q', the low energy Yukawa coupling is

$$\lambda_{\rm top} = \frac{\lambda_1}{\sqrt{1+\alpha_q^2\lambda_1^2/\lambda_2^2}\sqrt{1+\alpha_t^2\lambda_1^2/\lambda_3^2}}. \tag{10.9}$$

This form of the Yukawa coupling is very suggestive of equation (9.20). We can match λ_i to parameters of the AdS theory by expanding equation (9.16) in KK modes and canonically normalizing just the Higgs doublet:

$$\lambda_1 \to \frac{\lambda f_L f_R \sqrt{2}}{f_4\sqrt{Z_h}}, \qquad \alpha_q\lambda_1 f_\pi \to \lambda f_L f_R^{(1)}, \qquad \alpha_t\lambda_1 f_\pi \to \lambda f_L^{(1)} f_R,$$
$$\lambda_2 f_\pi \to m_R^{(1)}, \qquad \lambda_3 f_\pi \to m_L^{(1)}. \tag{10.10}$$

Here $m_L^{(1)}(\nu)$ and $f_L^{(1)}(\nu)$ are the mass and IR brane overlap of the lightest KK mode of a $(-,+)$ upper component fermion with bulk mass νk, and similarly for $m_R^{(1)}(\nu^c)$ and $f_R^{(1)}(\nu^c)$. Note that f_L and f_R have dimensions of $\sqrt{\rm mass}$ so these expressions match dimensionally. The ratio α_q/α_t is clearly necessary to account for the fact that $\lambda f_L f_R^{(1)}$ need not equal $\lambda f_L^{(1)} f_R$. We see that all of the λ_i's act as spurions for the soft breaking of $SU(5)$. In particular, λ_2 and λ_3 are proportional to the masses of $(-,+)$ modes, and if $SU(5)$ were restored on the UV brane, λ_2 and λ_3 would go to zero as all the $(-,+)$ modes would become $(+,+)$ zero modes.

We can write the expressions for $\lambda_{\rm top}$ in terms of boundary to boundary 5D propagators. On the IR brane, $(-,+)$ bulk fields look like tower of massive states with different overlaps:

$$\hat{G}(p; L_1, L_1)/\epsilon \sim \sum_i \frac{{f^{(i)}}^2}{p^2 + {m^{(i)}}^2}. \tag{10.11}$$

(We have analytically continued to momentum space.) As long as there is a large mass separation between the first state the second state, we can write approximately

$$\hat{G}(0; L_1, L_1)/\epsilon \sim \frac{{f^{(1)}}^2}{{m^{(1)}}^2}. \tag{10.12}$$

From the mapping in equation (10.10),

$$1 + \alpha_q^2 \lambda_1^2 / \lambda_2^2 \to Z_q, \qquad 1 + \alpha_t^2 \lambda_1^2 / \lambda_3^2 \to Z_{t^c}, \tag{10.13}$$

and we see that the Yukawa couplings in equations (9.20) and (10.9) match beautifully.

We can use equation (10.10) to identify the low energy f_π:

$$f_\pi = \frac{f_L^{(1)}}{\alpha_t f_L \sqrt{2}} f_4 \sqrt{Z_h} = \frac{f_R^{(1)}}{\alpha_q f_R \sqrt{2}} f_4 \sqrt{Z_h}. \tag{10.14}$$

This matches to equation (10.1) as long as we define α_t and α_q appropriately. Of course, these were unknown coefficients in the low energy theory anyway so it is not surprising that their value depends on the UV completion. More importantly, once we fix what we mean by f_π from the gauge sector, there is an unambiguous translation to the fermion sector. Note that when $\nu = \nu_c = 0$, $f_i^{(1)}/f_i \sim \sqrt{2}$, and $\alpha_i \sim 1$.

11

Tension with the High Energy Theory

Though we have successfully matched our AdS construction with low energy observables, there are relationships between the parameters of the littlest Higgs which although harmless from the low energy point of view, cause some tension once a UV completion in the form of a large N CFT is chosen, and we will see that in order to address these issues, we need to shrink the conformal window by taking $1/L_0$ to be smaller than $M_{\rm Pl}$. The UV scale can still be quite high, however, so in this sense we can still claim a viable UV completion of the littlest Higgs.

At the end of the day, the radiatively generated Higgs potential will take the form

$$V(h) = -m_h^2 h^\dagger h + \lambda_h (h^\dagger h)^2, \qquad v_{EW} = \sqrt{\frac{-m_h^2}{\lambda_h}}, \qquad m_{h_0} = \sqrt{-2m_h^2}, \qquad (11.1)$$

where $v_{EW} \sim 246$ GeV is the electoweak scale and m_{h_0} is the mass of the physical Higgs boson. Because $\lambda_{\rm top}$ is numerically larger than g_{EW}, the dominant contribution to the Higgs potential will come from top loops. From the low energy Coleman-

Weinberg potential, there is the logarithmic contribution to the Higgs doublet mass from the fermion sector [54],

$$\delta_{\text{fermion}} m_h^2 = -\frac{3\lambda_{\text{top}}^2}{8\pi^2} \frac{m_{q'}^2 m_{t'}^2}{m_{q'}^2 - m_{t'}^2} \log \frac{m_{q'}^2}{m_{t'}^2} \to -\frac{3\lambda_{\text{top}}^2}{8\pi^2} m_{t'}^2, \tag{11.2}$$

where in the last step, we have taken the special case $m_{t'} = m_{q'}$, which minimizes the contribution to the Higgs doublet mass for fixed λ_{top}. (We are assuming $\alpha_t = \alpha_q = 1$ for simplicity.) In this limit, $m_{t'} = 2\sqrt{2}\lambda_{\text{top}} f_\pi$,[1] and the contribution to the Higgs doublet mass is bounded by

$$\delta_{\text{fermion}} m_h^2 = -\frac{3\lambda_{\text{top}}^4 f_\pi^2}{\pi^2}. \tag{11.3}$$

The physical Higgs will be roughly a factor of $\lambda_{\text{top}}/4$ lighter than the t', and to the extent that λ_{top} is small, we will have a light Higgs boson. Of course, $\lambda_{\text{top}} \sim 1$, so numerically there is not much of a separation of scales. While it may not be a total disaster if $m_{h_0} \sim m_{t'}$, the mass of the t' is set by f_π which in turn sets the mass of the W':

$$m_{W'} = \frac{g' f}{2} = m_{t'} \frac{g'}{4\sqrt{2}\lambda_{\text{top}}}. \tag{11.4}$$

If $g_1 = g_2$, then $g' = 2g_{EW}$, and $m_{W'}$ would generically be *lighter* than the Higgs boson.

The obvious way to relieve this tension is to raise g' by increasing g_2, but there is a limit to how high we can push g_2 without perturbation theory breaking down in AdS space. Even without Planck brane gauge kinetic terms, the largest g_2 can be is $4\pi/\sqrt{\log \epsilon^{-1}}$, assuming $g_\rho \lesssim 4\pi$. If $\epsilon \sim 10^{-15}$, then g' cannot be much larger than $3.5 g_{EW}$. Therefore, if we want the t' and W' to be roughly degenerate, we have to

[1] When $\alpha_i \neq 1$, the mass of the t' can be lighter than $2\sqrt{2}\lambda_{\text{top}} f_\pi$ even in the limit $m_{t'} = m_{q'}$.

shrink the size of AdS space. In CFT language, the $SU(2)_i$ beta function is very large in a large N CFT:

$$\frac{b_{CFT}}{8\pi^2} \sim \frac{1}{g_\rho^2} \sim \frac{N}{16\pi^2}, \tag{11.5}$$

so all gauge coupling run to zero in the infrared. If we leave the confinement scale fixed, the way to increase gauge couplings is to have gauge coupling running begin at a lower scale. We will explore the possibility of shrinking the conformal window more thoroughly in Section 13.

Even if we do decrease $1/L_0$, we may still want to increase the separation between the partner masses and the electroweak scale. In the limit $m_{t'} = m_{q'}$, the fermion contibution to the Higgs quartic coupling is [54]

$$\delta_{\text{fermion}}\lambda_h = \frac{\lambda_{\text{top}}^4}{\pi^2}, \tag{11.6}$$

so ignoring the gauge sector, the electroweak scale would not be very different from f_π:

$$v_{EW} = \sqrt{\frac{-m_h^2}{\lambda_h}} = \sqrt{3} f_\pi. \tag{11.7}$$

Of course, there is a positive contribution to m_h^2 coming from the gauge sector [7]

$$\delta_{\text{gauge}} m_h^2 = \frac{9}{64\pi^2} g_{EW}^2 f^2 \log \frac{m_\rho^2}{m_{W'}^2}, \tag{11.8}$$

which grows large if we are able to increase the mass of W', so v_{EW} will certainly be smaller than the value in equation (11.7). Also, there are other sources of $SU(5)$ symmetry breaking in a realistic model that would tend to give a positive contribution to m_h^2, such as the inclusion of $U(1)_Y$ effects and the (unspecified) mechanism to remove the η field from the spectrum.

Taken together, the final m_h^2 value will be

$$m_h^2 = \delta_{\text{fermion}} m_h^2 + \delta_{\text{gauge}} m_h^2 + \delta_{\text{other}} m_h^2. \tag{11.9}$$

The first two pieces are finite and calculable in our model, and while in principle $\delta_{\text{other}} m_h^2$ could be calculable if the additional $SU(5)$ violating effects are nonlocal in AdS, in general we expect the IR brane to be a complicated place which could admit small sources of local $SU(5)$ violation which might not be unambiguously determined. In order to increase the separation between v_{EW} and f_π, we will present calculations where we allow ourselves to add $\delta_{\text{other}} m_h^2$ contributions, but we will limit ourselves to 10% fine-tuning, meaning that $|m_h^2|/|\delta m_h^2|$ must be greater than .1 for each individual contribution. We will also show that in certain regions of parameter space, $\delta_{\text{fermion}} m_h^2$ and $\delta_{\text{gauge}} m_h^2$ can balance each other without including a $\delta_{\text{other}} m_h^2$ piece.

We remark that this philosophy towards tuning is very different than the one presented in [2]. In our case, we have a natural mechanism for generating a large Higgs quartic coupling, so for fixed electroweak scale, the Higgs mass $m_{h_0} = \sqrt{2\lambda_h} v_{EW}$ is reasonably heavy. However, because λ_{top} is large, we have to do some amount of tuning to increase the separation between v_{EW} and f_π. In [2], some amount of tuning between fermion contributions to the radiative potential is needed to get a hierarchy between v_{EW} and f_π, and this tuning does not yield a very large Higgs quartic, so the Higgs boson is correspondingly very light (though within experimental bounds). In our model, we require additional sources of symmetry breaking to avoid precision electroweak constraints, and in their model, they require additional sources of symmetry breaking to allow for a greater range in the Higgs mass. However, whereas we posit additional unknown sources of symmetry breaking to decrease the

absolute value of a relevant parameter ($-m_h^2$), they introduce additional interactions to increase the value of a marginal parameter (λ_h). In addition, we expect that a similar level of tuning would be necessary in [2] even if λ_{top} and g_{EW} were smaller, whereas in our case, the ratio between v_{EW} and f_π is naturally on the order of these small parameters.

12

Collective Breaking in AdS Space

The Higgs doublet receives a mass and quartic coupling via quantum corrections. To evaluate these corrections, we will calculate the Coleman-Weinberg potential [27] to one-loop order in a background with non-zero Σ. Expanding the potential $V(\Sigma)$ in the Goldstone fields, we can easily identify the quantum corrections to the Higgs mass and quartic coupling. At the end of the day, we will take the $f_4 \to \infty$ limit in order to decouple all information about how $SU(5)$ is broken to $SO(5)$ on the IR brane. In the next section, we will present numerical calculations with specific values of the parameters in order to illustrate the tensions mentioned in the Section 11. In this section, we focus on trying to understand the structure of the Coleman-Weinberg integrals.

What is most fascinating about the littlest Higgs in AdS space is that the expressions for the mass and quartic coupling manifestly exhibit collective breaking. The 5D Coleman-Weinberg potential is a function of 5D propagators evaluated on the IR brane (See Appendix C for the form of these propagators). In both the gauge boson

and fermion case, there are two relevant (rescaled) propagators which we can write schematically as

$$G = \hat{G}^{(+,+)}(p; L_1, L_1), \qquad G_{\rm br} = \hat{G}^{(-,+)}(p; L_1, L_1), \tag{12.1}$$

corresponding to fields with $(+,+)$ and $(-,+)$ boundary conditions. If all of the fields that coupled to Σ had the same boundary conditions on the UV brane, then $SU(5)$ would be a good symmetry everywhere in AdS space and the Higgs would be an exact Goldstone. The degree to which $SU(5)$ is broken on the UV brane tells us the degree to which the Higgs is a pseudo-Goldstone boson, so the expression for the Higgs mass and quartic coupling will be proportional to $(G_{\rm br} - G)$. Indeed, by collective breaking, the expressions will be proportional to *two* factors of $(G_{\rm br} - G)$, showing that two "coupling constants" have to be non-zero for the Higgs to acquire a radiative potential.

We begin with the gauge sector. The gauge bosons couples to Σ on the IR brane through the Σ kinetic term:

$$\mathcal{L}_\Sigma = \sqrt{-g_{\rm ind}}\delta(z-L_1) g_{\rm ind}^{\mu\nu} \frac{f_5^2}{8} \,{\rm tr}(D_\mu \Sigma)^\dagger (D_\nu \Sigma) \supset \epsilon^2 \frac{f_5^2 g_5^2}{8} A^{\mu a} A_\mu^b \,{\rm tr}(T_a \Sigma + \Sigma T_a^T)(T_b^T \Sigma^\dagger + \Sigma^\dagger T_b). \tag{12.2}$$

The (rescaled) mass-squared matrix for the gauge boson in the background Σ is therefore

$$M_{ab}^2 = \frac{f_5^2 g_5^2}{4} \,{\rm tr}(T_a \Sigma + \Sigma T_a^T)(T_b^T \Sigma^\dagger + \Sigma^\dagger T_b). \tag{12.3}$$

To generate the effective potential for Σ to 1-loop order, we consider an arbitrary

number of mass insertions, analytically continuing the propagators to Euclidean space:

$$\delta_{\text{gauge}}\left(\sqrt{-g_{\text{ind}}}V(\Sigma)\right) = \frac{3}{2}\int \frac{p^3 dp}{8\pi^2}\,\text{tr}\sum_{n=0}^{\infty}\frac{(-1)^n}{n}(\hat{G}\cdot M^2)^n = \frac{3}{2}\,\text{tr}\int\frac{p^3 dp}{8\pi^2}\log(1+\hat{G}\cdot M^2), \tag{12.4}$$

where $\hat{G}_{ab} = \hat{G}_a(p; L_1, L_1)\delta_{ab}$ are the rescaled propagators for the $SU(5)$ gauge bosons, and a labels the generators of $SU(5)$. (The factor of 3 accounts for the three polarizations of each gauge boson.) The propagators for the $SU(2)_i$ subgroups will be labeled G_i for $i = 1, 2$, and the propagators for the rest of $SU(5)$ will be labeled G_{br} to indicate that those propagators have Dirichlet boundary conditions on the UV brane.

Using the fact that $\text{tr}\log X = \log\det X$, we can evaluate equation (12.4) exactly. Expanding $V(\Sigma)$ in powers of the Goldstone fields, the mass correction to the Higgs potential from gauge bosons loops is (including wavefunction renormalization for the Higgs):

$$\delta_{\text{gauge}}m_h^2 = \frac{9}{16Z_h\epsilon^2}\int\frac{p^3 dp}{8\pi^2}\frac{f_5^2 g_5^4\,(G_{\text{br}}-G_1)\,(G_{\text{br}}-G_2)}{(1+f_5^2 g_5^2 G_{\text{br}}/2)(1+f_5^2 g_5^2(G_1+G_2)/4)}. \tag{12.5}$$

In the numerator, we manifestly see collective breaking, in that both $G_1 \neq G_{\text{br}}$ and $G_2 \neq G_{\text{br}}$ in order for the Higgs to get a radiative potential from the gauge sector. As already mentioned, we want to take the $f_5 \to \infty$ limit. The resulting expression only depends on the AdS parameters through $f_\pi = 2/(L_1 g_\rho)$ and the propagators themselves:

$$\delta_{\text{gauge}}m_h^2 = \frac{9}{2f_\pi^2}\int\frac{p^3 dp}{8\pi^2}\frac{(G_{\text{br}}-G_1)\,(G_{\text{br}}-G_2)}{G_{\text{br}}(G_1+G_2)}. \tag{12.6}$$

We will discuss the physical meaning of this integrand after we calculate the Higgs quartic.

In the littlest Higgs, there is a radiatively generated trilinear coupling ϕhh and ϕ^2 mass term. Looking the at the fermion coupling in equation (9.16) and the fermion content in equation (9.14), it is clear that there is still a global $SU(2)$ symmetry present in the fermion sector that protects the triplet from radiative corrections, so all contributions to the ϕ potential will come from gauge boson loops.[1] Using the Coleman-Weinberg potential we can calculate the contribution to the triplet mass and ϕhh coupling to 1-loop order in the $f_5 \to \infty$ limit. To go to this limit, we need to canonically normalize ϕ, and we use $Z_h = Z_\phi$:

$$\delta_{\text{gauge}} m_\phi^2 = \frac{3}{f_\pi^2} \int \frac{dpp^3}{8\pi^2} \frac{2G_{\text{br}}^2 + 4G_1G_2 - 3G_{\text{br}}(G_1+G_2)}{G_{\text{br}}(G_1+G_2)}, \tag{12.7}$$

$$\delta_{\text{gauge}} \lambda_{\phi hh} = \frac{3}{2f_\pi^3} \int \frac{dpp^3}{8\pi^2} \frac{G_1 - G_2}{G_1+G_2}. \tag{12.8}$$

In the case $G_1 = G_2$, we see that no ϕhh coupling is generated, corresponding to the T-parity limit of the theory. The direct contribution of the gauge bosons to the Higgs quartic is

$$\delta_{\text{gauge}} \lambda_h' = -\frac{3}{4f_\pi^4} \int \frac{p^3 dp}{8\pi^2} \frac{3G_{\text{br}}^2(G_{\text{br}}^2 - G_1^2 - G_2^2) + G_{\text{br}}(G_{\text{br}}^2 - G_1G_2)(G_1+G_2) + 3G_1^2G_2^2}{G_{\text{br}}^2(G_1+G_2)^2}. \tag{12.9}$$

After integrating out the heavy triplet, the total gauge contribution to the Higgs quartic is

$$\delta_{\text{gauge}} \lambda_h = \delta_{\text{gauge}} \lambda_h' - \frac{(\delta_{\text{gauge}} \lambda_{\phi hh})^2}{\delta_{\text{gauge}} m_\phi^2}. \tag{12.10}$$

Collective breaking is certainly not manifest in this form, but we can check that collective breaking occurs slice by slice in momentum space. Imagine doing each momentum integral from p_0 to $p_0 + \Delta p_0$. The contribution from this slice to $\delta_{\text{gauge}} \lambda_h$

[1] In particular, in this model there is no danger of having a negative triplet mass squared.

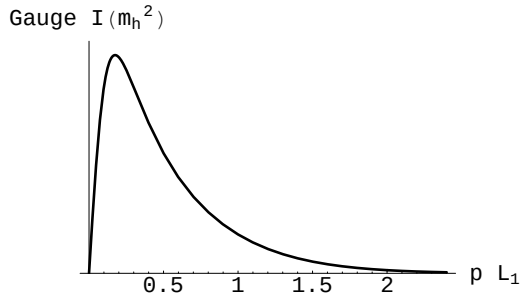

Figure 12.1: The gauge boson integrand for $\delta_{\text{gauge}} m_h^2$ using the parameters of Model 1c. The linear behavior near $p = 0$ corresponds to the quadratic sensitivity of this operator below the mass of the W'. The W' has mass around $.18/L_1$ and the ρ-like resonances appear at $2.4/L_1$.

is

$$\frac{1}{f_\pi^4}\frac{\Delta p_0 p_0^3}{8\pi^2}\frac{(G_{\text{br}}-G_1)\,(G_{\text{br}}-G_2)}{G_{\text{br}}^2(G_1+G_2)^2}\frac{E_4(G_{\text{br}},G_1,G_2)}{E_2(G_{\text{br}},G_1,G_2)}\bigg|_{p=p_0}, \tag{12.11}$$

where E_i are unenlightening i-th order polynomials. We see readily that the gauge contribution to λ_h vanishes in each slice of momentum space unless both G_1 and G_2 are different from G_{br}.

Before proceeding to analyze the fermion contribution, it is interesting to ask whether these 1-loop contributions match our expectations from the low energy theory. Expanding the integrand in equation (12.6) to lowest order in momenta and integrating with a hard momentum cutoff Λ_0:

$$\delta_{\text{gauge}} m_h^2 \sim \int^{\Lambda_0} I(p\to 0)\,dp = \frac{9 g_{EW}^2 \Lambda_0^2}{64\pi^2} + \mathcal{O}(\Lambda_0^4/f_\pi^2), \tag{12.12}$$

which is exactly the expected quadratically divergent contribution to the Higgs mass from a W boson loop. Figure 12.1 is a plot of the integrand of equation (12.6) with the parameters of Model 1c from the next section. At low energies, we see the linear behavior in p corresponding to the quadratic divergence from the W loops. At

momenta around $m_{W'} \sim .18/L_1$, this divergence is softened by the appearance of the W' partner. The $1/p$ behavior between $m_{W'}$ and $m_\rho \sim 2.4/L_1$ reflects a logarithmic threshold correction, and at $p \sim m_\rho$, the integrand dies off exponentially fast.

Note that the peak in the m_h^2 integrand is almost exactly at $m_{W'}$. More generally, when there is a quadratic divergence at low energies that is cutoff by the existence of new states, the integrands are roughly of the form (ignoring coupling constants):

$$I(p) \sim \frac{p^3}{8\pi^2}\frac{1}{f_\pi^2 p^2}\prod_i\left(1-\frac{p^2}{p^2+m_i^2}\right) \sim \frac{p^3}{8\pi^2}\frac{1}{f_\pi^2 p^2}\left(1-\frac{p^2}{p^2+m_{\text{partner}}^2}\right)^N, \quad (12.13)$$

where m_i is the mass of any partner particle whose appearance would cutoff the quadratic divergence, and in the last step, we have gone to the limit where all N of the partners are degenerate with mass m_{partner}. The peak in $I(p)$ is at

$$p \sim \frac{m_{\text{partner}}}{\sqrt{2N-1}}. \quad (12.14)$$

For the gauge quadratic divergence to the Higgs mass, $N = 1$ because there is only the W' partner particle, and indeed the peak in Figure 12.1 is at the mass of the W'. We can do the integral over p of $I(p)$:

$$\int I(p)\,dp = \frac{m_{\text{partner}}^2}{(4\pi f_\pi)^2}\log\frac{\Lambda^2}{m_{\text{partner}}^2} \quad (N=1), \qquad \frac{m_{\text{partner}}^2}{(4\pi f_\pi)^2}\frac{1}{N-1} \quad (N>1). \quad (12.15)$$

These factors are what a low energy observer would call "unknown $\mathcal{O}(1)$ coefficients" that multiply quadratically sensitive operators. In the example of a single W' ($N = 1$), there is still a logarithmic divergence, and indeed the ρ-like resonances provide an effective cutoff $\Lambda \sim m_\rho$ for $\delta_{\text{gauge}} m_h^2$.

The expressions for the quartic coupling are also very interesting. Expanding equations (12.7), (12.8) and (12.9) in momenta and integrating up to Λ_0:

$$\delta_{\text{gauge}} m_\phi^2 \sim \frac{3g_{EW}^2}{8\pi^2}\Lambda_0^2 + \mathcal{O}(\Lambda_0^4/f_\pi^2), \qquad \delta_{\text{gauge}}\lambda_{\phi hh} \sim \frac{3(g_1^2-g_2^2)}{64\pi^2(g_1^2+g_2^2)}\frac{\Lambda_0^4}{f_\pi^3} + \mathcal{O}(\Lambda_0^6/f_\pi^5),$$

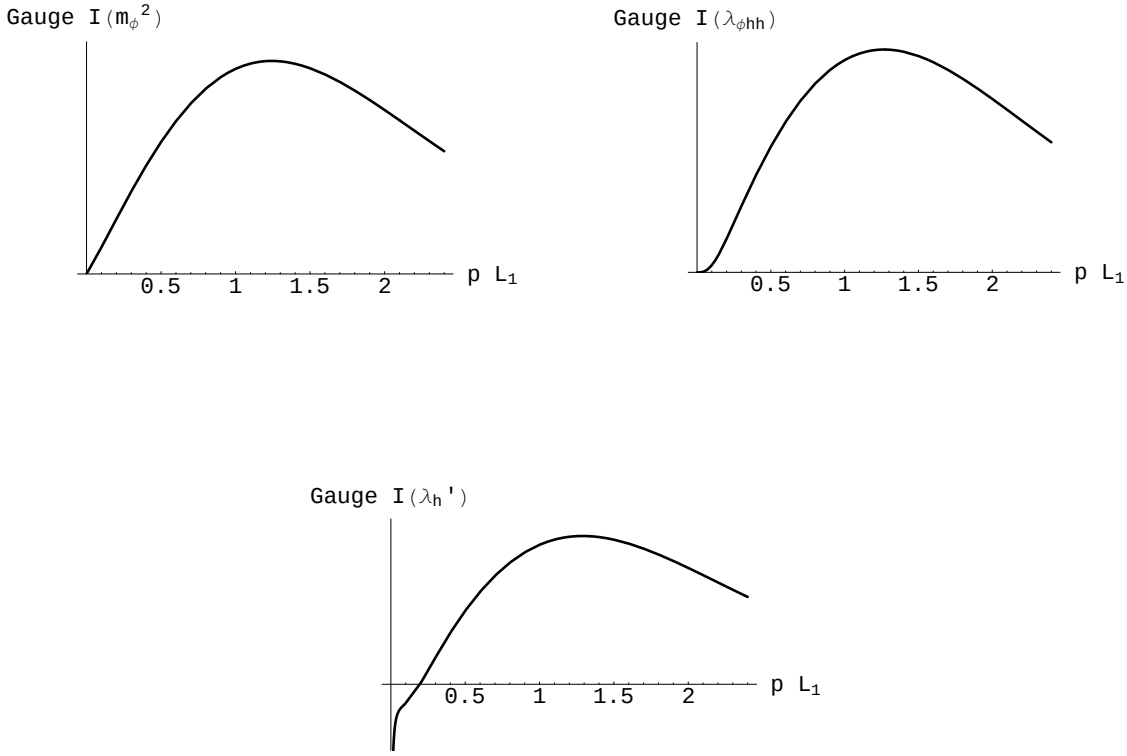

Figure 12.2: The gauge boson integrands for $\delta_{\text{gauge}} m_\phi^2$, $\delta_{\text{gauge}} \lambda_{\phi hh}$, and $\delta_{\text{gauge}} \lambda_h'$ using the parameters of Model 1c. The mass of the first ρ-like resonances is $\sim 2.4/L_1$, and all of these integrands become exponentially small at momenta corresponding to the second ρ-like resonances $\sim 5.5/L_1$. See the text for why the peaks of these integrands are at $p \sim 1.3/L_1$. Note the $-1/p$ behavior of $\delta_{\text{gauge}} \lambda_h'$ near $p = 0$, corresponding to expected low energy logarithmic running of the Higgs quartic.

$$\delta_{\text{gauge}} \lambda_h' \sim -\frac{9 g_{EW}^4}{256 \pi^2} \log \Lambda_0^2 + \mathcal{O}(\Lambda_0^2 / f_\pi^2). \tag{12.16}$$

To leading order in Λ_0, $\delta_{\text{gauge}} \lambda_h$ comes entirely from $\delta_{\text{gauge}} \lambda_h'$. This logarithmic divergence is the standard contribution to a doublet scalar from a W boson loop. Looking at the integrands in Figure 12.2, we see that each one rises linearly until it peaks at $\sim 1.3/L_1$. The linear behavior reflects the fact that the low energy operators which generate the Higgs quartic coupling are quadratically sensitive to the cutoff. How-

ever, there is no state in the spectrum at $\sim 1.3/L_1$ where the quadratic divergence is softened. Rather, the ρ-like states appear at $\sim 2.4/L_1$ but $N = 2$ because along with the $(+,+)$ gauge bosons, the appearance of the first KK mode of the $(-,+)$ gauge bosons or the second KK mode of the $(+,-)$ gauge bosons would restore enough of the $SU(5)$ global symmetry to protect the Higgs mass.[2] At momenta $p \sim 5.5/L_1$ the integrands are exponentially suppressed, as one might expect as this is the scale of the next-to-lightest KK gauge boson modes.

Now for the fermion contribution to the Higgs potential. The bulk fermions couple to the IR brane scalar Σ via

$$\mathcal{L}_{\text{Yukawa}} = \sqrt{-g_{\text{ind}}}\delta(z - L_1)(\lambda \bar{\mathbf{Q}} \Sigma \mathbf{Q^c} + h.c.). \tag{12.17}$$

Unlike equation (9.16), we are explicitly using bulk Dirac notation, though recall that the boundary conditions eliminate the lower (upper) Weyl fermion in $\mathbf{Q}$ ($\mathbf{Q^c}$) on the IR brane. In order to form a fermion loop and contract the fields, we need two such Yukawa insertions, so the one-loop effective potential for Σ is

$$\delta_{\text{fermion}} \left(\sqrt{-g_{\text{ind}}} V(\Sigma)\right) = -3 \,\text{tr} \int \frac{p^3 dp}{8\pi^2} \log(1 + \hat{S} \cdot M \cdot \hat{S}^c \cdot M^\dagger), \tag{12.18}$$

where $\hat{S}_{ab} = \hat{S}_a \delta_{ab}$ are bulk 5D propagators (with Dirac indices) for $\mathbf{Q}$, and similarly for $\hat{S}^c$. The index a runs over a fundamental of $SU(5)$, and the rescaled mass matrix in a background Σ is

$$M_{ab} = \frac{\lambda}{\epsilon} \Sigma_{ab}. \tag{12.19}$$

[2]The $(+,-)$ modes technically only exist in the $f_4 \to \infty$ limit. The first KK $(+,-)$ mode is the W' and the second KK mode is another ρ-like state which is roughly degenerate with the first $(-,+)$ KK mode. We can either restore $SU(5)$ near the UV brane or near the IR brane, and in this sense $N = 2$ and $m_{\text{partner}} = m_\rho \sim g_\rho f_\pi$.

The trace in equation (12.18) runs over both $SU(5)$ and Dirac indices, and the factor of 3 takes into account the $SU(3)_C$ charges of $\mathbf{Q}$ and $\mathbf{Q^c}$.

Because of our choice of boundary conditions on the IR brane, we can easily do the trace over Dirac indices. From Appendix C, the (rescaled) bulk fermion propagators take the schematic form

$$\hat{S}(p; L_1, L_1; \nu) = (A\not{p} + B\gamma^5 + C)P_L, \qquad \hat{S}^c(p; L_1, L_1; \nu^c) = (A^c\not{p} + B^c\gamma^5 + C^c)P_R, \tag{12.20}$$

where $P_{L,R} = (1 \mp \gamma^5)/2$. Using the trace properties of the σ matrices:

$$\hat{S} = \begin{pmatrix} C - B & 0 \\ A\bar{\sigma}\cdot p & 0 \end{pmatrix}, \qquad \hat{S^c} = \begin{pmatrix} 0 & A^c\sigma\cdot p \\ 0 & C^c + B^c \end{pmatrix}, \qquad \mathrm{Tr}(\hat{S}\hat{S^c})^n = 2(p^2 A A^c)^n. \tag{12.21}$$

Note that $A = \hat{G}(p; L_1, L_1; \nu)$, so equation (12.18) can be rewritten as

$$\delta_{\mathrm{fermion}}\left(\sqrt{-g_{\mathrm{ind}}}V(\Sigma)\right) = -3\,\mathrm{tr}\int\frac{p^3dp}{8\pi^2}2\log(1 + p^2\hat{G}\cdot M\cdot\hat{G^c}\cdot M^\dagger), \tag{12.22}$$

where now the trace runs only over $SU(5)$ indices.

We can proceed as in the gauge boson case and compute the Higgs mass and quartic coupling. We designate propagators for modes with $(+,+)$ boundary conditions as G and G^c, and with $(-,+)$ boundary conditions as G_{br} and G^c_{br}. These propagators are functions of ν and ν^c, respectively. After canonically normalizing h and taking the $f_4 \to \infty$ limit:

$$\delta_{\mathrm{fermion}}m_h^2 = -\frac{12}{f_\pi^2}\int\frac{p^3dp}{8\pi^2}\frac{\hat{\lambda}^2p^2(G_{\mathrm{br}} - G)(G^c_{\mathrm{br}} - G^c)}{(1 + \hat{\lambda}^2p^2GG^c_{\mathrm{br}})(1 + \hat{\lambda}^2p^2G_{\mathrm{br}}G^c)}, \tag{12.23}$$

$$\delta_{\mathrm{fermion}}\lambda_h = -\frac{4\lambda^2}{f_\pi^4}\int\frac{p^3dp}{8\pi^2}\frac{p^2(G_{\mathrm{br}} - G)(G^c_{\mathrm{br}} - G^c)}{\left(1 + p^2\hat{\lambda}^2GG^c_{\mathrm{br}}\right)^2\left(1 + p^2\hat{\lambda}^2G_{\mathrm{br}}G^c\right)^2}F(G, G_{\mathrm{br}}, G^c, G^c_{\mathrm{br}}), \tag{12.24}$$

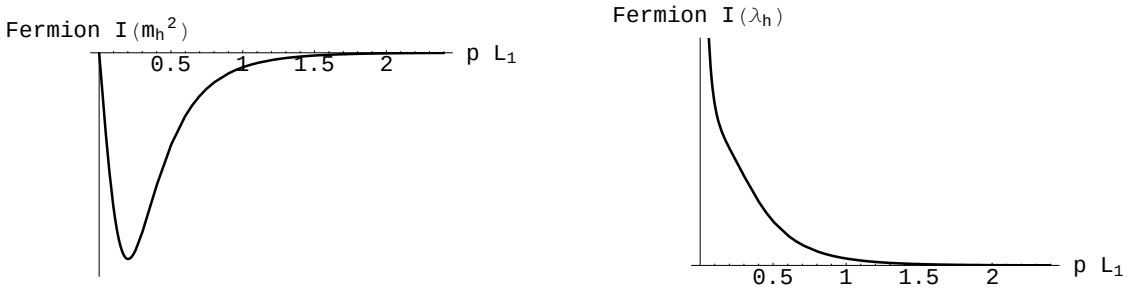

Figure 12.3: The fermion integrands for $\delta_{\rm gauge} m_h^2$ and $\delta_{\rm gauge}\lambda_h$ using the parameters of Model 1c. The linear behavior of the mass integrand and the $1/p$ behavior of the quartic integrand reflect the expected quadratic and logarithmic sensitivity of these operators at energies beneath the mass of the fermion partners. The q' and t' are degenerate with mass $\sim .36/L_1$. See the text for why the peak of the mass integrand is at $p \sim .2/L_1$.

where $\hat{\lambda} = \lambda/\epsilon$ and $F(G, G_{\rm br}, G^c, G^c_{\rm br})$ is

$$F(G, G_{\rm br}, G^c, G^c_{\rm br}) = 4 + \hat{\lambda}^2 p^2 (3GG^c + 3G_{\rm br}G^c_{\rm br} + GG^c_{\rm br} + G_{\rm br}G^c) + 4\hat{\lambda}^4 p^4 GG_{\rm br}G^c G^c_{\rm br}. \tag{12.25}$$

These expressions manifestly exhibit collective breaking.

It is again very instructive to match the results with our expectations from effective field theory. As in the bosonic case, we can expand the integrands to lowest order in momenta and integrate with a hard momentum cutoff Λ_0:

$$\delta_{\rm fermion} m_h^2 \sim -\frac{3\lambda_{\rm top}^2}{8\pi^2}\Lambda_0^2 + \mathcal{O}(\Lambda_0^4/f_\pi^2), \qquad \delta_{\rm fermion}\lambda_h \sim \frac{3\lambda_{\rm top}^2}{16\pi^2}\log\Lambda_0^2 + \mathcal{O}(\Lambda_0^4/f_\pi^4). \tag{12.26}$$

These are precisely the low energy expectations for the contribution of top loops to the Higgs doublet mass and quartic. The integrands from equations (12.23) and (12.24) appear in Figure 12.3. The mass integrand starts off linearly, corresponding to the low energy quadratic divergence. In Model 1c, the q' and t' are degenerate

with mass $\sim .36/L_1$, so $N = 2$ and the peak in the integrand is at $p \sim .2/L_1$ as expected. The quartic integrand is dominated by the $1/p$ piece corresponding to the logarithmic low energy behavior, though there is a slight bump at the mass of the q' and t'. Unlike the quartic integrands in the gauge sector, these integrals are already very suppressed at the mass of the KK fermion modes $\sim \pi/L_1$, which is as expected because the quartic contribution is finite at one-loop with the fermion content of [54].

13

Numerical Examples

Now that we understand the structure of the Coleman-Weinberg integrals, we want to input specific values of the AdS parameters to find the generic value of the physical Higgs mass in this setup. In order to deal with the infrared logarithmic divergences in the quartic coupling, we do each Coleman-Weinberg integral from $p = m_{h_0}$ to ∞, iterating the calculations until we get a stable m_{h_0} value. We choose the parameters of our theory to fit the known top Yukawa coupling, electroweak gauge coupling, and electroweak scale. In Model 1, we allow for an unknown $\delta_{\text{other}} m_h^2$ contribution to the Higgs potential in order to fix the pion decay constant at $f_\pi = 1$ TeV, and this will generically require fine-tuning at the 10% level. In Model 2, we arrange the gauge and fermion contributions to the doublet mass to cancel against each other with no considerable fine-tuning by shrinking the conformal window, but in these models f_π will be significantly lower, and hence the t', q' and W' partners will be generically lighter. Finally in Model 3, we show a compromise where we shrink the conformal window but still allow for a $\delta_{\text{other}} m_h^2$ piece, yielding sufficiently heavy partner particles

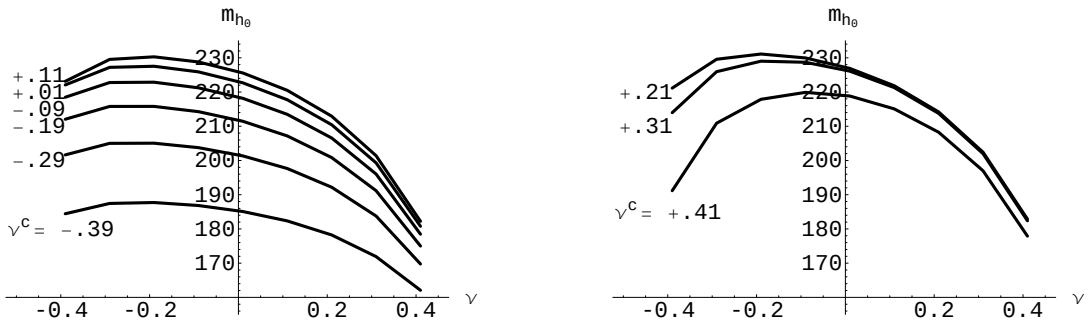

Figure 13.1: Values of the physical Higgs mass in Model 1, keeping $f_\pi = 1$ TeV fixed and varying the bulk masses ν and ν^c ($g' = 2g_{EW}$). Outside of the region $|\nu|, |\nu^c| \lesssim .4$, it is difficult to satisfy the condition $\lambda_{\text{top}} = 1$.

with no considerable fine-tuning (25%).

We begin in Model 1 by choosing the brane separation to generate the full hierarchy between M_{Pl} and f_π, namely $\epsilon \sim 10^{-15}$. Once this AdS geometry is fixed, it is clear from equation (9.3) that in order for g_ρ to remain perturbative, we need the gauge kinetic terms on the UV boundary to be close to zero (*i.e.* choose the Landau pole of the gauge couplings to be as close to the UV as possible) and therefore we must take approximately $g_1 = g_2$. In terms of the electroweak gauge coupling, $g' = 2g_{EW}$. When we do consider cases where $g_1 \neq g_2$, we take $z_2 = 0$ for simplicity. We still have the freedom to choose the bulk masses of the fermions. Looking at equation (10.1), the requirement of $\lambda_{\text{top}} = 1$ restricts the range of ν and ν^c to around $|\nu|, |\nu^c| \lesssim .4$. As remarked earlier in equation (11.2), to minimize the logarithmic correction to m_h^2 from the fermion sector, we want the t' and q' fermion partners to be roughly degenerate, and this corresponds to the limit $\nu = -\nu^c$. To make the t' and q' as light as possible, we want to send ν as large as possible while still maintaining the desired top Yukawa coupling, corresponding to $\nu \to 0.4$.

The details of Model 1 are presented in Table 13.1, with some variations of the parameters to illustrate the stability of these results. In particular, we allow g' to be larger than $2g_{EW}$ in Model 1c to raise the W' mass. With the addition of a $\delta_{\text{other}} m_h^2$ contribution to the Higgs potential, there is no problem getting a viable phenomenology which reproduces the electroweak scale while fixing $f_\pi = 1$ TeV. Figure 13.1 is a plot of the physical Higgs mass as a function of ν and ν^c when $g' = 2g_{EW}$. Generically the physical Higgs falls within the range $m_{h_0} \sim 150-250$ GeV. As expected, the lightest physical Higgs occurs when $\nu \sim -\nu^c \sim 0.4$. Because $\lambda_{\text{top}} \sim 1$, the fermionic contribution to the Higgs doublet mass is generically large, ranging from $\sim 300-500$ GeV, whereas for $g' = 2g_{EW}$, the gauge contribution is fixed at ~ 80 GeV. This large difference between the gauge and fermion contributions to the doublet mass is expected from equations (11.2) and (11.8). Fine-tuning of the mass parameters is at the $\sim 10\%-20\%$ level, and $\delta_{\text{other}} m_h^2$ is responsible for canceling nearly all of the fermionic contribution. The large quartic coupling comes almost entirely from the fermion sector, though the contributions equalize as g' increases.

The goal of Model 2 is to see if it is possible to reduce the amount of fine-tuning and balance the gauge and fermion contributions. Once the brane separation ϵ is chosen, we have very little freedom in the gauge sector if we want g_ρ to be perturbative. However, simply reducing the scale of the UV brane will not help very much. The real problem is the numerically large difference between the gauge and fermion contributions mentioned above, and short of raising g_{EW} or lowering λ_{top}, our only freedom is to raise the mass of the W', but this can only get us so far. In order to dispense with the $\delta_{\text{other}} m_h^2$ piece altogether, we have to bring the overall contributions down,

and this can be accomplished by lowering the pion decay constant f_π. Of course, doing so will cause the W' to be unacceptably light unless we also raise the value of g'. By decreasing the brane separation to make ϵ larger than 10^{-15}, we can crank the gauge coupling to $g' = (\text{a few})g_{EW}$ while still keeping a perturbative g_ρ. Table 13.2 presents the parameters of Model 2 where no $\delta_{\text{other}} m_h^2$ piece is included. In Model 2a, we see that simply increasing ϵ yields a very light W'. Model 2b is much safer, though g_ρ is approaching the edge of the perturbative regime. In Model 2c, the conformal window is very small, and we see that there is no problem having reasonably heavy partners without including a $\delta_{\text{other}} m_h^2$ contribution to artificially raise f_π as long as the conformal window is small enough.

Finally, Model 3 represents a compromise between the competing tensions of the theory. We allow a $\delta_{\text{other}} m_h^2$ piece to enforce $f_\pi = 800$ GeV, but we shrink the conformal window to allow $g' \sim 4g_{EW}$, effectively putting the UV brane at the intermediate scale. To have the lightest q' and t' possible, we push ν and $-\nu^c$ to the edge of the region where we can satisfy the condition $\lambda_{\text{top}} = 1$. This model comes the closest to realizing the original vision of the littlest Higgs, in that the value of f_π does not involve an unacceptable level of fine-tuning, the q', t' and W' partners are around 1 TeV in mass, and the scale m_ρ where we see resonances of the strong dynamics is near 10 TeV. Note that $g_\rho \sim 10$ in this model, so we are imagining a very small N CFT. We see that the mass of the Higgs is around 200 GeV, though this value increases substantially if we reduce g' or ν.

In summary, the littlest Higgs in AdS space has a healthy phenomenology if we allow ourselves maximal freedom to raise the mass of the W', lower the mass of the

q' and t', and include some (unknown) sources of additional $SU(5)$ violation to get a less negative doublet mass value. In CFT language, we see that the favored regions of parameter space are small N theories with small conformal windows, though with some amount of fune-tuning we can still have small g_ρ and ϵ. Note that these tensions are numerical tensions and not parametric tensions. If we could lower λ_{top} and g_{EW}, then we could have an exceptionally light Higgs boson with no fine-tuning. The extent to which these dimensionless parameters are large are the degree to which we have to work to enforce a large separation between the pion decay constant and the electroweak scale.

	Model 1a	Model 1b	Model 1c
L_1	$(2.6\text{ TeV})^{-1}$	$(2.6\text{ TeV})^{-1}$	$(5.2\text{ TeV})^{-1}$
ϵ	10^{-15}	10^{-15}	10^{-15}
g_{EW}	0.63	0.63	0.63
v_{EW}	246 GeV	246 GeV	246 GeV
g'	$2g_{EW}$	$2g_{EW}$	$3g_{EW}$
g_ρ	5.2	5.2	10.4
f_π	1.0 TeV	1.0 TeV	1.0 TeV
m_ρ	6.2 TeV	6.2 TeV	12.2 TeV
λ_{top}	1.0	1.0	1.0
ν	$+0.42$	$+0.20$	$+0.49$
ν^c	-0.42	-0.10	-0.49
λ	0.26	0.23	0.11
$m_{W'}$	630 GeV	630 GeV	950 GeV
$m_{t'}$	2.0 TeV	3.0 TeV	1.9 TeV
$m_{q'}$	2.0 TeV	3.5 TeV	1.9 TeV
m_{h_0}	160 GeV	210 GeV	210 GeV
$\delta_{\text{gauge}}m_h^2$	$+(80\text{ GeV})^2$	$+(80\text{ GeV})^2$	$+(130\text{ GeV})^2$
$\delta_{\text{fermion}}m_h^2$	$-(310\text{ GeV})^2$	$-(440\text{ GeV})^2$	$-(330\text{ GeV})^2$
$\delta_{\text{other}}m_h^2$	$+(270\text{ GeV})^2$	$+(410\text{ GeV})^2$	$+(270\text{ GeV})^2$
$\delta_{\text{gauge}}\lambda_h$	0.04	0.04	0.15
$\delta_{\text{fermion}}\lambda_h$	0.18	0.32	0.20
m_ϕ	430 GeV	430 GeV	1240 GeV
$\lambda_{\phi hh}$	—	—	560 GeV

Table 13.1: Parameters and results for Model 1. In this model, we allow the addition of a $\delta_{\text{other}}m_h^2$ contribution to the Higgs potential in order to set the pion decay constant $f_\pi = 1$ TeV. By fixing $\epsilon = 10^{-15}$, we are limited in how high we can push the g' coupling, and hence the mass of the W'. Fine-tuning in this model is usually of the order of 10% – 20%.

	Model 2a	Model 2b	Model 2c
L_1	$(530\text{ GeV})^{-1}$	$(1.7\text{ TeV})^{-1}$	$(1.3\text{ TeV})^{-1}$
ϵ	10^{-5}	10^{-5}	10^{-1}
g_{EW}	0.63	0.63	0.63
v_{EW}	246 GeV	246 GeV	246 GeV
g'	$2g_{EW}$	$5g_{EW}$	$8g_{EW}$
g_ρ	3.0	10.5	7.6
f_π	580 GeV	420 GeV	340 GeV
m_ρ	1.2 TeV	5.2 TeV	3.0 TeV
λ_{top}	1.0	1.0	1.0
ν	$+0.17$	$+0.49$	$+0.49$
ν^c	-0.17	-0.49	-0.49
λ	0.63	0.08	0.10
$m_{W'}$	360 GeV	650 GeV	850 GeV
$m_{t'}$	820 GeV	940 GeV	520 GeV
$m_{q'}$	820 GeV	940 GeV	520 GeV
m_{h_0}	120 GeV	220 GeV	260 GeV
$\delta_{\text{gauge}} m_h^2$	$+(20\text{ GeV})^2$	$+(80\text{ GeV})^2$	$+(70\text{ GeV})^2$
$\delta_{\text{fermion}} m_h^2$	$-(90\text{ GeV})^2$	$-(180\text{ GeV})^2$	$-(200\text{ GeV})^2$
$\delta_{\text{gauge}} \lambda_h$	0.01	0.15	0.07
$\delta_{\text{fermion}} \lambda_h$	0.12	0.26	0.51
m_ϕ	90 GeV	860 GeV	880 GeV
$\lambda_{\phi hh}$	—	800 GeV	1.1 TeV

Table 13.2: Parameters and results for Model 2. In this model, we do not set f_π by hand, and rely on a natural cancellation between the gauge and fermion sectors to generate the hierarchy between f_π and v_{EW}. As such, f_π is quite low, and we need to raise g' so as not to have too light a W'. In order to allow for larger gauge couplings, we need to shrink the size of the conformal window.

	Model 3a	Model 3b	Model 3c
L_1	$(4.2\text{ TeV})^{-1}$	$(4.0\text{ TeV})^{-1}$	$(3.7\text{ TeV})^{-1}$
ϵ	10^{-8}	10^{-10}	10^{-12}
g_{EW}	0.63	0.63	0.63
v_{EW}	246 GeV	246 GeV	246 GeV
g'	$4g_{EW}$	$3.5g_{EW}$	$3.0g_{EW}$
g_ρ	10.4	10.1	9.2
f_π	800 GeV	800 GeV	800 GeV
m_ρ	9.8 TeV	9.5 TeV	8.7 TeV
λ_{top}	1.0	1.0	1.0
ν	+0.49	+0.48	+0.48
ν^c	−0.49	−0.48	−0.48
λ	0.08	0.08	0.10
$m_{W'}$	1.0 TeV	850 GeV	730 GeV
$m_{t'}$	1.6 TeV	1.5 TeV	1.5 TeV
$m_{q'}$	1.6 TeV	1.5 TeV	1.5 TeV
m_{h_0}	210 GeV	210 GeV	190 GeV
$\delta_{\text{gauge}}m_h^2$	$+(110\text{ GeV})^2$	$+(130\text{ GeV})^2$	$+(100\text{ GeV})^2$
$\delta_{\text{fermion}}m_h^2$	$-(290\text{ GeV})^2$	$-(300\text{ GeV})^2$	$-(270\text{ GeV})^2$
$\delta_{\text{other}}m_h^2$	$+(220\text{ GeV})^2$	$+(220\text{ GeV})^2$	$+(200\text{ GeV})^2$
$\delta_{\text{gauge}}\lambda_h$	0.15	0.14	0.12
$\delta_{\text{fermion}}\lambda_h$	0.22	0.22	0.19
m_ϕ	1.3 TeV	1.1 TeV	900 GeV
$\lambda_{\phi hh}$	930 GeV	630 GeV	360 GeV

Table 13.3: Parameters and results for Model 3. In this model, we try to equalize the contributions to the Higgs potential from $\delta_{\text{gauge}}m_h^2$, $\delta_{\text{fermion}}m_h^2$, and $\delta_{\text{other}}m_h^2$. The pion decay constant is fixed at $f_\pi = 800$ GeV. The conformal window is smaller than Model 1 but larger than Model 2, and there is more freedom in the choice of g'. In order for the fermionic contribution to the Higgs potential to be small, we adjusted ν and ν^c such that t' and q' were as light as possible while still allowing $\lambda_{\text{top}} = 1$. Note that as we decrease ϵ, we are forced to decrease g', so the W' mass decreases.

14

Toward a Realistic Model with T-Parity

To construct a realistic little Higgs model, we need to include the entire fermion sector of the standard model. One construction is to simply introduce the remaining fermions on the IR brane and include explicit $SO(5)$ violating couplings between these fermions and the Higgs doublet. This would give rise to a divergent Higgs mass sensitive to the local Planck scale (*i.e.* $1/L_1$), but because the non-top Yukawa couplings are sufficiently small, these quadratic divergences would not spoil the successes of the littlest Higgs. While this construction is consistent, it is not particularly elegant. Not only does it not explain the hierarchy in the Yukawa couplings, but it does not yield a manifestly finite Coleman-Weinberg potential.

In this section, we sketch one possible AdS implementation of the littlest Higgs where all the fermions live in the bulk of AdS, and the interactions on the IR brane preserve the $SO(5)$ symmetry protecting the Higgs mass. Just like in Section 12, the

Higgs potential is generated only through loops that stretch from the IR brane to the UV brane. We would also like to take advantage of some of the previous successes of AdS model building; for example, if the bulk fermions have different bulk masses, we can naturally generate a hierarchy in the Yukawa couplings while simultaneously suppressing flavor changing neutral currents [45, 41, 50, 49]. As we will see, however, there is a tension between Yukawa coupling hierarchies and T-parity.

Given this tension, one may wonder why we want to implement T-parity in the first place. A main constraint on little Higgs theories has been corrections to precision electroweak observables coming from couplings between standard model fields and the new massive gauge fields and scalars in the little Higgs [48, 33, 34, 43, 55, 21, 78]. If these new bosons have mass around 1 TeV, then they generate dimension six standard model operators through tree-level exchange suppressed by the scale 1 TeV. However, precision electroweak data suggests that the natural suppression scale should be closer to $5 - 10$ TeV [14]. The difference between the mass scale necessary to stabilize the electroweak scale (1 TeV) and the mass scale suggested by precision electroweak data (10 TeV) is known as the "little hierarchy" problem. In AdS_5 language, there is no symmetry that forbids the IR brane operator

$$\sqrt{-g_{\mathrm{ind}}}\delta(z - L_1)\,\mathrm{tr}\,(F_{\mu\nu}\Sigma F^{*\mu\nu}\Sigma^*)\,, \tag{14.1}$$

and when electroweak symmetry is broken, this operator will yield a contribution to the S parameter of order $(v_{EW}/f_\pi)^2$. As we have seen, while there is a parametric separation between v_{EW} and f_π, numerically the scales can be close and S may be dangerously large.

In models with T-parity [22, 23, 60], there is $\mathbf{Z}_2$ symmetry under which the stan-

dard model fields (including the Higgs) are even but the new massive gauge fields and scalars are odd. Therefore, tree-level exchange of non-SM bosons is forbidden and the dimension six operators generated by integrating out non-SM bosons are suppressed by a loop factor. T-parity is a simple solution to the little hierarchy problem, and generically little Higgs theories with T-parity are safe from excessive precision electroweak corrections. Of course, another way to avoid precision electroweak constraints is to consider a little Higgs mechanism with a custodial $SU(2)$ symmetry [20, 19], and it would be interesting to try to implement such little Higgs theories in AdS space.

In the original T-parity formulation of the $SU(5)/SO(5)$ littlest Higgs [23], fermions transformed non-linearly under the $SU(5)$ global symmetry, making it difficult to imagine the bulk fermion content of an AdS extension. In [60], the $SU(5)/SO(5)$ littlest Higgs was extended to an $SU(5)^2/SO(5)$ model in which all fermions transform linearly under $SU(5)^2$ symmetry, making it much easier to imagine a UV completion of the low energy effective theory. One difficulty of implementing a realistic $SU(5)^2/SO(5)$ model in AdS space (or even a $SU(5)/SO(5)$ without T-parity), is the necessity gauging $U(1)_B$ in the bulk. Because of this $U(1)_B$, we are forced to introduce a top-type and a bottom-type quark doublet in the bulk, and then use boundary conditions on the UV brane to identify a linear combination of the two doublets as the standard model quark doublet. Therefore, this model has a large number of $SU(5)$ muliplets to allow for T-parity and the $U(1)_B$ nuisance, and it may be interesting to see the effect of such a large number of bulk fermions on the $SU(3)_C$ and $SU(2)_{EW}$ beta functions to see whether we maintain perturbative gauge couplings.

The bulk symmetry in this model is $SU(5)_L \times SU(5)_R$ which is broken to a diagonal $SO(5)_V$ on the IR brane. We can characterize this breaking pattern by the vacuum expectation values of three scalars. Imagine three 5×5 matrix fields Φ_L, Φ_R, and Φ_T on the IR brane that transform under $SU(5)_L \times SU(5)_R$ as

$$\Phi_L \to L\Phi_L L^T, \qquad \Phi_R \to R\Phi_R R^T, \qquad \Phi_T \to L\Phi_T R^\dagger, \tag{14.2}$$

where $L \in SU(5)_L$ and $R \in SU(5)_R$. These fields take vacuum expectation values

$$\langle \Phi_L \rangle = \Sigma_0, \qquad \langle \Phi_R \rangle = \Sigma_0, \qquad \langle \Phi_T \rangle = \mathbb{1}. \tag{14.3}$$

We see readily that the vevs of $\Phi_i, i = L, R$ break $SU(5)_i$ to $SO(5)_i$, and the vev of Φ_T selects the diagonal subgroup of $SO(5)_L \times SO(5)_R$.

Let T_i^a be the generators of $SO(5)_i$ and X_i^a be the generators of $SU(5)_i/SO(5)_i$. The Goldstone matrices of $SU(5)^2/SO(5)$ can be parametrized as

$$\Pi_L = \pi_L^a X_L^a, \qquad \Pi_R = \pi_R^a X_R^a, \qquad \Pi_T = \pi_T^a (T_L^a - T_R^a). \tag{14.4}$$

Performing the broken symmetry on the vacuum, the CCWZ prescription [28, 18] tells us that

$$\Sigma_L = e^{2i\Pi_L/f_5}\Sigma_0, \qquad \Sigma_R = e^{2i\Pi_R/f_5}\Sigma_0, \qquad \Sigma_T = e^{i\Pi_L/f_5} e^{2i\Pi_T/f_5} e^{-i\Pi_R/f_5}, \tag{14.5}$$

transform like their counterparts in equation (14.2). For simplicity, we have given each Σ field the same 5D decay constant f_5, which as before will be taken to infinity in any calculation.

In addition to introducing an $SU(3)_C \times U(1)_B$ bulk gauge symmetry, we also gauge a $SU(2)_{L1} \times SU(2)_{L2} \times SU(2)_R \times U(1)_Y$ subgroup of $SU(5)^2$, *i.e.* we give this subgroup

Neumann boundary conditions on the UV brane.[1] The subgroup is imbedded as

$$Q^a_{L1} = \begin{pmatrix} \sigma^a/2 & & \\ & & \\ & & \end{pmatrix}_L, \qquad Q^a_{L2} = \begin{pmatrix} & & \\ & & \\ & & -\sigma^{*a}/2 \end{pmatrix}_L, \qquad Q^a_R = \begin{pmatrix} \sigma^a/2 & & \\ & & \\ & & -\sigma^{*a}/2 \end{pmatrix}_R, \tag{14.6}$$

$$A = \frac{1}{2}\,\mathrm{diag}(1,1,0,-1,-1)_L, \tag{14.7}$$

where subscripts L and R on the matrices indicate whether the gauge generator belongs to $SU(5)_L$ or $SU(5)_R$. The hypercharge generator is $Y = A + B$, and when $SU(5)^2$ breaks to $SO(5)$, the electroweak $SU(2)$ is generated by

$$Q^a_{EW} = Q^a_{L1} + Q^a_{L2} + Q^a_R. \tag{14.8}$$

Note that the same subgroup of $SU(5)_L$ is gauged as in Section 9.

We identify the Goldstone matrix Π_L with the Goldstone matrix in the original $SU(5)/SO(5)$ little Higgs. As shown in [60] the Goldstones in Π_R and Π_T are either eaten by the broken $SU(2)$ gauge bosons or can be given large masses through radiatively generated gauge interactions or through plaquette operators. These plaquette operators live on the IR brane and explicitly break $SU(5)^2$ even before the Φ fields take their vaccum expectation value. However, they do so in a way that maintains the $SU(2)^3$ subgroup of $SU(5)^2$, so the low energy gauge structure is not modified.

In the fermion sector, the action of T-parity effectively maps a $\bar{\mathbf{5}}$ of $SU(5)_L$ onto a $\mathbf{5}$ of $SU(5)_L$ and leaves representations of $SU(5)_R$ unchanged. One linear combination of the $\bar{\mathbf{5}}_L$ and $\mathbf{5}_L$ becomes a standard model fermion, and a $\mathbf{5}_R$ marries the other combination to become the heavy T-odd partner to the standard model fermion.

[1] In order to give $U(1)_Y$ a different gauge coupling from $SU(2)_{Li}$ we also introduce boundary gauge kinetic terms.

Therefore, for each $SU(5)$ multiplet Ψ corresponding to a standard model fermion, we introduce three bulk Dirac fermions $\mathbf{\Psi}_{L1}$, $\mathbf{\Psi}_{L2}$, and $\mathbf{\Psi}_R$. We choose these fields to have non-vanishing upper (left-handed) components on the IR brane. These upper component Weyl fields Ψ_{L1}, Ψ_{L2}, and Ψ_R transform under $SU(5)_L \times SU(5)_R$ as:

	$SU(5)_L$	$SU(5)_R$	Other Quantum Numbers
Ψ_{L1}	$\bar{\mathbf{5}}$	–	Defined by Ψ
Ψ_{L2}	$\mathbf{5}$	–	Defined by Ψ
Ψ_R	–	$\mathbf{5}$	Conjugate to Ψ

(14.9)

In the last column we mean that Ψ_{L1} and Ψ_{L2} have identical $SU(3)_C \times U(1)_B$ quantum numbers and Ψ_R has the conjugate quantum numbers. For convenience, we also introduce the notation for bulk Dirac fermions $\mathbf{\Psi}^c_{L1}$, $\mathbf{\Psi}^c_{L2}$, and $\mathbf{\Psi}^c_R$ whose lower (right-handed) components are non-vanishing on the IR brane. These lower component Weyl fields Ψ^c_{L1}, Ψ^c_{L2}, and Ψ^c_R transform under $SU(5)_L \times SU(5)_R$ the same way as Ψ_{L1}, Ψ_{L2}, and Ψ_R but have opposite other quantum numbers to their counterparts.

	$SU(5)_L$	$SU(5)_R$	Other Quantum Numbers
Ψ^c_{L1}	$\bar{\mathbf{5}}$	–	Conjugate to Ψ
Ψ^c_{L2}	$\mathbf{5}$	–	Conjugate to Ψ
Ψ^c_R	–	$\mathbf{5}$	Defined by Ψ

(14.10)

We now define the action of T-parity. Start with the 5×5 matrices

$$\Omega = \begin{pmatrix} -\mathbb{1} & & \\ & 1 & \\ & & -\mathbb{1} \end{pmatrix}, \qquad Z = \Sigma_0 \Omega, \qquad Z^2 = \Omega^2 = \mathbb{1}. \tag{14.11}$$

Let A_i be the $SU(5)_i$ gauge fields for $i = L, R$. The action of T-parity looks like charge conjugation on $SU(5)_L$.

$$A_L \to -ZA_L^T Z, \qquad A_R \to \Omega A_R \Omega. \tag{14.12}$$

In terms of the gauge fields on the UV brane, T-parity maps $SU(2)_{L1}$ to $SU(2)_{L2}$ and leaves $SU(2)_R$ and $U(1)_Y$ invariant. Note that T-parity forces the gauge couplings g_{L1} and g_{L2} to be equal. Before $SU(2)^3$ is broken to the electroweak $SU(2)$, there are two T-even gauge bosons and one T-odd gauge boson.

$$Q^a_{EW} = Q^a_{L1} + Q^a_{L2} + Q^a_R, \qquad Q^a_+ = Q^a_{L1} + Q^a_{L2} - 2Q^a_R, \qquad Q^a_- = Q^a_{L1} - Q^a_{L2}. \tag{14.13}$$

After $SU(2)^3$ breaks to $SU(2)$, $Q^a_\pm$ get masses. Q^a_- has a mass $g_L f_4 \sim 1$ TeV, and by T-parity it cannot contribute to tree-level dimension six operators. However, Q^a_+ can contribute to tree-level dimension six operators, so we must choose $SU(2)_R$ to have a large $g_R \sim 4\pi$ gauge coupling in order for Q^a_+ to get a mass of order $g_R f_4 \sim 10$ TeV. Also, this forces Q^a_+ to be mostly Q^a_R, and if standard model fields are uncharged under $SU(2)_R$, then precision electroweak corrections from tree-level Q^a_+ exchange is suppressed. Note that in order to really have a large g_R, we would have to have a very small conformal window.

On the Goldstone matrices, T-parity acts as

$$\Sigma_L \to Z\Sigma_L^\dagger Z, \qquad \Sigma_R \to \Omega \Sigma_R \Omega, \qquad \Sigma_T \to Z\Sigma_L \Sigma_T \Omega. \tag{14.14}$$

The action of T-parity on Σ_T is indeed a $\mathbf{Z}_2$ symmetry. On the fields in Π_L as defined in (9.8), h is T-even, and η and ϕ are T-odd, therefore ϕ and η can safely have 1 TeV masses without affecting precision electroweak data. Also, it is a quick check that the Goldstone kinetic terms are invariant under T-parity.

Finally, the action of T-parity on the fermions must be consistent with the gauge sector in equation (14.12). Again, T-parity looks like charge conjugations between a $\bar{\mathbf{5}}_L$ ($\mathbf{\Psi}_{L1}$) and a $\mathbf{5}_L$ ($\mathbf{\Psi}_{L2}$):

$$\mathbf{\Psi}_{L1} \to Z\mathbf{\Psi}_{L2}, \qquad \mathbf{\Psi}_{L2} \to Z\mathbf{\Psi}_{L1}, \qquad \mathbf{\Psi}_R \to \Omega\mathbf{\Psi}_R, \tag{14.15}$$

with similar formulas for the Ψ^c fermions. Before introducing the specific quantum numbers of the standard model fields, note that we can give mass to the T-odd combination of Ψ_{L1} and Ψ_{L2} via the interaction on the TeV brane:

$$\mathcal{L}_{T-\text{odd mass}} = \sqrt{-g_{\text{ind}}}\delta(z - L_1)\kappa\left(\Psi_{L1}\Sigma_T\Psi_R + \Psi_{L2}\Sigma_L\Sigma_T\Psi_R + h.c.\right). \tag{14.16}$$

We can write down a similar interaction for Ψ^c. Because Σ_T depends on Π_L, one might worry that this interaction could give rise to a radiative correction the the Higgs mass. In the case that Ψ is supposed to describe an electroweak doublet, Ψ_{L1}, Ψ_{L2}, and Ψ_R have boundary conditions that happen to preserve an $SU(3)^2$ symmetry that is enough to protect the Higgs mass. If Ψ describes an electroweak singlet however, there is no symmetry protecting the Higgs mass and there will be a radiatively generated potential. Just as for the top sector from Section 12, though, the interaction in equation (14.16) exhibits collective breaking to the extent that a potential is only generated if both Ψ_{Li} and Ψ_R have $SU(5)$ violating boundary conditions.

The T-invariant Yukawa interactions between Ψ, Ψ^c, and the Higgs take the form

$$\mathcal{L}_{\text{Higgs}} = \sqrt{-g_{\text{ind}}}\delta(z - L_1)\lambda\left(\Psi_{L1}\Sigma_L\Psi^c_{L1} + \Psi_{L2}\Sigma_L^\dagger\Psi^c_{L2} + h.c.\right). \tag{14.17}$$

This is simply the T-invariant generalization of equation (9.16). Already, we can see the tension between Yukawa coupling hierarchies and the masses of the T-odd fermion

partners. If λ is $\mathcal{O}(1)$, we know we can generate the Yukawa coupling hierarchy through the different overlaps of Ψ_L and Ψ_L^c with the IR brane for each generation. However, the same overlap functions would enter into equation (14.16). We could of course make κ large, insist that Ψ_R and Ψ_R^c have maximum overlap with the IR brane, and also split the Yukawa hierarchy equally between the Ψ_L and Ψ_L^c overlaps. But given that the electron mass is a factor of 10^6 lighter than the top quark, we would find that the T-odd partner to the electron is $\sqrt{10^6} = 10^3$ lighter than the T-odd partner of the top quark! We will discuss this issue further at the end of this section.

We now give the quantum numbers of a standard model generation. As mentioned already, there are slight complications coming from the fact that we need to gauge $U(1)_B$. This forces us to introduce a top-type doublet and a bottom-type doublet. Ignoring a possible right-handed neutrino, we have the following $SU(5)_L \times SU(5)_R$ matter content, using the notation of equations (14.9) and (14.10):

	$SU(3)_C$	$U(1)_B$
U	$\mathbf{3}$	$+2/3$
U^c	$\bar{\mathbf{3}}$	$-2/3$
D	$\mathbf{3}$	$-1/3$
D^c	$\bar{\mathbf{3}}$	$+1/3$
L	$-$	-1
L^c	$-$	$+1$

(14.18)

Looking at the top sector in detail, we imbed the top-type doublet and top singlet

fields as

$$U_{L1} = \begin{pmatrix} q_1^U \\ - \\ - \end{pmatrix}, \qquad U_{L2} = \begin{pmatrix} - \\ - \\ q_2^U \end{pmatrix}, \qquad U_R = \begin{pmatrix} q_M^U \\ - \\ - \end{pmatrix}, \tag{14.19}$$

$$U_{L1}^c = \begin{pmatrix} - \\ u_1^c \\ - \end{pmatrix}, \qquad U_{L2}^c = \begin{pmatrix} - \\ u_2^c \\ - \end{pmatrix}, \qquad U_R^c = \begin{pmatrix} - \\ u_M^c \\ - \end{pmatrix}, \tag{14.20}$$

where dashes indicate fields that have Dirichlet boundary conditions on the UV brane and therefore do not have zero modes. As in Section 10, the physical top doublet and singlet will be mixtures of these zero modes and components from the KK modes. After $SU(2)^3$ breaks to $SU(2)_{EW}$, the q^U and u^c fields have the right standard model quantum numbers. At low energies, the interaction in equation (14.16) generates the mass terms

$$\mathcal{L}_{\text{mass}} \sim m_q^U \; q_M^U (q_1^U + q_2^U) + m_u \; u_M (u_1 + u_2), \tag{14.21}$$

so at low energies, the fields

$$q_{\text{even}}^U = \frac{1}{\sqrt{2}}(q_1^U - q_2^U), \qquad u_{\text{even}}^c = \frac{1}{\sqrt{2}}(u_1^c - u_2^c), \tag{14.22}$$

are massless, T-even fermions, and the orthogonal T-odd combinations get masses m_q^U and m_u. At energies below the T-odd masses, the interaction in equation (14.17) generates the Yukawa coupling

$$\mathcal{L}_{\text{Yukawa}} \sim \lambda^U \, q_{\text{even}}^U h u_{\text{even}}^c. \tag{14.23}$$

As in Section 9, the physical Yukawa coupling involves wavefunction renormalization from mixing with heavy KK modes.

By this prescription, we will have a massless $q^U_{\rm even}$ and a massless $q^D_{\rm even}$ both with the quantum numbers of a quark doublet. We want to identify one combination of $q^U_{\rm even}$ and $q^D_{\rm even}$ to be the standard model quark doublet and the other combination to be heavy. Looking at the D field:

$$D_{L1} = \begin{pmatrix} - \\ - \\ q_2^D \end{pmatrix}, \qquad D_{L2} = \begin{pmatrix} q_1^D \\ - \\ - \end{pmatrix}, \qquad D_R = \begin{pmatrix} - \\ - \\ q_M^D \end{pmatrix}. \tag{14.24}$$

(The subscripts 1, 2 on q_1^D and q_2^D indicate whether the field transforms under $SU(2)_{L1}$ or $SU(2)_{L2}$, and *not* whether they came from the field D_{L1} or D_{L2}.) Consistent with $SU(2)_i$, we can set boundary conditions on the UV brane for $(q_1^U - q_1^D)$, $(q_2^U - q_2^D)$, and $(q_M^U - q_M^D)$ to vanish. The $(q_M^U - q_M^D)$ boundary condition is necessary because without it, there would be an additional massless doublet. At the end of the day, the combination

$$q_{\rm even} = \frac{1}{\sqrt{2}}(q^U_{\rm even} + q^D_{\rm even}) \tag{14.25}$$

is the massless standard model quark doublet and it couples in the appropriate way to u^c and d^c. Again, the physical standard model fermions will be mixtures of these T-even zero modes with components of T-even KK states. In the lepton sector, we imbed the lepton doublet and singlet analogously to equations (14.19) and (14.19), but if we do not have a right-handed neutrino, we do not need to have a separate electron-type and neutrino-type lepton doublet.

While it might be interesting to calculate the Higgs radiative potential in this T-parity extension of the AdS_5 littlest Higgs, there is a basic model building question that needs to be addressed before such a calculation would become meaningful. As

we saw in Section 12, the Higgs potential depends on the bulk propagators for the fermions, and these in turn depend heavily on the choice of fermion bulk masses. If we simply want to reproduce the Higgs Yukawa matrix and ignore flavor-violating four-fermion operators, then we can simply choose some reasonable fermion bulk masses that give $\mathcal{O}(1)$ overlap with the IR brane and then dial the Yukawa matrix by hand on IR brane to get the desired low energy Yukawa structure. In this case, the mass of *all* the T-odd fermions can be pushed up to around 10 TeV with a reasonable value of κ in equation (14.16). (See [60] for a reason why the T-odd fermions most likely need to be closer to 1 TeV.)

If, however, we want to naturally explain the smallness of four-fermion operators that contribute to FCNCs, then we want the different fermion generations to be localized in different parts of the bulk. This means that there will be a hierarchy in the overlap of the different generations with the IR brane, and while this feature is desirable from the point of view of trying to understand the Yukawa hierarchy, it is disastrous in light of equation (14.16), where the overlap functions also determine the masses of the T-odd fermions. We expect this to be a general issue with trying to build AdS models of the little Higgs with T-parity. The problem is not with T-parity itself; indeed, for a single generation where flavor is not an issue we can easily incorporate T-parity in AdS space. The problem is that T-parity wants to be flavor blind (*i.e.* all of the T-odd fermions need to have roughly the same mass), whereas our implementation of T-parity makes explicit reference to flavor because the T-odd mass terms inherit flavor specific overlap functions. We may have some freedom to generate the Yukawa hierarchy through a combination of overlap functions

and IR brane matrix elements, but in the context of AdS model building, there is no explanation for why these two effects would naturally work in the same direction. There may be other implementations of T-parity in AdS space that avoid these issues, but in this model there is an important tension between T-parity and flavor.

15

Future Directions

We have seen that the collective breaking structure of little Higgs theories can be naturally implemented in AdS space. The 5D Coleman-Weinberg potential has a particularly illuminating structure, in that corrections to the Higgs potential are proportional to *two* differences of 5D Greens functions. In this part of the thesis, we have worked out the gauge and fermion structure for the $SU(5)/SO(5)$ littlest Higgs, but the construction can be easily extended to other little Higgs theories. The AdS/CFT correspondence tells us exactly how to implement the gauge and Goldstone sector of any G/H little Higgs theory. The only possible challenge is trying to figure out the bulk G fermion content, and in general it is desirable to start with a low energy theory where the fermions come in linear representations of G.

From the top-down point of view, we have found a UV completion of the littlest Higgs that concisely explains the hierarchy between the Planck scale and electroweak scale. We start at some high scale with a large N conformal field theory. The size of AdS space represents the logarithmic running of some operator which eventually

breaks conformality in the infrared, and this guarantees a natural hierarchy between $M_{\rm Pl}$ and the 10 TeV scale. Because conformality is broken, the CFT confines, yielding an $SU(5)/SO(5)$s worth of "pions." Collective breaking insures that the pion corresponding to the Higgs boson is light, and this generates a natural hierarchy between $f_\pi \sim 1$ TeV and the electroweak scale.

We have seen a number of tensions in this model that one could guess from the low energy theory. Large N CFTs with a large conformal window lead to very small gauge couplings, and if we want to raise the mass of the W' to phenomenologically healthy values, we need to shrink the size of the conformal window. If we allow for T-parity, then a light W' may be acceptable, but in the context of AdS space, we saw a tension between flavor physics, precision electroweak tests, and little Higgs theories. If T-parity is indeed the reason for the smallness of precision electroweak corrections, then we have to explain why the masses of T-odd fermion partners do not exhibit the same flavor hierarchy as the fermions themselves. It may be interesting to look at AdS models of little Higgs theories with custodial $SU(2)$ symmetry where it appears easier to separate flavor physics from precision electroweak tests.

In AdS space, locality in the warped dimension guaranteed that our Higgs potential was finite, but one might wonder how important the extra dimension actually was for our construction to succeed. Even if we took $\epsilon = L_0/L_1$ to be $1/2$, the Higgs potential would still be finite, suggesting that the physics relevant for pseudo-Goldstone phenomenology is heavily localized near the IR brane. In fact, as shown in [66], the Higgs potential can be made completely free of 1-loop quadratic divergences if one simply postulates the existence of ρ-like mesons. Of course, the properties of the ρ

are inherited from the strong dynamics, and AdS/CFT is a simple way to understand ρ-like states. But given the difficulty of having heavy W' states in large N CFTs, it would be nice if we had a framework other than AdS/CFT to understand the radiative potentials for pseudo-Goldstone bosons.

In [75], we will show that in the right context, pseudo-Goldstone phenomenology can be made largely independent of strong dynamics. In essence, a low energy observer cannot tell whether a gauge quadratic divergence is cut off by a ρ-like or a W'-like state, so if our only problem with a large conformal window is that W' states are generically much lighter than ρ states, then we should work in a framework where we can decouple the ρ-like states. In particular, we will show that the $SU(5)/SO(5)$ littlest Higgs can actually arise in ordinary QCD with five flavors, and the gauge contribution to the Higgs potential is completely finite at one-loop. This UV complete theory will have light W' and W'' states responsible for cutting off divergences in the Higgs potential, but the QCD ρ mesons will play a much smaller role in the low energy phenomenology. This will open a new avenue to construct simple UV completions of little Higgs models.

Appendices

Appendix A

Matrix Elements Calculations

In this appendix we present the explicit matrix elements for the decays considered in the text. We begin with the Same-Spin decay channel $q' \to q + W' \to q + W + A'$. The matrix element is given by,

$i\mathcal{M}$ =

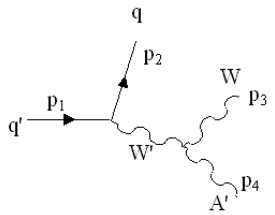

$$= g_2 \bar{u}(p_2)\gamma_\mu P_L u(p_1) \frac{i}{q^2 - m_{W'}^2}\left(-g^{\mu\nu} + \frac{q^\mu q^\nu}{m_{W'}^2}\right)$$

$$\times \; e\left(g_{\rho\nu}(-q - p_3)_\sigma + g_{\nu\sigma}(p_4 + q)_\rho + g_{\sigma\rho}(p_3 - p_4)_\nu\right)\epsilon^\sigma(p_4)\epsilon^\rho(p_3)$$

We have borrowed the usual Standard Model coupling for the vertices. The probability amplitude is then,

$$\sum_{pol} |\mathcal{M}|^2 = c_2(t_{qW})^2 + c_1 t_{qW} + c_0$$

Where the coefficient functions are,

$$c_2 = \frac{1}{(q^2 - m_{W'}^2)^2} \frac{m_W^4 + (m_{A'}^2 - q^2)^2 + 2m_W^2(5m_{A'}^2 - q^2)}{m_W^2 m_{A'}^2}$$

$$\begin{aligned} c_1 &= \frac{1}{(q^2 - m_{W'}^2)^2} \frac{1}{m_{W'}^2 m_{A'}^2 m_W^2} \\ &\times (-(m_{q'}^2 - m_q^2)(m_W^2 - m_{A'}^2)(m_{A'}^4 + 10m_W^2 m_{A'}^2 + m_{A'}^4 - q^4) \\ &+ m_{W'}^2(-m_W^6 - 11m_W^4 m_{A'}^2 - 11m_W^2 m_{A'}^4 - m_{A'}^6 + 3m_W^4 q^2 \\ &+ 14m_W^2 m_{A'}^2 q^2 + 3m_{A'}^4 q^2 - 3m_W^2 q^4 - 3m_{A'}^2 q^4 + q^6 \\ &+ m_{q'}^2(m_W^4 - 10m_W^2 m_{A'}^2 - 3m_{A'}^4 + 4m_{A'}^2 S - q^4)) \\ &+ (m_q^2(-3m_W^4 + m_{A'}^4 - q^4 + m_W^2(-10m_{A'}^2 + 4q^2)))) \end{aligned}$$

The last term, c_0 is too complicated to present and carries little significance. It is not hard to show that c_2 is always positive for any real choice of q^2.

Next we are interested in the corresponding SUSY decay chain shown in Fig. (A.1). The first vertex is given by,

$$-g_2 V_{11}\ \bar{d} P_R \tilde{C}^c\ \tilde{u} \quad \text{and} \quad -g_2 U_{11}^*\ \bar{\tilde{C}} P_L u\ \tilde{d}^* \tag{A-1}$$

respectively. The $\tilde{N}\tilde{C}W^+$ vertex is given by,

$$g_2 W_\mu^- \bar{\tilde{N}}_i \gamma^\mu (\mathcal{O}_{ij}^L P_L + \mathcal{O}_{ij}^R P_R) \tilde{C}_j \tag{A-2}$$

The matrix element for the decay initiated by a down-type squark is,

$$\mathcal{M}_{\tilde{d}} = g_2^2 U_{11}^*\ \bar{u}_{\tilde{N}}(p_4) \gamma^\mu (\mathcal{O}_{11}^L P_L + \mathcal{O}_{11}^R P_R) \frac{\not{q} + M_{\tilde{C}}}{q^2 - M_{\tilde{C}}^2} P_L v_u(p_2) \epsilon_\mu(p_3) \tag{A-3}$$

$$= U_{11}^*\ \bar{u}_{\tilde{N}}(p_4) \gamma^\mu \frac{a\not{q} + bM_{\tilde{C}}}{q^2 - M_{\tilde{C}}^2} v_u(p_2) \epsilon_\mu(p_3) \tag{A-4}$$

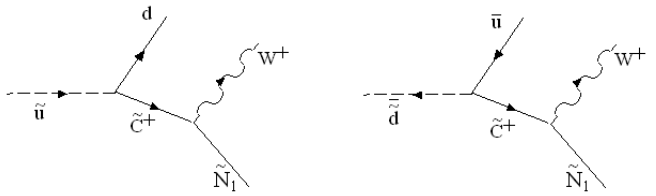

Figure A.1: Two different process contributing to squark decay into $\tilde{C}^+$ and a quark. The chargino consequently decays into $W^\pm$ and LSP.

where,

$$a = g_2^2 O_{11}^R \quad \text{and} \quad b = g_2^2 O_{11}^L \tag{A-5}$$

The squared amplitude is given by,

$$|\mathcal{M}_{\bar{\tilde{d}}}|^2 = \frac{(b^2 m_{\tilde{C}}^2 - a^2 q^2)(q^2 - 2m_W^2 + m_{\tilde{N}}^2)}{2m_W^2 (q^2 - m_{\tilde{C}}^2)^2}\, t_{qW} + \text{Const.} \tag{A-6}$$

Therefore, in the narrow width limit, the slope depends on the difference $b^2 - a^2$. The problem is that the second diagram contributing to this process (with an up-squark decay) has the opposite sign for this coefficient. Notice that,

$$\begin{aligned} \bar{d} P_R \tilde{C}^c \tilde{u} &= -(\tilde{C}^c)^T P_R \bar{d}^T \tilde{u} = -\bar{\tilde{C}} C^T P_R \bar{d}^T \tilde{u} \\ &= -\bar{\tilde{C}} P_R C^T \bar{d}^T \tilde{u} = -\bar{\tilde{C}} P_R C^T \bar{d}^T \tilde{u} \\ &= \bar{\tilde{C}} P_R d^c \tilde{u} \end{aligned} \tag{A-7}$$

When contracting this operator with the $\tilde{N}\tilde{C}W^+$ vertex we get the opposite spin structure,

$$\begin{aligned} \mathcal{M}_{\tilde{u}} &= g_2^2 V_{11}\ \bar{u}_{\tilde{N}}(p_4)\gamma^\mu (\mathcal{O}_{11}^L P_L + \mathcal{O}_{11}^R P_R) \frac{\not{q} + M_{\tilde{C}}}{q^2 - M_{\tilde{C}}^2} P_R v_d(p_2) \epsilon_\mu(p_3) \\ &= V_{11}\ \bar{u}_{\tilde{N}}(p_4)\gamma^\mu \frac{b\not{q} + aM_{\tilde{C}}}{q^2 - M_{\tilde{C}}^2} v_u(p_2) \epsilon_\mu(p_3) \end{aligned} \tag{A-8}$$

Experimentally, we cannot distinguish between up quarks and down quarks. We must therefore average over the two contributions,

$$\sum_{\tilde{u},\tilde{d}} |\mathcal{M}|^2 \propto (b^2 - a^2)(f_d(U_{11}^*)^2 - f_u(V_{11})^2)t_{qW} + \text{Const.} \tag{A-9}$$

f_d and f_u is the fraction of events with a down-squark or up-squark, respectively.

Appendix B

HERWIG Implementation

In this appendix we review the implementation of matrix elements into HERWIG[1]. This section is relevant to any Monte-Carlo program using the S and F functions of Eijk and Kleiss [76] to calculate helicity amplitudes. The usage of these functions results in very efficient computations. The price the user has to pay is the complexity of the expressions. These functions are then used in the spin correlations algorithm devised by Knowles and Collins [29, 58]. We hope to provide a brief but fairly self-consistent presentation below.

HERWIG is an event generator consisting of roughly 5 phases (for a complete description of the program consult [32]):

1. Hard process, where the particles in the main $2 \to 2, 3$ event are generated, e.g. $q\ q \to g\ g$ or $e^+e^- \to q\bar{q}$.

2. The parton shower phase involving the QCD evolution from the collision energy to the infrared cutoff.

[1]HERWIG stands for Hadron Emission Reactions with Interfering Gluons

3. Decay of heavy unstable particles before hadronization, such as top quark and SUSY partners.

4. Hadronization stage

5. Decay of unstable hadrons.

We are mainly concerned with the third step. In order to decay any unstable particle (e.g. gluino, squark etc.), one must provide HERWIG with its different decay channels and the corresponding matrix elements. To keep track of spin correlations the matrix element must include the external polarizations. For example, let's consider the decay of a heavy fermion into a fermion and a scalar (top decay into bottom and higgs). The matrix element is given by,

$$i\mathcal{M} = ig\bar{u}(q, \lambda_2)u(p, \lambda_1) \tag{B-1}$$

In order to compute this spinor product, HERWIG requires the user to express it in terms of the S and F functions of Eijk and Kleiss [76] defined below. This facilitates the algebra, but obscures the expression. Let's briefly recall the construction.

One begins by expressing any polarization in terms of massless spinors (for a pedagogical review, see[56]). Two basic 4-momenta, k_0, k_1 are chosen such that,

$$k_0 \cdot k_0 = 0, k_0 \cdot k_1 = 0, k_1 \cdot k_1 = -1 \tag{B-2}$$

The basic left and right helicities are then defined via,

$$u_L(k_0)\bar{u}_L(k_0) = P_L \not{k}_0, \quad u_R(k_0) = \not{k}_1 u_L(k_0) \tag{B-3}$$

The helicity spinor for any other momenta (not collinear with k_0) is then given by,

$$u_\lambda(k) = \not{k} u_{-\lambda}(k_0)/\sqrt{2k_0 \cdot k} \tag{B-4}$$

A massive spinor is nothing but the linear combination of two massless spinors of opposite helicities. It can be written as,

$$\begin{aligned} u(p,\lambda) &= \frac{(\not{p} + m)\ u_{-\lambda}(k_2)}{\sqrt{2p \cdot k_2}} \\ &= \frac{1}{\sqrt{2p \cdot k_2}} \left(S_\lambda(k_1, k_2)\ u_\lambda(k_1) + m\ u_{-\lambda}(k_2)\right) \end{aligned} \tag{B-5}$$

where $p = k_1 + k_2$ is decomposed into two massless 4-vectors and the S function is defined as,

$$S_\lambda(k_1, k_2) = \bar{u}_\lambda(k_1) u_{-\lambda}(k_2) = (S_{-\lambda}(k_2, k_1))^* = -S_\lambda(k_2, k_1) \tag{B-6}$$

Notice that, $|S_\lambda(k_1, k_2)|^2 = m^2$.

All expressions can therefore be reduced into products of massless spinors, with the possibility of having a γ^μ matrix sandwiched in between. It proves useful to define the F function as well,

$$F(k_1, \lambda_1, p, k_2, \lambda_2, M) = \bar{u}_{\lambda_1}(k_2)\ (\not{p} + M)\ u_{\lambda_2}(k_2) \tag{B-7}$$

for some p which is not light-like. Matrix elements for many typical processes were already implemented in HERWIG by P. Richardson. As an example, the above matrix

element (B-1) can be written as,

$$\begin{aligned}
\mathcal{M} &= g\bar{u}(q,\lambda_2)u(p,\lambda_1) \\
&= g\frac{1}{\sqrt{2p\cdot p_2}}\frac{1}{\sqrt{2q\cdot q_2}}\left(S^*_{\lambda_2}(q_1,q_2)\bar{u}_{\lambda_2}(q_1)+m_2\bar{u}_{-\lambda_2}(q_2)\right)(\not{p}+m_1)\,u_{-\lambda_1}(p_2) \\
&= \frac{1}{\sqrt{2p\cdot p_2}}\frac{1}{\sqrt{2q\cdot q_2}} \\
&\times\ g\left(S_{-\lambda_2}(q_2,q_1)F(q_1,\lambda_2,p,p_2,-\lambda_1,m_1)+m_2F(q_2,-\lambda_2,p,p_2,-\lambda_1,m_1)\right)
\end{aligned}$$

For a massless spin-1 particle the external polarization $\epsilon^\mu(k,\lambda)$ can be expressed as,

$$\epsilon^\mu(k,\lambda)=\bar{u}_\lambda(k)\gamma^\mu u_\lambda(k_1)/\sqrt{4k\cdot k_1} \tag{B-8}$$

where k_1 is any light-like momentum not collinear with k.

The extra polarization of a massive spin-1 particle adds an extra complication to the calculation. Since the only massive gauge bosons in the MSSM are the $W^\pm$ and Z, it is easier to simply insert the entire matrix element (e.g. $t\to b+e^+\nu_e$ rather than $t\to b+W^+$ and $W^+\to e^+\nu_e$). In Same-Spin theories, there are many massive gauge bosons around and it proves useful to develop the needed formalism and implement it in HERWIG.

Looking at the massless polarization (B-8) it is easy to guess the form of a massive one in terms of spinors,

$$\epsilon^\mu(p,\lambda_1,\lambda_2)=\frac{1}{(2\sqrt{2}m)}\,\bar{u}(p,\lambda_1)\gamma^\mu v(p,\lambda_2) \tag{B-9}$$

where, $p^2=m^2$ and $\lambda_{1,2}$ are the usual spinor polarizations. This might seem wrong at first, as it seems to imply 4 polarizations rather than the required 3, but as we

will see in a moment, $(+,+)$ and $(-,-)$ both correspond to the scalar polarization. First, let's verify that this indeed reproduces the correct polarization sum,

$$\begin{aligned}\sum_{\lambda_1,\lambda_2}\epsilon_\mu(p,\lambda_1,\lambda_2)\epsilon^*_\nu(p,\lambda_1,\lambda_2)/(8m^2) &= \sum_{\lambda_1,\lambda_2} Tr(u(p,\lambda_1)\bar{u}(p,\lambda_1)\gamma_\mu v(p,\lambda_2)\bar{v}(p,\lambda_2)\gamma_\nu)/(8m^2)\\ &= Tr((\not{p}+m)\gamma_\mu(\not{p}-m)\gamma_\nu)/(8m^2)\\ &= \left(-g_{\mu\nu}+\frac{p_\mu p_\nu}{m^2}\right)\end{aligned}$$

It is straight forward to show that (B-9) corresponds to the different polarizations directly. First note that,

$$\begin{aligned}&\epsilon_\mu \quad (p,\lambda_1,\lambda_2) = \frac{1}{2\sqrt{2}m}\frac{1}{2p\cdot p_1}\\ &\times \quad \left(S^*_{\lambda_1}(p_1,p_2)\bar{u}_{\lambda_1}(p_1)+m\ \bar{u}_{-\lambda_1}(p_2)\right)\gamma_\mu\left(S_{\lambda_2}(p_1,p_2)u_{\lambda_2}(p_1)-m\ u_{-\lambda_2}(p_2)\right)\\ &= \begin{cases}\bar{u}_\lambda(p_1)\gamma_\mu u_\lambda(p_1)-\bar{u}_\lambda(p_2)\gamma_\mu u_\lambda(p_2)\ /2\sqrt{2}m & \lambda_1\equiv\lambda=\lambda_2\\ \frac{\left(S_{-\lambda}-S^*_\lambda\right)}{m}\ \bar{u}_\lambda(p_2)\gamma_\mu u_\lambda(p_1)\ /2\sqrt{2}m & \lambda_1\equiv\lambda\neq\lambda_2\end{cases}\end{aligned}$$

In the rest frame of the particle we can take $\vec{p_1}=\hat{z}|p|/2$ and $\vec{p_2}=-\hat{z}|p|/2$, so that $p=p_1+p_2=(m,\vec{0})$ and the massless spinors are given by,

$$u_-(p_1)=\sqrt{2m}\begin{pmatrix}0\\1\\0\\0\end{pmatrix}\qquad u_+(p_1)=\sqrt{2m}\begin{pmatrix}0\\0\\1\\0\end{pmatrix} \tag{B-10}$$

With a few lines of arithmetic one can verify that,

$$\begin{aligned}\epsilon_\mu(p,-,-) &= ((1,0,0,m)-(1,0,0,-m))/(2\sqrt{2}m) = (0,0,0,1/\sqrt{2})\\ \epsilon_\mu(p,+,+) &= ((1,0,0,m)-(1,0,0,-m))/(2\sqrt{2}m) = (0,0,0,1/\sqrt{2})\\ \epsilon_\mu(p,-,+) &= 2(0,m,im,0)/(2\sqrt{2}m) = (0,1/\sqrt{2},i/\sqrt{2},0)\\ \epsilon_\mu(p,+,-) &= 2(0,m,-im,0)/(2\sqrt{2}m) = (0,1/\sqrt{2},-i/\sqrt{2},0)\end{aligned}$$

and so we conclude that $\epsilon^\mu(-,+) = \epsilon^\mu_L$, $\epsilon^\mu(+,-) = \epsilon^\mu_R$ and $\epsilon^\mu(-,-) = \epsilon^\mu(+,+) = \epsilon^\mu_0/\sqrt{2}$. It is now straight forward, albeit tedious, to express any matrix element involving an external massive gauge boson in terms of S and F functions and implement it into HERWIG.

We begin with the matrix element for a gauge boson decay into a fermion - anti-fermion pair,

$$i\mathcal{M} = iA_\lambda \bar{u}(k,\lambda_2)\gamma^\mu P_\lambda v(q,\lambda_4)\ \ \epsilon_\mu(p,\lambda_1,\lambda_2) \tag{B-11}$$

The corresponding expressions are,

$$\begin{aligned}
\mathcal{M}((\lambda_1,\lambda_1),\lambda_3,\lambda_4) &= \frac{\sqrt{2}}{\sqrt{4p\cdot p_2 2k\cdot k_2 2q\cdot q_2}} \\
&\times \ (\ A_{-\lambda_1}F(k_2,-\lambda_3,k,p_1,\lambda_1,m_2)\ F(p_1,\lambda_1,q,q_2,-\lambda_4,-m_3) \\
&+ \ (p_1\to p_2,\ \lambda_1\to-\lambda_1)\ )
\end{aligned}$$

$$\begin{aligned}
\mathcal{M}((\lambda_1,-\lambda_1),\lambda_3,\lambda_4) &= \frac{1}{\sqrt{4p\cdot p_2 2k\cdot k_2 2q\cdot q_2}} \\
&\times \ \left(\frac{S_{-\lambda_1}(p_1,p_2)-S^*_{\lambda_1}(p_1,p_2)}{m_1}\right) \\
&\times \ (\ A_{-\lambda_1}F(k_2,-\lambda_3,k,p_2,\lambda_1,m_2)\ F(p_1,\lambda_1,q,q_2,-\lambda_4,-m_3) \\
&\qquad + (p_1\leftrightarrow p_2,\ \lambda_1\to-\lambda_1)\ \ )
\end{aligned}$$

The factor of $\sqrt{2}$ above is to guarantee proper normalization of the longitudinal mode. With a little bit of care it is easy to obtain the other two diagrams $f(\bar{f})\to f(\bar{f})+g.b.$. To turn a fermion into an anti-fermion or vice-versa simply send $m\to -m$. The incoming gauge-boson polarization becomes an outgoing one by conjugation,

$$\epsilon_\mu \to \epsilon^*_\mu = \bar{v}(p,\lambda_2)\gamma_\mu u(p,\lambda_1) = \lambda_1\lambda_2\ \bar{u}(p,-\lambda_1)\gamma_\mu v(p,-\lambda_2) \tag{B-12}$$

So we simply have to send $\lambda_1 \to -\lambda_1$ in the expressions above, and an overall minus sign in front of the $\mathcal{M}((\lambda_1, -\lambda_1), \lambda_3, \lambda_4)$ amplitude due to the $\lambda_1\lambda_2$ factor.

The last diagram we consider is the non-Abelian vertex including 3 external massive spin-1 polarizations.

$i\mathcal{M}$ =

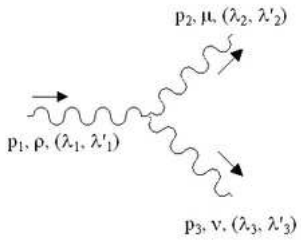

$$
\begin{aligned}
&= ig\left(g^{\mu\nu}(p_3-p_2)^\rho + g^{\nu\rho}(-p_1-p_3)^\mu + g^{\rho\mu}(p_2+p_1)^\nu\right) \\
&\times \ \epsilon_\rho(p_1,\lambda_1,\lambda_1')\ \epsilon_\mu^*(p_2,\lambda_2,\lambda_2')\ \epsilon_\nu^*(p_3,\lambda_3,\lambda_3')
\end{aligned}
$$

We give the corresponding expression for the first term only. The other terms can be obtained by trivial permutations and using (B-12) for the outgoing polarizations.

$$
\begin{aligned}
i\mathcal{M} &\supset \epsilon_\mu^*(p_2,\lambda_2,\lambda_2')\epsilon_\nu^*(p_3,\lambda_3,\lambda_3')g^{\mu\nu}(p_3-p_2)^\rho\epsilon_\rho(p_1,\lambda_1,\lambda_1') \qquad \text{(B-13)} \\
&= \frac{1}{16\sqrt{2}m_1m_2m_3}A(\lambda_2,\lambda_2',\lambda_3,\lambda_3')B(\lambda_1,\lambda_1')
\end{aligned}
$$

where,

$$A(\lambda_2,\lambda_2',\lambda_3,\lambda_3') = \begin{cases} \lambda_2 = \lambda_2' & \frac{1}{m_3^2}\left(F(q_3',\lambda_3,p_3,q_2,\lambda_2,m_3)F(q_2,\lambda_2,p_3,q_3',\lambda_3',-m_3)\right. \\ & -F(q_3',\lambda_3,p_3,q_2',\lambda_2,m_3)F(q_2',\lambda_2,p_3,q_3',\lambda_3',-m_3) \\ & \left. +\,\lambda_3\to-\lambda_3\right) \\ \lambda_2 = -\lambda_2' & \frac{1}{m_3^2}\left(\frac{S(q_2,q_2',-\lambda_2)-S^*(q_2,q_2',\lambda_2)}{m_2}\right)\times \\ & \left(F(q_3',\lambda_3,p_3,q_2',\lambda_2,m_3)F(q_2,\lambda_2,p_3,q_3',\lambda_3',-m_3)\right. \\ & \left. +(\lambda_3\to-\lambda_3,q_2'\leftrightarrow q_2)\right) \end{cases}$$

and,

$$B(\lambda_1,\lambda_1') = \begin{cases} \lambda_1 = \lambda_1' & \left(F(q_1,\lambda_1,p_3-p_2,q_1,\lambda_1,0)-F(q_1',-\lambda_1,p_3-p_2,q_1',-\lambda_1,0)\right) \\ \lambda_1 = -\lambda_1' & \left(\frac{S(q_1,q_1',-\lambda_1)-S^*(q_1,q_1',\lambda_1)}{m_1}F(q_1,\lambda_1,p_3-p_2,q_1',\lambda_1,0)\right) \end{cases}$$

Here, the momentum is written in terms of two massless momenta $p_i = q_i + q_i'$, with $q_i^2 = (q_i')^2 = 0$ and $p_i^2 = m_i^2$.

Appendix C

Summary of Bulk Fields in AdS Space

In this appendix, we briefly summarize the main results and conventions for bulk fields in AdS space. All the results below can be found in the literature (see for example [30, 2, 45, 41]), though there are different conventions for the naming of left- and right-handed fermions, and we try to stick to the conventions of [45]. Throughout, we use the choice of metric given by equation (8.1), which is most convenient for our purposes.

Let us begin with scalars in the bulk. The lagrangian for a complex scalar field in 5D with arbitrary boundary mass terms and a bulk source J is,

$$\mathcal{L}_\phi = \sqrt{g}\left(g^{MN}\partial_M\phi^*\partial_N\phi - M^2|\phi|^2 - J\phi\right) + \sqrt{-g_{\text{ind}}}m_0^2|\phi|^2\delta(z-L_0) + \sqrt{-g_{\text{ind}}}m_1^2|\phi|^2\delta(z-L_1). \tag{C-1}$$

The induced metric on the branes is $g^{\mu\nu}_{\text{ind}}(z) = \eta^{\mu\nu}/(kz)^2$. The boundary terms are merely a handy way of imposing boundary conditions on the fields in the lagrangian

formulation. Rescaling the fields in the lagrangian simplifies things somewhat and allow for a unified treatment of fields with different spins, so let $\phi \to \hat{\phi} = (kz)^{-2}\phi$. The lagrangian is then (ignoring the boundary terms since they will only change the boundary conditions of the Greens function),

$$\mathcal{L}_\phi = (kz)\left(\left(-\hat{\phi}^*\partial^\mu\partial_\mu\hat{\phi} + \hat{\phi}^*\left(\partial_z^2 + \frac{1}{z}\partial_z - \frac{4}{z^2}\right)\hat{\phi}\right) - \frac{M^2}{(kz)^2}|\hat{\phi}|^2 - \frac{\sqrt{g}}{(kz)}\hat{J}\hat{\phi}\right). \quad \text{(C-2)}$$

The rescaled Greens function $\hat{G}(x,x',z,z') = (kz)^{-2}(kz')^{-2}G(x,x',z,z')$ satisfies the following differential equation (moving to momentum space in the transverse direction),

$$\left(p^2 + \partial_z^2 + \frac{1}{z}\partial_z - \frac{\alpha^2}{z^2}\right)\hat{G}(p;z,z') = \frac{1}{kz}\delta(z-z'), \quad \text{(C-3)}$$

where $\alpha^2 = M^2/k^2 + 4$.

Let us move on to consider gauge bosons in AdS space. Similar to the scalar case, the 5D gauge boson lagrangian is given by

$$\mathcal{L}_{\text{gauge}} = -\frac{1}{4g_5^2}\sqrt{g}g^{AB}g^{MN}F_{AM}F_{BN} - \frac{z_0}{4g_5^2}\sqrt{-g_{\text{ind}}}g_{\text{ind}}^{\mu\nu}g_{\text{ind}}^{\alpha\beta}F_{\mu\alpha}F_{\nu\beta}\delta(z-L_0), \quad \text{(C-4)}$$

where we have dropped a possible IR brane kinetic term since it plays no role in our analysis. Working in $A_5 = 0$ and $\partial_\mu A^\mu = 0$ gauge, the situation is identical to the scalar case, except that the rescaled field is $\hat{A}_\mu = (kz)^{-1}A_\mu$, and so the rescaled propagator is $\eta_{\mu\nu}\hat{G}(p;z,z') = (kz)^{-1}(kz')^{-1}\eta_{\mu\nu}G(p;z,z')$. The propagator satisfies equation (C-3) with $\alpha = 1$.

In curved backgrounds, the spin of a field is defined with respect to the Lorentz group acting on the comoving coordinates (the local tangent space). The vierbein e_A^a is the object which connects the comoving frame (a index) with the spacetime coordinates (A index). The spin-connection w_{bcA} tells us how the comoving reference

frame changes as we go in different spacetime directions (hence the two internal indices a and b and one spacetime index A). In 5 dimensions, Dirac fermions form an irreducible representation of the Lorentz group. The lagrangian for a Dirac field in the bulk is

$$\mathcal{L}_{\text{fermion}} = \sqrt{g}\left(e_a^A\left(\frac{i}{2}\bar{\Psi}\gamma^a(\partial_A - \overleftarrow{\partial}_A)\Psi + \frac{w_{bcA}}{8}\bar{\Psi}\{\gamma^a,\sigma^{bc}\}\Psi\right) - m\bar{\Psi}\Psi - \bar{\Psi}J\right), \tag{C-5}$$

where $e_a^A = \text{diag}(1,1,1,1,1)/kz$ is the inverse vierbein. Since the metric is diagonal, the spin-connection is non-zero only when $b = A$ or $c = A$, giving no contribution to the fermionic action. Again, rescaling $\Psi \to \hat{\Psi} = (kz)^{-5/2}\Psi$ the lagrangian takes the form,

$$\mathcal{L}_{\text{fermion}} = (kz)\left(\hat{\bar{\Psi}}i\partial\!\!\!/\hat{\Psi} - \hat{\bar{\Psi}}\left(\frac{m}{kz} + \frac{1}{2z}\gamma_5\right)\hat{\Psi} - \hat{\bar{\Psi}}\gamma_5\partial_z\hat{\Psi} - \frac{\sqrt{g}}{kz}\hat{\bar{\Psi}}J\right). \tag{C-6}$$

Therefore, the rescaled fermion Greens function have to satisfy,

$$\left(p\!\!\!/ + \frac{\nu}{z} + \gamma_5\left(\frac{1}{2z} + \partial_z\right)\right)\hat{S}(p;z,z';\nu) = \frac{-1}{kz}\delta(z-z'), \tag{C-7}$$

where we have introduced the ratio $\nu \equiv m/k$. If we let

$$\hat{S}^{(\pm,\pm)}(p;z,z';\nu) = \left(-p\!\!\!/ - \gamma_5\left(\partial_z + \frac{1}{2z}\right) + \frac{\nu}{z}\right)(P_L\hat{G}_L^{(\pm,\pm)} + P_R\hat{G}_R^{(\mp,\mp)}), \tag{C-8}$$

we see that $\hat{G}$ has to satisfy equation (C-3) again with $\alpha = |1/2 \mp \nu|$ with the minus (plus) sign for the left- (right-) handed propagator. The $\pm$ signs on the Gs refer to the choice of boundary conditions for the fields.

So it all comes down to solving equation (C-3). The boundary conditions are as follows. We can choose either Neumann (even) or Dirichlet (odd) boundary conditions

on the two branes. For the fermions the boundary conditions for the left- and right-handed components have to be opposite from each other since as we will see they are coupled through the equations of motion. The solution to equation (C-3) is simple and is given in [30, 42] (note that we have analytically continued to Euclidean space so that $p^2 \to -p^2$):

$$\hat{G}(p;z,z') = \frac{-L_0}{R_1 - R_0}\Big(I_\alpha(|p|z_<) - R_0 K_\alpha(|p|z_<)\Big)\Big(I_\alpha(|p|z_>) - R_1 K_\alpha(|p|z_>)\Big), \tag{C-9}$$

where $z_>$ ($z_<$) is the greater (lesser) of (z, z'), I_α and K_α are the modified Bessel's functions and the ratios R_0, R_1 depend on the choice of boundary conditions on the UV/IR branes. For the gauge boson:

$$R_0^{(+)} = \frac{I_{\alpha-1}(|p|L_0) - z_0|p|I_\alpha(|p|L_0)}{-K_{\alpha-1}(|p|L_0) - z_0|p|K_\alpha(|p|L_0)}, \qquad R_0^{(-)} = \frac{I_\alpha(|p|L_0)}{K_\alpha(|p|L_0)},$$
$$R_1^{(+)} = \frac{I_{\alpha-1}(|p|L_1)}{-K_{\alpha-1}(|p|L_1)}, \qquad R_1^{(-)} = \frac{I_\alpha(|p|L_1)}{K_\alpha(|p|L_1)}. \tag{C-10}$$

For the fermions, the ratios are different for the left- and right-handed components of the Dirac field. To simplify the expressions somewhat let $\alpha = |1/2 \mp \nu|$ and $\beta = 1/2 \mp \nu$:

$$R_0^{(+)} = -\frac{|p|L_0 I_{\alpha-1}(|p|L_0) - (\alpha-\beta)\, I_\alpha(|p|L_0)}{|p|L_0 K_{\alpha-1}(|p|L_0) + (\alpha-\beta)\, K_\alpha(|p|L_0)}, \qquad R_0^{(-)} = \frac{I_\alpha(|p|L_0)}{K_\alpha(|p|L_0)},$$
$$R_1^{(+)} = -\frac{|p|L_1 I_{\alpha-1}(|p|L_1) - (\alpha-\beta)\, I_\alpha(|p|L_1)}{|p|L_1 K_{\alpha-1}(|p|L_1) + (\alpha-\beta)\, K_\alpha(|p|L_1)}, \qquad R_1^{(-)} = \frac{I_\alpha(|p|L_1)}{K_\alpha(|p|L_1)}. \tag{C-11}$$

Note that when $\alpha = \beta$, this simply reduces to the same ratios as for gauge bosons with no boundary kinetic terms. We ignore possible boundary kinetic/mass terms for fermions since we do not need them in this paper.

It is important to know the low energy expansion of these propagators with even boundary conditions on the IR bane evaluated at the IR brane, in order to match the UV theory with the IR theory. For the gauge bosons we have,

$$\hat{G}^{(+,+)}(p; L_1, L_1) = \frac{\epsilon^2}{L_0 \log(\epsilon^{-1})} \frac{1}{p^2} + \mathcal{O}(p^0), \qquad \hat{G}^{(-,+)}(p; L_1, L_1) = \frac{L_0}{2}(1+\epsilon^2) + \mathcal{O}(p^2). \tag{C-12}$$

Notice that the expansion of $\hat{G}^{(+,+)}$ is as expected: it is the gauge boson zero-mode overlap function squared, divided by p^2. For the fermions the low energy expansion gives,

$$\begin{aligned}
\hat{G}_L^{(+,+)}(p; L_1, L_1; \nu) &= \frac{\epsilon}{p^2}\frac{1}{L_1}\left(\frac{1+2\nu}{1-\epsilon^{1+2\nu}}\right) + \mathcal{O}(p^0) = \frac{\epsilon}{p^2} f_L(\nu)^2, \\
\hat{G}_L^{(-,+)}(p; L_1, L_1; \nu) &= \epsilon L_1 \left(\frac{1-\epsilon^{1-2\nu}}{1-2\nu}\right) + \mathcal{O}(p^2) = \epsilon \frac{1}{f_R(\nu)^2}, \\
\hat{G}_R^{(+,+)}(p; L_1, L_1; \nu) &= \frac{\epsilon}{p^2}\frac{1}{L_1}\left(\frac{1-2\nu}{1-\epsilon^{1-2\nu}}\right) + \mathcal{O}(p^0) = \frac{\epsilon}{p^2} f_R(\nu)^2, \\
\hat{G}_R^{(-,+)}(p; L_1, L_1; \nu) &= \epsilon L_1 \left(\frac{1-\epsilon^{1+2\nu}}{1+2\nu}\right) + \mathcal{O}(p^2) = \epsilon \frac{1}{f_L(\nu)^2}.
\end{aligned} \tag{C-13}$$

Notice that $G_L^{(+,+)}$ ($G_R^{(+,+)}$) is nothing but the left (right) zero-mode overlap function squared divided by p^2. It is amusing that $G_L^{(-,+)}$ ($G_R^{(-,+)}$) is simply the inverse of the *right* (*left*) zero-mode overlap function.

The KK spectrum of the theory is found in the poles of the propagator in equation (C-9). Since the numerator of the propagator is everywhere analytic, the poles must be at $R_1(p) - R_0(p) = 0$. Analytically continuing back to Minkowski space the masses are given by the solutions to

$$R_1(im_n) = R_0(im_n), \tag{C-14}$$

where R_1 and R_0 for fermions and gauge bosons are given above for the different choices of boundary conditions. For instance, in the case of odd boundary conditions

on both branes for a right-handed fermion field we have,

$$\frac{J_\alpha(m_n L_1)}{Y_\alpha(m_n L_1)} = \frac{J_\alpha(m_n L_0)}{Y_\alpha(m_n L_0)} \tag{C-15}$$

where $\alpha = |1/2 + \nu|$. Solving this equation for m_n, one obtains the KK spectrum. A similar story holds for gauge boson masses.

Now for the Kaluza-Klein decomposition of the different fields. We will present the details for the fermion KK modes only [45]. Starting from the lagrangian given by equation (C-5) we decompose the 5D Dirac fields into,

$$\Psi_{L,R}(x,z) = \sum_n \psi_n^{L,R}(x,z)(kz)^2 f_n^{L,R}(z). \tag{C-16}$$

To get the usual 4D lagrangian for left- and right-handed fermions we demand that,

$$\int dz (f_n^L)^* f_m^L = \int dz (f_n^R)^* f_m^R = \delta_{m,n}, \tag{C-17}$$

$$(\pm z\partial_z - \nu)\, f_n^{L,R}(z) = -m_n z f_n^{R,L}(z), \tag{C-18}$$

where m_n is the 4-dimensional mass for the different KK modes. The boundary conditions on $f_n^{L,R}$ are simply $f_n^{L*}(L_0) f_n^R(L_0) = f_n^{L*}(L_1) f_n^R(L_1) = 0$, which tells us that either the left- or right-handed component of the bulk field must have vanishing boundary conditions on each brane. Equation (C-18) implies the following second-order differential equation for the left- and right-handed components:

$$\left(z^2\partial_z^2 + z^2 m_n^2 - \nu(\nu \mp 1)\right) f_n^{L,R} = 0. \tag{C-19}$$

To begin with, we look for zero modes, $m_n = 0$. Solving equation (C-18) for the zero modes we get (for $\nu \neq \mp 1/2$),

$$f_0^{L,R}(z) = \frac{1}{L_1^{1/2}} \sqrt{\frac{1 \pm 2\nu}{1 - \epsilon^{1\pm 2\nu}}} \left(\frac{z}{L_1}\right)^{\pm\nu}. \tag{C-20}$$

For the case $\nu = -1/2$ ($\nu = 1/2$) for left- (right-) handed fermions the wave-function is $f_0 = z^{-1/2}/\sqrt{-\log(\epsilon)}$.

For the massive KK modes we need to solve equation (C-19). For $\nu \neq \frac{1}{2} + N$ the solutions are simply Bessel functions

$$f_n^{L,R}(z) = \sqrt{z}\left(A_n^{L,R} J_{\frac{1}{2}\mp\nu}(m_n z) + B_n^{L,R} Y_{\frac{1}{2}\mp\nu}(m_n z)\right) \tag{C-21}$$

However, note that the left- and right-handed solutions are not independent because they are coupled through the first-order equation (C-18). The spectrum and normalization for the massive wave-function are found by imposing the different boundary conditions, together with equation (C-17). From equation (C-18) we see that if we choose Dirichlet boundary conditions for the right- (left-) handed mode we must choose the modified Neumann boundary condition $(z\partial_z \mp \nu)\, f_n^{L,R}(z) = 0$ for the left- (right-) handed modes. In the case of odd boundary conditions on both branes for a right-handed field, for instance, we recover the same constraint on m_n as equation (C-15).

Bibliography

[1] Atlas detector and physics performance. technical design report. vol. 1 and 2. CERN-LHCC-99-15.

[2] Kaustubh Agashe, Roberto Contino, and Alex Pomarol. The minimal composite higgs model. *Nucl. Phys.*, B719:165–187, 2005.

[3] Kaustubh Agashe, Antonio Delgado, Michael J. May, and Raman Sundrum. Rs1, custodial isospin and precision tests. *JHEP*, 08:050, 2003.

[4] B. C. Allanach et al. The snowmass points and slopes: Benchmarks for susy searches. *Eur. Phys. J.*, C25:113–123, 2002.

[5] Alexandre Alves, Oscar Eboli, and Tilman Plehn. It's a gluino. 2006.

[6] Thomas Appelquist, Hsin-Chia Cheng, and Bogdan A. Dobrescu. Bounds on universal extra dimensions. *Phys. Rev.*, D64:035002, 2001.

[7] N. Arkani-Hamed, A. G. Cohen, E. Katz, and A. E. Nelson. The littlest higgs. *JHEP*, 07:034, 2002.

[8] N. Arkani-Hamed et al. The minimal moose for a little higgs. *JHEP*, 08:021, 2002.

[9] Nima Arkani-Hamed, Andrew G. Cohen, and Howard Georgi. (de)constructing dimensions. *Phys. Rev. Lett.*, 86:4757–4761, 2001.

[10] Nima Arkani-Hamed, Andrew G. Cohen, and Howard Georgi. Electroweak symmetry breaking from dimensional deconstruction. *Phys. Lett.*, B513:232–240, 2001.

[11] Nima Arkani-Hamed, Andrew G. Cohen, Thomas Gregoire, and Jay G. Wacker. Phenomenology of electroweak symmetry breaking from theory space. *JHEP*, 08:020, 2002.

[12] Nima Arkani-Hamed, Gordon L. Kane, Jesse Thaler, and Lian-Tao Wang. Supersymmetry and the lhc inverse problem. 2005.

[13] Nima Arkani-Hamed, Massimo Porrati, and Lisa Randall. Holography and phenomenology. *JHEP*, 08:017, 2001.

[14] Riccardo Barbieri and Alessandro Strumia. What is the limit on the higgs mass? *Phys. Lett.*, B462:144–149, 1999.

[15] Vernon D. Barger and R. J. N. Phillips. Collider physics. REDWOOD CITY, USA: ADDISON-WESLEY (1987) 592 P. (FRONTIERS IN PHYSICS, 71).

[16] A. J. Barr. Using lepton charge asymmetry to investigate the spin of supersymmetric particles at the lhc. *Phys. Lett.*, B596:205–212, 2004.

[17] A. J. Barr. Measuring slepton spin at the lhc. 2005.

[18] Jr. Callan, Curtis G., Sidney R. Coleman, J. Wess, and Bruno Zumino. Structure of phenomenological lagrangians. 2. *Phys. Rev.*, 177:2247–2250, 1969.

[19] Spencer Chang. A 'littlest higgs' model with custodial su(2) symmetry. *JHEP*, 12:057, 2003.

[20] Spencer Chang and Jay G. Wacker. Little higgs and custodial su(2). *Phys. Rev.*, D69:035002, 2004.

[21] Mu-Chun Chen and Sally Dawson. One-loop radiative corrections to the rho parameter in the littlest higgs model. *Phys. Rev.*, D70:015003, 2004.

[22] Hsin-Chia Cheng and Ian Low. Tev symmetry and the little hierarchy problem. *JHEP*, 09:051, 2003.

[23] Hsin-Chia Cheng and Ian Low. Little hierarchy, little higgses, and a little symmetry. *JHEP*, 08:061, 2004.

[24] Hsin-Chia Cheng, Ian Low, and Lian-Tao Wang. Top partners in little higgs theories with t-parity. 2005.

[25] Hsin-Chia Cheng, Konstantin T. Matchev, and Martin Schmaltz. Bosonic supersymmetry? getting fooled at the lhc. *Phys. Rev.*, D66:056006, 2002.

[26] D. J. H. Chung et al. The soft supersymmetry-breaking lagrangian: Theory and applications. *Phys. Rept.*, 407:1–203, 2005.

[27] Sidney R. Coleman and E. Weinberg. Radiative corrections as the origin of spontaneous symmetry breaking. *Phys. Rev.*, D7:1888–1910, 1973.

[28] Sidney R. Coleman, J. Wess, and Bruno Zumino. Structure of phenomenological lagrangians. 1. *Phys. Rev.*, 177:2239–2247, 1969.

[29] John C. Collins. Spin correlations in monte carlo event generators. *Nucl. Phys.*, B304:794, 1988.

[30] Roberto Contino, Yasunori Nomura, and Alex Pomarol. Higgs as a holographic pseudo-goldstone boson. *Nucl. Phys.*, B671:148–174, 2003.

[31] Roberto Contino and Alex Pomarol. Holography for fermions. *JHEP*, 11:058, 2004.

[32] G. Corcella et al. Herwig 6.5 release note. 2002.

[33] Csaba Csaki, Jay Hubisz, Graham D. Kribs, Patrick Meade, and John Terning. Big corrections from a little higgs. *Phys. Rev.*, D67:115002, 2003.

[34] Csaba Csaki, Jay Hubisz, Graham D. Kribs, Patrick Meade, and John Terning. Variations of little higgs models and their electroweak constraints. *Phys. Rev.*, D68:035009, 2003.

[35] AseshKrishna Datta, Gordon L. Kane, and Manuel Toharia. Is it susy? 2005.

[36] AseshKrishna Datta, Kyoungchul Kong, and Konstantin T. Matchev. Discrimination of supersymmetry and universal extra dimensions at hadron colliders. *Phys. Rev.*, D72:096006, 2005.

[37] Michael J. Dugan, Howard Georgi, and David B. Kaplan. Anatomy of a composite higgs model. *Nucl. Phys.*, B254:299, 1985.

[38] Howard Georgi and David B. Kaplan. Composite higgs and custodial su(2). *Phys. Lett.*, B145:216, 1984.

[39] Howard Georgi, David B. Kaplan, and Peter Galison. Calculation of the composite higgs mass. *Phys. Lett.*, B143:152, 1984.

[40] Howard Georgi and Lisa Randall. Flavor conserving cp violation in invisible axion models. *Nucl. Phys.*, B276:241, 1986.

[41] Tony Gherghetta and Alex Pomarol. Bulk fields and supersymmetry in a slice of ads. *Nucl. Phys.*, B586:141–162, 2000.

[42] Tony Gherghetta and Alex Pomarol. A warped supersymmetric standard model. *Nucl. Phys.*, B602:3–22, 2001.

[43] Thomas Gregoire, David R. Smith, and Jay G. Wacker. What precision electroweak physics says about the su(6)/sp(6) little higgs. *Phys. Rev.*, D69:115008, 2004.

[44] Thomas Gregoire and Jay G. Wacker. Mooses, topology and higgs. *JHEP*, 08:019, 2002.

[45] Yuval Grossman and Matthias Neubert. Neutrino masses and mixings in non-factorizable geometry. *Phys. Lett.*, B474:361–371, 2000.

[46] S. S. Gubser, Igor R. Klebanov, and Alexander M. Polyakov. Gauge theory correlators from non-critical string theory. *Phys. Lett.*, B428:105–114, 1998.

[47] Tao Han. *private communication.*

[48] JoAnne L. Hewett, Frank J. Petriello, and Thomas G. Rizzo. Constraining the littlest higgs. ((u)). *JHEP*, 10:062, 2003.

[49] Stephan J. Huber. Flavor violation and warped geometry. *Nucl. Phys.*, B666:269–288, 2003.

[50] Stephan J. Huber and Qaisar Shafi. Fermion masses, mixings and proton decay in a randall- sundrum model. *Phys. Lett.*, B498:256–262, 2001.

[51] David B. Kaplan and Howard Georgi. Su(2) x u(1) breaking by vacuum misalignment. *Phys. Lett.*, B136:183, 1984.

[52] David B. Kaplan, Howard Georgi, and Savas Dimopoulos. Composite higgs scalars. *Phys. Lett.*, B136:187, 1984.

[53] David E. Kaplan and Martin Schmaltz. The little higgs from a simple group. *JHEP*, 10:039, 2003.

[54] Emanuel Katz, Jae-yong Lee, Ann E. Nelson, and Devin G. E. Walker. A composite little higgs model. *JHEP*, 10:088, 2005.

[55] Can Kilic and Rakhi Mahbubani. Precision electroweak observables in the minimal moose little higgs model. *JHEP*, 07:013, 2004.

[56] R. Kleiss and W. James Stirling. Spinor techniques for calculating p anti-p $\rightarrow$ w+- / z0 + jets. *Nucl. Phys.*, B262:235–262, 1985.

[57] I. G. Knowles. Angular correlations in qcd. *Nucl. Phys.*, B304:767, 1988.

[58] I. G. Knowles. Spin correlations in parton - parton scattering. *Nucl. Phys.*, B310:571, 1988.

[59] I. G. Knowles. A linear algorithm for calculating spin correlations in hadronic collisions. *Comput. Phys. Commun.*, 58:271–284, 1990.

[60] Ian Low. T parity and the littlest higgs. *JHEP*, 10:067, 2004.

[61] Ian Low, Witold Skiba, and David Smith. Little higgses from an antisymmetric condensate. *Phys. Rev.*, D66:072001, 2002.

[62] C. Macesanu, C. D. McMullen, and S. Nandi. Collider implications of models with extra dimensions. 2002.

[63] Juan M. Maldacena. The large n limit of superconformal field theories and supergravity. *Adv. Theor. Math. Phys.*, 2:231–252, 1998.

[64] Aneesh Manohar and Howard Georgi. Chiral quarks and the nonrelativistic quark model. *Nucl. Phys.*, B234:189, 1984.

[65] Patrick Meade and Matthew Reece. Top partners at the lhc: Spin and mass measurement. 2006.

[66] Maurizio Piai, Aaron Pierce, and Jay G. Wacker. Composite vector mesons from qcd to the little higgs. 2004.

[67] Massimo Porrati. Mass and gauge invariance. iv: Holography for the karch-randall model. *Phys. Rev.*, D65:044015, 2002.

[68] Lisa Randall and Raman Sundrum. An alternative to compactification. *Phys. Rev. Lett.*, 83:4690–4693, 1999.

[69] Lisa Randall and Raman Sundrum. A large mass hierarchy from a small extra dimension. *Phys. Rev. Lett.*, 83:3370–3373, 1999.

[70] R. Rattazzi and A. Zaffaroni. Comments on the holographic picture of the randall-sundrum model. *JHEP*, 04:021, 2001.

[71] Peter Richardson. Spin correlations in monte carlo simulations. *JHEP*, 11:029, 2001.

[72] Witold Skiba and John Terning. A simple model of two little higgses. *Phys. Rev.*, D68:075001, 2003.

[73] Jennifer M. Smillie and Bryan R. Webber. Distinguishing spins in supersymmetric and universal extra dimension models at the large hadron collider. *JHEP*, 10:069, 2005.

[74] Gerard 't Hooft. A planar diagram theory for strong interactions. *Nucl. Phys.*, B72:461, 1974.

[75] Jesse Thaler. Little technicolor. *JHEP*, 07:024, 2005.

[76] B. van Eijk and R. Kleiss. On the calculation of the exact g g → z b anti-b cross- section including z decay and b quark mass effects. In *Aachen 1990, Proceedings, Large Hadron Collider, vol. 2* 183-194. CERN Geneva - CERN-90-10-B (90/12,rec.Jul.91) 183- 194.

[77] Edward Witten. Anti-de sitter space and holography. *Adv. Theor. Math. Phys.*, 2:253–291, 1998.

[78] Chong-xing Yue and Wei Wang. The branching ratio r(b) in the littlest higgs model. *Nucl. Phys.*, B683:48–66, 2004.